Understanding Pathways Regulating Liver versus Pancreas Fate Decision and beta-cell Regeneration

A Dissertation
Presented to
The Academic Faculty

by

Jin Xu

In Partial Fulfillment
of the Requirements for the Degree
Doctor of Philosophy in Biology in the
School of Biological Sciences

Georgia Institute of Technology
August 2017

Understanding Pathways Regulating Liver versus Pancreas Fate Decision and beta-cell Regeneration

Approved by:

Dr. Chong Shin, Advisor
School of Biological Sciences
Georgia Institute of Technology

Dr. Francesca Storici
School of Biological Sciences
Georgia Institute of Technology

Dr. Alfred Merrill
School of Biological Sciences
Georgia Institute of Technology

Dr. Yury Chernoff
School of Biological Sciences
Georgia Institute of Technology

Dr. Young Jang
School of Biological Sciences
Georgia Institute of Technology

Date Approved: July 17, 2017

ACKNOWLEDGEMENTS

I would like to extend my deepest gratitude to my advisor Dr. Chong Shin for her invaluable guidance. My success would not have been possible without the continuous support and nurturing of her. I am also grateful to my committee members, Dr. Francesca Storici, Dr. Alfred Merrill, Dr. Yury Chernoff, and Dr. Young Jang for their insightful questions and discussions on my thesis proposal and for reviewing this dissertation. I also wish to thank my parents and my friends for their unconditional support and love.

TABLE OF CONTENTS

LIST OF FIGURES

SUMMARY

The liver and pancreas originate from common endodermal progenitors in early development. Single-cell lineage tracing experiments using zebrafish model system have demonstrated that Bone morphogenetic protein 2b (Bmp2b) signaling is essential in determining the fate of these bipotential progenitors towards the liver or pancreas. However, key downstream targets in the Bmp2b signaling regulatory network remains largely unknown. Therefore, we performed transcriptome analyses to identify genes that respond to altered levels of Bmp2b signaling. We found *four and a half LIM domains 1b* (*fhl1b*) as a novel target of Bmp2b signaling. *fhl1b* is primarily expressed in the prospective liver primordium. By loss of *fhl1b* using morpholino and overexpression of *fhl1b* combined with single cell lineage tracing, we showed *fhl1b* favors the specification of liver and suppresses the induction of pancreatic cells. These data reveal novel and critical functions of Fhl1b in regulating the hepatic versus pancreatic fate decision as a Bmp2b downstream target.

Diabetes is characterized by compromised glucose regulation. Both type 1 and type 2 diabetes patients suffer from losing functional β-cells along the progression of the disease. Given its function in suppressing pancreas induction with concomitant stimulation of liver, we conducted loss- and gain-of-function studies of *fhl1b* using a zebrafish model of type 1 diabetes. We conclude that *fhl1b* regulates the regeneration of β-cells mainly via modulating ductal progenitor-to-β-cell neogenesis. In addition to Bmp2b signaling pathway, we identified inhibitors of non-canonical IκB kinases, TANK-binding kinase 1 (TBK1) and IκB kinase ε (IKKε), as enhancers of β-cell regeneration.

TBK1/IKKε inhibitors promoted β-cell regeneration through enhancing β-cell-specific proliferation. Our results also suggested that this effect is achieved by up-regulating cAMP levels via suppressing activation of Pde3a in zebrafish. TBK1/IKKε inhibitors augmented function and proliferation of β-cells in mammalian islets including human islets *in vitro*. TBK1/IKKε inhibitors also improved glycemic control in streptozotocin (STZ)-induced diabetic mice with increased β-cell proliferation, and total insulin content *in vivo*. Therefore, our work shows an evolutionarily conserved and critical role of TBK1/IKKε suppression in expanding functional β-cell mass, and a strong clinical potential of TBK1/IKKε suppression in diabetes treatment.

The work presented in this dissertation contributed to the following publications:

Xu, J., Cui, J., Del Campo, A., and Shin, C.H. (2016). Four and a Half LIM Domains 1b (Fhl1b) Is Essential for Regulating the Liver versus Pancreas Fate Decision and for β-Cell Regeneration. PLOS Genet *12*, e1005831.

Xu, J., Tapadar, S.*, Weaver, J.D.*, Raji, I.O., Pithadia, D.J., Oyelere, A.K., García, A.J., Shin, C.H. Inhibition of TBK1/IKKε Promotes Regeneration of Pancreatic β-cells. Under review (*contributed equally).

CHAPTER 1
INTRODUCTION

The liver and pancreas are two essential organs regulating glucose metabolism. Cells residing in them produce hormones and enzymes in response to environmental signals inside the body, to facilitate maintaining physiological homeostasis. In pancreas, endocrine cells are clustered together, forming pancreatic islets. These tiny structures are engulfed in exocrine pancreatic cells, and only constitute a very small portion of the entire organ. However, hormones secreted by endocrine cells, especially glucagon and insulin, play key roles in controlling glucose levels. Endocrine cells, including glucagon-producing α-cells, insulin-producing β-cells, somatostatin-producing δ-cells, produce functionally distinct hormones to balance glucose production and storage in body. The majority of pancreas consists of exocrine cells. The exocrine cells, along with hepatic cells, generate digestive enzymes, that are transported by ductal system to intestine to assist ingesting nutrients. Among these various types of cells, the insulin-secreting β-cells have continuously been the focus of researches in academia, and of topics in general media, due to their direct association with the development of diabetes.

Diabetes is characterized by compromised glucose regulation. Both type I and type II diabetes patients suffer from losing functional insulin-producing β-cells along progression of the disease. However, the symptoms can be ameliorated by simply replenishing the pancreas with functional β-cells. One current approach is to transplant functional β-cells to patients, which heavily relies on the availability of cadaver donors. This approach faces many drawbacks. Besides the scarcity of donors, lifelong immunosuppression may be required, which usually leads to adverse effects (Cogger and

Nostro, 2015). Hence, developing alternative sources for high-quality, and ideally, compatible β-cells has become the mission of many studies. One intensively explored direction of these researches is to induce embryonic stem cells (ESCs) to differentiate into functional insulin-producing β-cells. Combining with patient-specific induced pluripotent cells, this strategy could easily generate sufficient material *in vitro* for transplantation, with no immunosuppression treatment necessary. Therefore, understanding the regulatory signaling pathways during normal organogenesis can be exploited to optimize the current protocol, benefiting the promotion of cell-based transplantation for diabetes treatment. Another promising direction for diabetes treatment is to enhance the expansion of functional β-cells. For patients with less severe loss of β-cells, expanding the remaining functional β-cell population *in vivo* could be one of the easiest and least costing methods. In addition, transplantation-based treatment will also benefit from increased proliferation of β-cells during *in vitro* culture to prepare sufficient supplies, and during and after operation to achieve higher therapeutic efficiency.

.

1.1 Pathways in normal development of liver and pancreas

After gastrulation, the three primary germ layers are segregated. The endodermal cells continuously migrate to form a tube-like structure, before the budding of digestive organ primordia. Meanwhile, these endodermal cells are highly plastic and competent. The fate of these cells are delicately regulated by the signals and cues produced from surrounding mesenchymal tissues, orchestrating the following patterning and organogenesis (Wells and Melton, 2000; Zorn and Wells, 2009). For liver and pancreas specification and development, the patterning of foregut endodermal region is critical to

ensure the proper differentiation of functionally diverse cell types. The anterior-posterior and dorsal-ventral patterning for the following organogenesis is finely controlled by many growth factor signaling pathways, including Wnt (Lancman et al., 2013; McLin et al., 2007; Ober et al., 2006), fibroblast growth factor (FGF) (Shin et al., 2011; Shin et al., 2007), bone morphogenetic protein (BMP) (Chung et al., 2010; Chung et al., 2008; Shin et al., 2007; Zaret, 2008), retinoic acid (RA) (Kinkel et al., 2008; Ostrom et al., 2008; Stafford and Prince, 2002), hedgehog (Hh) (Chung and Stainier, 2008; diIorio et al., 2002), and Notch (Murtaugh et al., 2003; Ninov et al., 2012; Shih et al., 2012).

Studying the early development of liver and pancreas sheds light in our understanding of the onset of certain congenital diseases, the impaired structure and function of tissues and organs involved in these diseases, and providing potential treatment clues. Furthermore, the rapidly thriving approach of using *in vitro* induction and culture to produce sufficient functional cells from ESCs or pluripotent cells, to supply transplantation-based disease treatment, is also taking advantages of the accumulated understanding of early development. Many induction protocols have been developed and successfully generated insulin-producing β-cells. These protocols use signaling molecules to guide the differentiation path of ESCs, mimicking endogenous dynamics of changing pathways shaping the fates of progenitor cells (Pagliuca et al., 2014; Rezania et al., 2014; Russ et al., 2015).

1.2 Pathways in pancreatic β-cell regeneration

Unlike the robust regenerative capacity of liver, through proliferation of abundant hepatocytes or activation of progenitor cell population in the ductal system (Huang et al., 2014; Michalopoulos, 2007), the spontaneous regeneration of pancreatic β-cells is weak. Previous studies have shown that β-cell regeneration can be promoted by either enhancing the proliferation of residual β-cells (Dor et al., 2004) or stimulating neogenesis of β-cells from non-β-cells. Non-β-cells could be progenitor cells residing in the extra- and/or intra-pancreatic ductal systems (Xu et al., 2008) or other mature cell types including glucagon-expressing α-cells (Thorel et al., 2010) or digestive enzyme-secreting acinar cells (Zhou et al., 2008). Although the regulatory network controlling pancreatic β-cell development is well-explored (Arda et al., 2013; Pan and Wright, 2011), the signaling pathways mediating β-cell regeneration remain largely unknown. Recently, the Adenosine signaling pathway has been shown to increase β-cell proliferation during homeostasis and regeneration (Andersson et al., 2012; Annes et al., 2012). In addition, the growth factor (insulin/IGF-1) signaling pathway and NFAT-DYRK1A signaling were reported to be activated to promote β-cell proliferation (El Ouaamari et al., 2015; Wang et al., 2015a). Nevertheless, few studies have pinpointed extrinsic signaling pathways, including Bmp signaling, that can induce *de novo* formation of β-cells during regeneration with a limited focus on determining the origin of newly formed β-cells (Stanger and Hebrok, 2013; Ziv et al., 2013). More importantly, to expand the clinical exploration on β-cell regeneration, whether manipulating these pathways successfully boosts up human β-cell regeneration is an inevitable question to be addressed.

1.3 Diabetes and the loss of functional β-cells

Diabetes mellitus is an epidemic healthcare challenge affecting around 380 million people worldwide, based on the International Diabetes Federation. According to 2014 National Diabetes Statistics Report, in the United States alone, 29.1 million people (9.3% of the population) have diabetes. What's more, 86 million people are predicted to have prediabetes, among which 15-30% will develop type 2 diabetes within five years. Patients with diabetes failed to produce sufficient insulin, or use insulin effectively. As the disease progresses, properly functional insulin-producing β-cells are getting scarce, resulting in severely compromised glucose homeostasis. In addition, patients with diabetes are at higher risk of serious health complications, such as heart disease, kidney failure, and blindness.

The direct cause of diabetic symptoms is the insufficiency or functional failure of insulin-producing β-cells, alone or in association with insulin resistance (Shaw et al., 2010). However, simply replenishing the pancreas with functional β-cells is competent to reverse the progression. This approach has been proven fruitful and employed widely (Wang et al., 2015b). It also has inspired many studies to obtain new β-cells through converting stem-cell or transdifferentiating non-β-cells into β-cells, or to discover small molecules or other compounds that can induce proliferation of β-cells. Due to both metabolic factors and immune components are closely linked to the progression of diabetes (Brezar et al., 2011; Donath and Shoelson, 2011; Esser et al., 2014), coupling expansion and protection of residual functional β-cells is critical in remedying diabetes. However, few currently available approaches achieved this goal.

1.4 Zebrafish as a model organism for developmental/regeneration studies and chemical testing

Zebrafish has been used as model organism for development for a few decades. The visually transparent small-sized body, *ex utero* development from fertilization, easy genetic manipulation and easy access to massive number of larvae, make zebrafish one of the ideal models to study early pattern and development events. The zebrafish liver and pancreas share their basic cell types with the mammalian liver and pancreas. All major types of hepatic and pancreatic cells are present in zebrafish, and they function in similar fashion as their mammalian counterparts. In addition, the signaling pathways that lead to the establishment of liver and pancreas are generally conserved from fish to mammals. Therefore, zebrafish provides a powerful tool to probe the mechanisms controlling establishment of the liver and pancreas from early embryonic progenitor cells, as well as the regeneration of these organs after damage. This knowledge is, in turn, applicable to refining protocols to generate renewable sources for clinical purposes.

Furthermore, with the rapidly advancing genetic techniques and accumulating pools of resources, studies are expanding to less explored yet important aspects of human diseases (Dooley and Zon, 2000). After successful establishment of zebrafish models of human diseases, they can be used to study various sides of the disease. As vertebrate, zebrafish acquires complexity in physiology and behavior similarly seen in mammalian systems, including human. One can easily monitor the real-time changes of other cell types or tissue in pathogenic condition with the assistance of endogenous fluorescent markers. To loyally establish a zebrafish model of human disease can be tricky. Not to

mention some diseases are initiated by a bunch of mixed factors, or progressed tardily with environmental influences, many diseases are not even thoroughly understood, making it extremely challenging to establish a model exposed to exactly the same genetic and/or environmental influence. However, researchers have adopted to use strategies phenotypically imitating human diseases (Moss et al., 2009).

Meanwhile, zebrafish has been embraced as a powerful platform to test and discover new effects of chemicals for quite some time (Rennekamp and Peterson, 2015). The small sized, massively reproduced population permits an economically efficient system for large scale screening. As vertebrate, zebrafish acquires complexity in physiology and behavior. The transparent body allows easy observation of changes *in vivo*. Last but not least, zebrafish is able to phenotypically imitate a wide range of diseases. It is also simple enough to administrate chemicals to zebrafish larvae, by directly adding the chemicals into the egg medium. Combining these points together, it makes zebrafish one of the ideal model organisms to test chemical properties.

1.5 Conclusion

Using zebrafish as a model organism to study (1) the fate decision of progenitor cells during normal development, and (2) β-cell regeneration embraces great advantages to provide insights in diabetes treatment. The loss of functional insulin-producing β-cells in progression of diabetes can be ameliorated by transplanting functional β-cells to patients, or expanding the remaining functional β-cells *in vivo*. In addition to traditional sources for transplantation, new protocols utilizing directed ESC differentiation to

produce supplies for transplantation have been developed based on the knowledge of regulatory signaling pathways during normal organogenesis, and will continuously benefit from more detailed and accurate understanding of this process. Easy access to massive zebrafish samples and convenient observation of *in vivo* changes in zebrafish models of diabetes enable expedited discoveries on new regulatory pathways and targets for diabetes treatment. These regeneration-specific targets could be potentially more efficient and safer in expanding endogenous β-cell population than strategies affecting general philological conditions.

CHAPTER 2
BMP2b SIGNALING ACTIVATES FOUR AND A HALF LIM DOMAINS 1b (Fhl1b) TO REGULATE THE LIVER VERSUS PANCREAS FATE DECISION

The work in this chapter contributes to the following publication:

Xu, J., et al. (2016). *PLOS Genetics*.

2.1 Abstract

The liver and pancreas, two essential organs regulating metabolism homeostasis, despite their distinct structures, cellular composition and physiological functions, originate from bipotential progenitors in early endoderm. Single-cell lineage tracing experiments using zebrafish model system have demonstrated that Bmp2b signaling plays a critical role in determining the fate of these bipotential hepatopancreatic progenitors towards the liver or pancreas. Nevertheless, the downstream regulatory network of Bmp2b signaling in this process is poorly understood. In our study, we identified *four and a half LIM domains 1b* (*fhl1b*) as a novel target of Bmp2b signaling. *fhl1b* is primarily expressed in the prospective liver primordium. Depletion of *fhl1b* by morpholino compromised specification of liver and enhanced induction of pancreatic cells, particularly endocrine cells. Conversely, overexpression of *fhl1b* promoted specification of liver and suppressed induction of pancreatic cells. By single-cell lineage tracing experiments, we showed that *fhl1b* depletion led the progenies of lateral endodermal progenitor cells, destined to

become liver cells in normal cases, to become pancreatic cells. Reversely, when *fhl1b* was overexpressed, the progenies of medially located endodermal progenitor cells, fated to differentiate into pancreatic and intestinal cells, turned into liver cells. Altogether, these data reveal novel and critical functions of Fhl1b in the hepatic versus pancreatic fate decision.

2.2 Introduction

Bone morphogenetic protein (Bmp) signaling has been shown to be heavily involved in endodermal progenitor fate decision, among other signaling pathways. In general, Bmp signaling induces the liver at the expense of *Pdx1*-expressing organs and tissues in various animal models (Chung et al., 2008; Rossi et al., 2001; Spagnoli and Brivanlou, 2008; Wandzioch and Zaret, 2009; Xu et al., 2011). To activate the expression of liver lineage genes, Bmp signaling can regulate the expression levels of zinc finger transcription factor Gata4 (Rossi et al., 2001; Shin et al., 2007), and epigenetically, promote histone acetylation at the liver gene regulatory elements (Xu et al., 2011). On the other hand, Bmp signaling may actively suppress the pancreas gene expression. *Pdx1* expression was inhibited in mice half-embryo cultures treated with Bmp4 at the 3-4 somite stage (Wandzioch and Zaret, 2009). *pdx1* expression gradient is formed in zebrafish endodermal progenitor cells based on their relative distance from Bmp2b signaling. The lateral endodermal progenitors close to the Bmp2b signal show minimum *pdx1* expression and differentiate into liver, while medial endodermal progenitors distant from the Bmp2b signal express high levels of *pdx1* and differentiate into pancreas and intestine (Chung et al., 2008). Furthermore, to successfully induce *PDX1* expression in human embryonic stem cells (hESCs) hence generate INSULIN-secreting β-cells, inhibition of BMP signaling is required based on recent studies and protocols (Kroon et al., 2008; Nostro et al., 2011; Pagliuca et al., 2014; Rezania et al., 2012). In addition, the induction of β-cells in zebrafish can be blocked by Bmp signaling activation cell-autonomously (Chung et al., 2010). However, how Bmp signaling facilitates liver specification at the expense of *pdx1*-expressing cells remains to be further elucidated, which necessitates the identification of downstream regulatory network. Furthermore, the

key question of whether Bmp signaling suppresses *Pdx1* expression to keep progenitors competent to differentiate into the liver or directly induces the liver gene program has not yet been answered.

In addition to the processes in normal development, it's been suggested that a progenitor cell population in the hepatopancreatic ductal (HPD) system may undergo differentiation upon stimuli in later stages. The HPD system connects the liver, gallbladder, and pancreas with the intestine, transporting products of multiple types of cells to the main location of nutrient ingestion. The HPD systems in amniotes and zebrafish are developmentally and structurally similar (Dong et al., 2007). In the HPD system of *fgf10* and *sox9* mutant zebrafish, hepatocyte-like and pancreatic-like cells can be observed within/adjacent to the system (Delous et al., 2012; Dong et al., 2007; Manfroid et al., 2012), indicating the existence of a progenitor cell population and its ability to differentiate into either liver or pancreas cells. Notch signaling and *pdx1* function have also been suggested to play essential roles in the induction of pancreatic endocrine cells from the progenitors in the HPD system of zebrafish (Kimmel et al., 2011). Consistent with expression studies in zebrafish, that *pdx1* is expressed in the HPD system and pancreas but not in liver (Field et al., 2003a), lineage tracing studies in mammals implied that the HPD system and the ventral pancreas, were derived from cells expressing both *Pdx1* and *Sox17*, a master regulator of the pancreaticobiliary ductal system (Spence et al., 2009). Intriguingly, the expression of Inhibitor of DNA binding 2 (Id2) protein, a cell-autonomous marker of Bmp signaling activity (Miyazono and Miyazawa, 2002), is excluded in the endocrine pancreas, and HPD system (Chung et al., 2010), which are the tissues that retain the potential to form pancreatic endocrine cells. In

a rat pancreatic epithelial cell line, Id2 has been implicated in repressing the function of key pancreatic endocrine transcription factor Neurod, which is essential for endocrine pancreas development (Hua et al., 2006). Nonetheless, the underlying mechanisms of how Bmp signaling orchestrates the proper lineage choice of the progenitors in the HPD system await further investigation.

The LIM (LIN-11, ISL-1, and MEC-3) domain is mediating protein-protein interaction without intrinsic catalytic activity (Kadrmas and Beckerle, 2004; Sang et al., 2014). The LIM proteins often contribute to biological activity as molecular adaptors or scaffolds to support the assembly of multimeric protein complexes (Chang et al., 2003). The four-and-a-half LIM (FHL) proteins contain four complete LIM domains with an N-terminal half LIM domain (Shathasivam et al., 2010). These proteins can be expressed in a cell- and tissue-specific manner to regulate cellular processes such as proliferation, differentiation, and adhesion/migration. However, little is known about their role in the cell fate choice between the liver and the pancreas.

Here, by transcriptome analysis, we identified a novel Bmp2b target, *four and a half LIM domains 1b* (*fhl1b*). *fhl1b* is primarily expressed in the prospective liver anlage. Loss- and gain-of-function as well as single-cell lineage tracing analyses indicate that Fhl1b inhibits specification of the pancreas and induces the liver.

2.3 Methods and materials

2.3.1 Zebrafish strains

Adult fish and embryos were raised and maintained under standard laboratory conditions (Westerfield, 2000). All animal work was performed according to procedures approved by the Institutional Animal Care and Use Committee at Georgia Institute of Technology. We used the following published transgenic lines: *Tg(P0-pax6b:*GFP*)*^{ulg515} (Delporte et al., 2008), *Tg(ins:GFP)*^{zf5} (Huang et al., 2001), *Tg(ins:dsRed)*^{m1018} (from W. Driever, Freiburg), *TgBAC(neurod:EGFP)*^{nl1} (Obholzer et al., 2008), *Tg(sox17:GFP)*^{s870} (Chung and Stainier, 2008), *Tg(hsp70l:bmp2b)*^{f13} (Chocron et al., 2007), *Tg(fabp10:dsRed, ela3l:GFP)*^{gz12} (Farooq et al., 2008), *Tg(-5.5ptf1a:DsRed)*^{ia6} (Leung et al., 2011), *Tg(ptf1a*:*GFP)*^{jh1} (Godinho et al., 2005), *Tg(ins:Kaede)*^{jh6} (Pisharath et al., 2007), and *Tg*(*ins*:*CFP-NTR*)^{s892} (Curado et al., 2007), and *Tg(fabp10a:CFP-Eco.NfsB)*^{gt1} (Huang et al., 2014). To generate the *Tg(hsp:fhl1b; hsp:GFP)*^{gt3}, *fhl1b* coding sequence was amplified (forward: 5'-CCGGAATTCATGGCAAGCCGGTCCAACTG-3', reverse: 5'-CCGGAATTCTTACAGTTTCTTGGAGCAGTCG-3') and cloned into a vector containing a multimerized minimal heat shock promoter, which drives *gfp* and *fhl1b* transcription bi-directionally in response to a heat shock (Bajoghli et al., 2004). Tol2-mediated transgenesis was achieved as described (Kawakami et al., 1998).

2.3.2 Microarray and phylogenetic analysis

Tg(sox17:GFP)^{s870} embryos were either crossed with *Tg(hsp70l:bmp2b)*^{f13} to induce overexpression of *bmp2b* at the 8-somite stage or treated with DMH1. For each condition, 100 embryos were used. At 20 hpf, *sox17*:GFP-positive endodermal cells from

dissected zebrafish trunks containing the organ-forming area were isolated by FACS and subjected to transcriptome profiling using the Zebrafish 44K gene expression microarray (Agilent Technologies). Data with an average fold change of 2 (*bmp2b* overexpressing) or 2.75 (DMH1-treated) at $p \leq 0.05$ were considered for GO analysis using PANTHER (http://www.pantherdb.org/). The phylogenetic tree of zebrafish Fhl1b (NM_199217) was constructed using Phylogeny.fr (Dereeper et al., 2008) with mammalian homologous proteins sorted by performing alignment on UniProtKB/Swiss-Prot database.

2.3.3 Reverse transcription quantitative real-time polymerase chain reaction

Total RNA was extracted using the Trizol Reagent (Invitrogen). cDNA synthesis was performed using Superscript III First-strand Synthesis System (Invitrogen). PCR was conducted using iTaq Universal SYBR Green Supermix in triplicate (Bio-Rad). Optimized primers targeting each gene were designed using Primer3 (Untergasser et al., 2012). The StepONE Plus PCR System (Applied Biosystems) was used to obtain the *C*t value. The relative gene expression of each sample was determined using the comparative *C*t method with *β-actin* as an internal control (Schmittgen and Livak, 2008). The following primers were used: *fhl1b*: forward 5'-GTGAGGAAAGACGAGAAACAAG-3', reverse 5'-GGCACATCGGAAACAATCAG-3'; *β-actin*: forward 5'-CGAGCTGTCTTCCCATCCA-3', reverse 5'-TCACCAACGTAGCTGTCTTTCTG-3'.

2.3.4 Embryo microinjection

Knockdown of *fhl1b* was performed via injection of individual *fhl1b* MO 1 (2 ng; 5'-CCCGCGAAAAGCTGTGAGAAATAAT-3') or MO 2 (2 ng; 5'-ATAAATATCTGTCCCCTCACCTGGC-3') or a combination of MO1 and 2 (4 ng; Gene Tools, LLC). A standard control MO (4 ng; 5'-CCTCTTACCTCAGTTACAATTTATA-3') targeting a human beta-globin intron mutation was used as a negative control (Gene Tools, LLC). *id2a* MO (5' -GCCTTCATGTTGACAGCAGGATTTC-3') (Uribe and Gross, 2010) and *tp53* MO (5'-GACCTCCTCTCCACTAAACTACGAT-3') (Robu et al., 2007)were purchased from Gene Tools, LLC. 4 ng of *id2a* MO or 2 ng of *tp53* MO was used. The primers annealing to the first (5'- GCAAAACACTTTGCTGTGGC-3') and the sixth (5'-GCCAGGTTGAGGGAGCATTT-3') coding exons were used to confirm the specificity of *fhl1b* MOs. Sense-strand-capped *fhl1b-P2A-mCherry* mRNA was synthesized with mMESSAGE mMACHINE kit (Ambion). For rescue experiments, embryos were injected with 200 pg of *fhl1b-P2A-mCherry* mRNA with a mixture of *fhl1b* MO 1 and 2.

2.3.5 *In situ* hybridization and immunohistochemistry

Whole-mount *in situ* hybridization was performed as previously described (Alexander et al., 1998), using the following probes: *pdx1* (Biemar et al., 2001), *neurod* (Korzh et al., 1998), *hhex* (Ho et al., 1999), and *fhl1b* (template for antisense RNA probe was amplified from embryonic cDNA with the following primers: forward: 5'-CCGCTCGAGATGGCAAGCCGGTCCAACTG-3', reverse: 5'-ACGGCTGGTCCTGGTAATTC-3'). Immunohistochemistry on whole-mount embryos

was performed as previously described (Dong et al., 2007) using the following antibodies: mouse anti-Glucagon (1:100; Sigma), mouse anti-2F11 (1:200; Abcam), mouse anti-β-catenin (1:100; BD Transduction Laboratories), rabbit anti-FHL1 (1:200; Abcam), chicken anti-GFP (1:1000; Aves Labs), rabbit anti-Somatostatin (1:100; MP Biomedicals), mouse anti-Islet1/2 (1:10; Developmental Studies Hybridoma Bank (DSHB), clone 39.4D5), guinea pig anti-Insulin (1:100; Sigma), rabbit anti-Prox1 (1:100; Millipore), guinea pig anti-Pdx1 (1:200; gift from C. Wright), rabbit anti-pan-Cadherin (1:1000; Sigma), goat anti-Fluorescein (1:100; Molecular Probes), and fluorescently conjugated Alexa antibodies (1:200; Molecular Probes). Nuclei were visualized with TOPRO (1:10000; Molecular Probes). For the TUNEL assay, embryos were fixed in 3% formaldehyde, preincubated in PBST, and then labeled with the TUNEL kit (Roche) for 1 hour at 37°C. For coimmunostaining with Prox1, sections were first incubated with primary antibodies, then with TUNEL solutions, and finally with secondary antibodies. Embryos were mounted in Vectashield (Vector Laboratories) and imaged on a Zeiss LSM 510 VIS confocal microscope.

2.3.6 *fhl1b* gene disruption with the CRISPR/Cas9 system

The guide RNA (gRNA) targeting sites, which are downstream of the start codon (gRNA 1: 5'- CTGTCGTGAGGACCTCAG-3', gRNA 2: 5'- AGTGGAAAGAAGTTCGTG-3'), were selected using the online application available at crispr.mit.edu. Complementary oligonucleotides corresponding to the target sequences were annealed as previously described (Jao et al., 2013). 1 µl of the annealed oligonucleotides was mixed with 500 ng of the gRNA cloning vector pDR274, 0.5 µl of BsaI-HF, 0.5 µl of T4 DNA ligase, 1 µl of

10× NEB buffer 2, 1 μl of 10× T4 ligase buffer, and water for a total of 10 μl. Digestion and ligation were performed in a single step as previously described (Jao et al., 2013). The gRNAs were transcribed using HindIII-digested expression vectors as templates and the MEGAshorscript T7 kit (Life Technologies). The *cas9* mRNA was transcribed using NotI-digested Cas9 expression vector and the mMESSAGE mMACHINE kit (Ambion). The mixture of 1 nl of *cas9* mRNA (300-450 ng/μl) and an individual or a combination of gRNA 1 and 2 (final concentration 12.5 ng/μl) were injected into one-cell stage embryos.

2.3.7 T7 Endonuclease I (T7EI) assay

The genomic region flanking the target sites was amplified using PCR (forward: 5'-ACTTACACATGAGGGGCTGTG-3', reverse: 5'-ATAGTCCTTAATGGAAAACATGCTG-3'). A total of 200 ng of the purified PCR products was denatured and re-annealed, as previously described (Jao et al., 2013) to facilitate heteroduplex formation. The re-annealed products were digested with 10 units of T7 endonuclease I (New England Biolabs) at 37°C for 30 min. The reaction was stopped by adding 1 μl of 0.5 M EDTA. Samples were analyzed by 2% agarose gel. Band intensity was quantified using ImageJ software (National Institutes of Health). Gene modification levels were estimated based on the following equation: $\%\ gene\ modification = 100 \times \left(1 - \left(1 - fraction\ cleaved\right)^{1/2}\right)$ % (Reyon et al., 2012).

2.3.8 DNA sequencing

For sequencing the target region in injected embryos, the PCR products were cloned into pGEM T-easy vector (Promega). Plasmid DNA was isolated from individual transformants and sequenced.

2.3.9 Chemical treatment and heat-shock experiment

Embryos were treated with 0.3 μM DMH1 (EMD Chemicals) from 12 hpf to 20 hpf or 3 μM SU 5402 (Tocris Bioscience) from 50 hpf to 72 hpf in egg water. To ablate β-cells, *Tg(ins:CFP-NTR)*^{s892} embryos were treated with freshly prepared 5 mM metronidazole (Mtz) (Sigma) from 84 hpf to 108 hpf in the dark, followed by 36-48 hours recovery. Before ablation, *Tg(ins:*Kaede*)*-expressing β-cells were converted from green to red by exposing them to UV light. Control embryos from the same batch were treated with DMSO in egg water. *Tg(hsp:fhl1b; hsp:GFP)*^{gt3} and *Tg(hsp70l:bmp2b)*^{f13} embryos were heat shocked at various stages by transferring them into egg water pre-warmed at 40°C and 37°C, respectively. After a 30-minute heat shock, embryos were returned into a 28°C incubator and harvested at various stages.

2.3.10 Lineage tracing

Tg(sox17:GFP)^{s870} embryos were injected with 2nl of 0.5% caged fluorescein dextran and allowed to develop until the 6-somite stage (corresponding to 12 hours-post-fertilization (hpf)). After manual dechorionation, embryos were mounted ventrally in a mold filled with egg water. Using a Nikon Eclipse Ti confocal microscope, we visualized

the endodermal sheet in live embryos at the 6-8 somite stage, and the A-P position of endodermal cells was determined by counting somites. Caged-fluorescein was activated in a single endodermal cell in each embryo with a 405 nm laser focused through a 40X objective lens. The uncaged embryos were fixed at various time points and stained with antibodies against GFP, the uncaged-Fluorescein, and Islet1 or Prox1.

2.3.11 Glucose measurements

Glucose measurements were performed on 3 times on 10 zebrafish larvae per condition using a fluorescence-based enzymatic detection kit (Biovision Inc.) (Andersson et al., 2012). The larvae were collected in 1.5 ml microcentrifuge tubes. Excess medium was removed and embryos were frozen on crushed dry ice. After thawing, 200µl PBS was added and the larvae were homogenized using a hand-held mechanical homogenizer. Reactions were assembled on ice in black, flat bottom 96-well plates (Costar). Standard curves were generated using glucose standard solution (according to instructions) and were included in each assay. To measure glucose in embryo extracts, 15 ul of sample were used. Control reactions without sample lysate were included in each row. Reactions were incubated for 30 minutes at 37°C in the dark. Fluorescence (excitation 535 nm; emission, 590 nm) was measured using a Safire II plate reader equipped with XFLUOR4 software (v 4.51).

Fluorescence values were corrected by subtracting measurements from control reactions without sample. Glucose levels were interpolated from standard curves. Each sample was measured in triplicate and each experiment repeated three times.

2.3.12 Statistical analysis

The *p*-values were calculated using an unpaired two-tailed Student *t*-test with Excel (Microsoft, Redmond, WA).

2.4 Results

2.4.1 *fhl1b* is a target of the Bmp2b pathway

To discover new Bmp2b downstream target genes potentially regulate the fate decision of bipotential hepatopancreatic progenitors, hence to facilitate unveiling the mechanism underneath, we performed microarray analyses on zebrafish endodermal cells exposed to increased or decreased Bmp signaling, before and during the organogenesis of liver and pancreas. The transgenic zebrafish line *Tg(sox17:*GFP*)*^{s870} labels all endodermal cell population with green fluorescent protein (GFP) (Chung and Stainier, 2008), enabling us to use fluorescence activated cell sorting (FACS) to exclusively collect them for analysis. For expression profiling of samples experienced enhanced Bmp2b signaling, zebrafish embryos were obtained from crossing *Tg(sox17:*GFP*)*^{s870} line with a heat-shock inducible *bmp2b* overexpressing transgenic zebrafish line, to precisely induce Bmp2b signaling before the fate decision of bipotential progenitor cells occurs. For expression profiling of samples with reduced Bmp signaling, embryos were obtained from *Tg(sox17:*GFP*)*^{s870} line, and treated with DMH1 (a highly selective inhibitor of the BMP type I receptors Alk3 (Bmpr1a) and Alk8 (Acvr1/Alk2)) (Hao et al., 2010), to decrease the level of Bmp2b signaling during fate decision. Endodermal cells from these treated embryos were dissociated and sorted. Total RNA was extracted from them and prepared for gene expression profiling analysis (Figure 2.1).

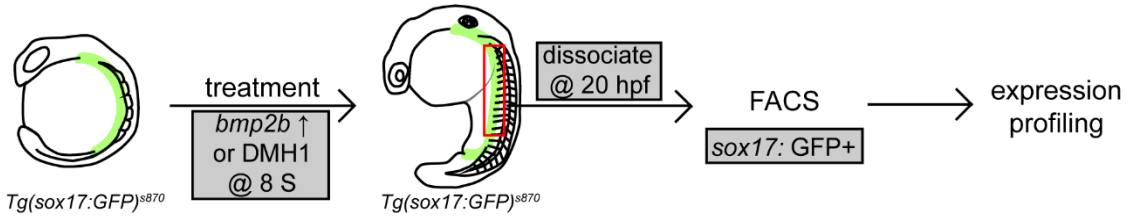

Figure 2.1 Scheme for the preparation of performing expression profiling to identify Bmp2b downstream genes.

Levels of Bmp2b signaling was pharmacologically or genetically manipulated in *Tg(sox17:GFP)*^{s870} embryos either by treating with DMH1 or inducing *bmp2b* expression at the 8-somite stage. *Tg(sox17:*GFP)^{s870}-positive endodermal cells from dissected zebrafish trunks containing the organ-forming area (red rectangle) were isolated by FACS and subjected to transcriptome profiling at 20 hpf.

Genes identified by the profiling analysis with the cutline of 2-fold (in the case of increased Bmp2b signaling) or 2.75-fold (in the case of decreased Bmp2b signaling) changes ($p \leq 0.05$) were clustered by biological processes, using Gene Ontology analysis by PANTHER program (http://www.pantherdb.org/). A total of 998 genes showed changes in increased Bmp2b signaling, and 1261 genes showed changes in decreased Bmp2b signaling, respectively. To find out genes that are direct downstream targets of Bmp2b signaling, we grouped genes that exhibited a change in expression in both conditions (Figure 2.2A). 56 genes met this criterion. Among them, *four and a half LIM domains 1b* (*fhl1b*), had a prominent change in expression (Figure 2.2B).

To confirm the microarray results of *fhl1b*, the mRNA transcription levels of *fhl1b* was assessed by reverse transcription quantitative real-time polymerase chain reaction (RT-qPCR), in embryos overexpressing *bmp2b* or treated with DMH1 (Figure 2.3A). To dissect the initiation developmental stage and level of *fhl1b* expression, total RNAs of variously staged embryos were extracted and reversed transcribed, then amplified by reduced-cycle PCR, using *fhl1b* primers and *β-actin* primers as internal control. Based on PCR results, the endogenous transcription of *fhl1b* starts around the 12-somite stage, following the endogenous *bmp2b* expression (Figure 2.3B.; (Chung et al., 2008)).

A

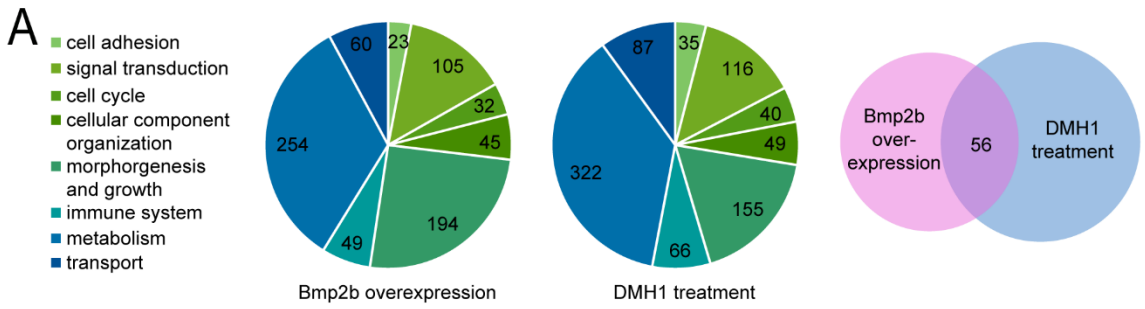

B

Genes		Bmp2b fold change	DMH1 fold change
BMP and activin membrane-bound inhibitor (Xenopus laevis) homolog a	bambia	2.65	-3.15
caspase a	caspa	7	-3.86
cellular retinoic acid binding protein 1a	crabp1a	10.64	-3.13
cytoglobin 1	cygb1	-2.65	7.88
erythrocyte membrane protein band 4.1 (elliptocytosis 1, RH-linked)	epb41b	2.57	-2.78
even-skipped homeobox 1	evx1	2.8	-2.68
four and a half LIM domains 1b	fhl1b	5.36	-2.44
gremlin 2, cysteine knot superfamily	grem2	2.75	-4.96
interleukin 1, beta	il1b	-2.07	6.36
ISL LIM homeobox 2a	isl2a	2.19	-3.63
NK2 transcription factor related 3	nkx2.3	5.75	-4.14
SMAD family member 6b	smad6b	3.01	-2.74

Figure 2.2 Strategy for the identification of Bmp2b downstream genes potentially associated with the liver versus pancreas fate decision.

(A) Functional clustering and distribution of known genes identified in the expression profiling with a *p*-value ≤ 0.05 and minimum a 2-fold change in *bmp2b* overexpressing or a 2.75-fold change in DMH1-treated embryos. 56 known genes showed significant changes in both *bmp2b* overexpressing and DMH1-treated embryos. (B) List of representative genes showing prominent changes both in DMH1-treated and *bmp2b*-overexrpessing conditions.

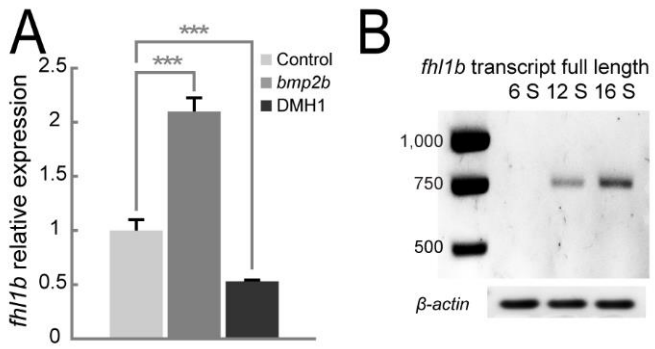

Figure 2.3 Confirmation of *fhl1b* expression from microarray results

(A) Quantitative real-time PCR analysis of *fhl1b* in *bmp2b*-overexpressing or DMH1-treated embryos at 20 hpf. *fhl1b* expression levels were normalized to the levels of *β-actin* and presented as fold changes (mean±SD) against control expression. Asterisks indicate statistical significance: ***, $P < 0.001$. (B) *fhl1b* full-length transcript starts to be expressed from the 12-somite stage onwards.

To investigate temporal and spatial expression pattern of *fhl1b* in the developing endodermal tissues, we performed double antibody and *in situ* hybridization staining. At 24 hours-post-fertilization (hpf), *fhl1b* is primarily expressed in the anterior part of the endoderm, which corresponds to the prospective liver region, (Figure 2.4A-B, black arrows). When combined with GFP staining in *Tg(sox17:GFP)*^{s870} embryos, the colocalization of *in situ* signal and GFP indicated that *fhl1b* is highly expressed in the endodermal tissues developing into liver (Figure 2.4E-E', black arrows; early-forming dorsal pancreatic bud, which develops into principal islet, containing endocrine pancreatic cells, is marked by dotted circles). Besides endodermal tissues, *fhl1b* expresses in the pronephric duct (Figure 2.4A and 2.4C, blue arrowheads) and heart (Figure 2.4A and 2.4C-D, black arrowheads) from 24 hpf onwards. At 30 hpf, levels of *fhl1b* expression maintain high in the liver (Figure 2.4C-D, and 2.3F, black arrows) when the liver is budding out from the medially migrated endodermal rod (Field et al., 2003b). *TgBAC(neurod:EGFP)*^{nl1} line marks pancreatic endocrine progenitors with EGFP. At 78 hpf, levels of *fhl1b* expression stay high in the differentiated liver (Figure 2.4G, black arrow). Levels of *fhl1b* expression are also high in patches of cells in the distal intestine (Figure 2.4G), low in the HPD system (Figure 2.4G, black bracket), and absent in most of the pancreatic cells except for a few cells in the periphery of the principal islet (Figure 2.4G, yellow arrow; figure 2.4G'-G", insets showing magnified views of *fhl1b* expression in the principal islet).

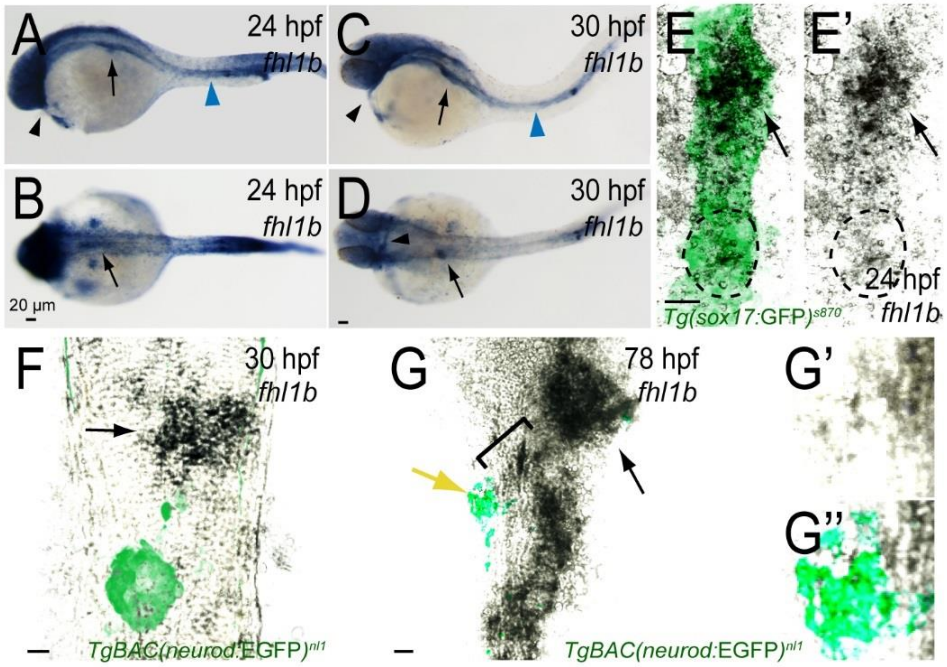

Figure 2.4 The expression pattern of *fhl1b* during early development.

(A-B) Whole-mount *in situ* hybridization showing the expression of *fhl1b* at 24 hpf. *fhl1b* is expressed in the anterior part of the endoderm, which corresponds to the prospective liver region (black arrows). Additionally, *fhl1b* is expressed in the pronephric duct (blue arrowhead) and heart (black arrowhead). (C-D) Whole-mount *in situ* hybridization showing the expression of *fhl1b* at 30 hpf. *fhl1b* continues to be highly expressed in the liver (black arrows) when the liver has started budding from the medially migrated endodermal rod. *fhl1b* also remains to be expressed in the pronephric duct (blue arrowhead) and heart (black arrowheads). (E-E') Double antibody and *in situ* hybridization staining of *fhl1b* at 24 hpf in *Tg(sox17:GFP)*^{s870} embryos. *fhl1b* is primarily expressed in the anterior part of the endoderm, which corresponds to the prospective liver anlage (black arrows). Black dotted circles point out the dorsal pancreatic bud. (F-G") Double antibody and *in situ* hybridization staining of *fhl1b* in *TgBAC(neurod:EGFP)*^{nl1} embryos at 30 (F) and 78 (G) hpf. *TgBAC(neurod:*EGFP*)*^{nl1} expression marks the posteriorly located pancreatic endocrine cells. At 78 hpf, the level of *fhl1b* expression is high in the liver (black arrow) and in patches of cells in the distal intestine, low in the HPD system (black bracket), and absent in most of the pancreatic cells (G). Magnified images for *fhl1b* and *TgBAC(neurod:*EGFP*)*^{nl1}expression in the principal islet are shown in insets. In the principal islet, *fhl1b* expression is confined to the peripheral boundary and does not significantly overlap with the *TgBAC(neurod:*EGFP*)*^{nl1} expression. Asterisks indicate statistical significance: ***, $P < 0.001$. E-G", confocal single-plane images combined with the projection images showing *Tg(sox17:*GFP*)*^{s870} (E-E') and *TgBAC(neurod:*EGFP*)*^{nl1} expression (F-G"), ventral views, anterior to the top. A and C, lateral views, anterior to the left. B and D, dorsal views, anterior to the left. n=10 per each time point and condition. Scale bars, 20 µm.

To confirm that Bmp2b signaling activates *fhl1b*, we checked the patterns and levels of *fhl1b* expression, in the excess or absence of Bmp2b signaling. Compared to control embryos (Figure 2.5A, black bracket; Figure 2.5D), embryos exposed to excessive levels of *bmp2b*, which was induced before the initiation of endogenous *bmp2b* expression, exhibited a drastic expansion of *fhl1b* expression (Figure 2.5B, black bracket; Figure 2.5D). On the other hand, embryos experienced decreased levels of Bmp signaling with DMH1 treatment showed a significant reduction of *fhl1b* expression, particularly in the liver at 30 hpf (Figure 2.5C, black bracket; Figure 2.5D). These results reassured that *fhl1b* is a target of Bmp2b signaling.

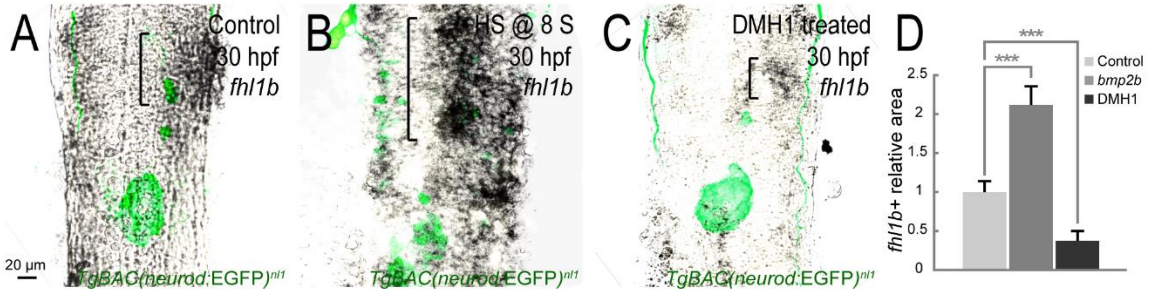

Figure 2.5 *fhl1b* is a target of the Bmp2b pathway.

(A-C) Double antibody and *in situ* hybridization staining showing the endogenous expression of *fhl1b* in the liver (black brackets), comparing control (A), *bmp2b*-overexpressing (B), and DMH1-treated (C) *TgBAC(neurod:EGFP)*^{nl1} embryos at 30 hpf. *fhl1b* expression was greatly expanded when *bmp2b* expression was induced at the 8-somite stage (B), but was dramatically reduced in DMH1-treated embryos (C). (D) Quantification of the *fhl1b*-positive *in situ* hybridization signal at 30 hpf. The areas of *fhl1b*-positive signal were selected and measured using Image J with normalization to control. 3 individual embryos were analyzed for each condition. Asterisks indicate statistical significance: ***, $P < 0.001$. A-C, confocal single-plane images combined with the projection images showing *TgBAC(neurod:*EGFP*)*^{nl1} expression (A-C), ventral views, anterior to the top. n=10 per each time point and condition. Scale bars, 20 μm.

To find the mammalian orthologs of *fhl1b*, we searched and compared the four and a half LIM domains proteins in mouse, rat, and human, and determined their evolutionary relationships. Based on the phylogenetic tree of zebrafish Fhl1b and the related proteins in mammals, Fhl1 was selected as the mouse ortholog of zebrafish Fhl1b (Figure 2.6A). Next we checked if the expression pattern of zebrafish *fhl1b* is conserved across species. Mouse Fhl1 shares 61% amino acid identity with zebrafish Fhl1b (Figure 2.6B).

We investigated mRNA and protein expression patterns of Fhl1 in developing mouse embryos. At embryonic day 8.5-9.5 (E8.5-9.5), *Fhl1* mRNA is detected in the foregut endoderm where the liver and the pancreas are derived (Wandzioch and Zaret, 2009) (Figure 2.7A). From E10.5 onwards, *Fhl1* is expressed in the liver (Figure 2.7A). At E14.5, Fhl1 proteins are highly expressed in the Prox1-positive liver cells (Figure 2.7B-B’’’), whereas their expression is weakly detected in the Prox1-positive pancreatic cells (Sosa-Pineda et al., 2000; Wang et al., 2005) (Figure 2.7C-C’’’). These findings suggest that similar to the expression pattern of zebrafish *fhl1b*, mouse *Fhl1* is primarily expressed in the developing liver. Taken together, these results indicate that the hepatopancreatic expression of Fhl1b and its mouse ortholog Fhl1 is evolutionarily conserved.

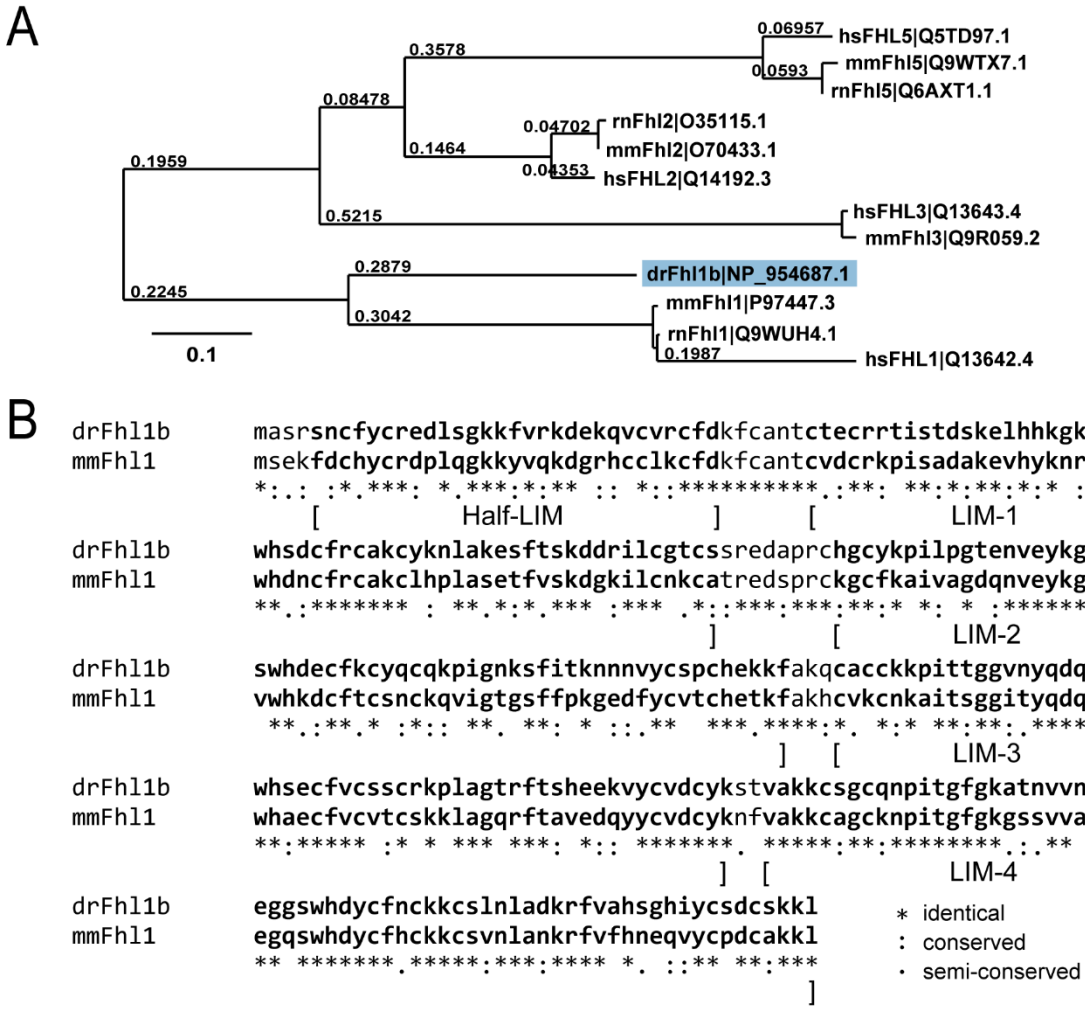

Figure 2.6 *Fhl1* is the mouse ortholog of zebrafish *fhl1b*.

(A) Phylogenetic tree of zebrafish Fhl1b (highlighted in blue) and the related proteins in mammals. This tree was constructed using Phylogeny.fr with sorted candidates from UniProtKB/Swiss-Prot database. Zebrafish (dr), Mouse (mm), Rat (rn), and Human (hs). (B) Alignment of zebrafish Fhl1b and mouse Fhl1 amino acid sequences. Identical residues are indicated with asterisks.

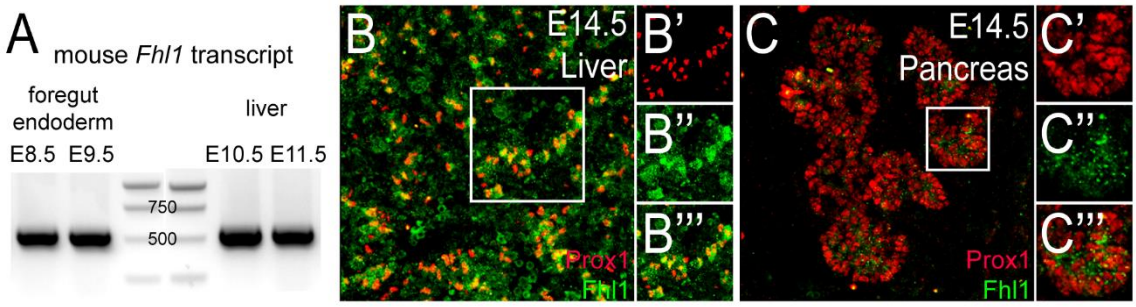

Figure 2.7 *Fhl1* is consistently expressed in the liver during mouse embryonic development.

(A-C’’’) Expression of Fhl1 in the developing mouse embryos. (A) *Fhl1* full-length transcript is expressed in the mouse foregut endoderm at embryonic day 8.5-9.5 (E8.5-9.5). From E10.5, *Fhl1* is consistently expressed in the liver. (B-C’’’) Immunofluorescent labeling of Fhl1 in the liver (B-B’’’) and pancreas (C-C’’’) of E14.5 mice (n=3). (B-B’’’) Fhl1 proteins are highly co-expressed in the Prox1-positive liver cells. (C-C’’’) Fhl1b proteins are weakly detected in the Prox1-positive pancreas cells. To better visualize hepatic and pancreatic Fhl1 expression, magnified images for Prox1 (red; top panel), Fhl1 (green; middle panel), and a merged view (bottom panel) are shown in insets in B’-B’’’ and C’-C’’’, respectively.

2.4.2 Loss-of-function and gain-of-function studies of *fhl1b*

2.4.2.1 Loss of *fhl1b* promotes pancreatic cells specification and compromises liver specification

To investigate the function of Fhl1b, especially during the process of endodermal progenitor fate decision, we disrupted the editing of *fhl1b* mRNA, hence reduce the levels of functional Fhl1b, with morpholino oligonucleotides (MOs). We tested two MOs, one (MO1) is against the splice acceptor site of the second exon, which includes the start codon; the other (MO2) is against the splice donor site of the third exon (Figure 2.6A). To validate the knockdown specificities and efficiency of *fhl1b* MOs, total RNA of MO-injected embryos was extracted, reverse transcribed, and PCR amplified with primers flanking the full-length coding sequence of *fhl1b* (Figure 2.8A). MO 1 and 2 successfully blocked the endogenous splice sites of *fhl1b.* A deletion of exon 2 (MO 1; Figure 2.8B, white asterisk) or a formation of a cryptic splice form of exon 3 (MO 2; Figure 2.8B, white asterisk) was detected. When a mixture of both MO 1 and 2 was injected, it led to the deletion of both exon 2 and 3 (MO 1 & 2; Figure 2.8B, white asterisk).

To check whether loss of *fhl1b* could result in the alteration of liver versus pancreas fate decision, shown as a phenotype of Bmp2b signaling suppression (Chung et al., 2010; Chung et al., 2008), we injected *Tg(ins:*GFP*)*^{zf5} embryos, in which all β-cells are labeled by GFP, with either single MO 1 or MO 2 as well as a mixture of MO 1 and 2. At 55 hpf, we examined the expression domain of GFP-positive cells in the pancreas and Prox1-positive cells in the liver using antibody staining, to score the change of sizes of these two organs. MO-injected embryos (morphants) showed reduced liver size and increased β-cell population (Figure 2.8C). To achieve high MO knockdown efficiency with low injection dose, throughout this study, *fhl1b* MOs were used as a mixture of MO

1 and 2 (2 ng of each) since each MO caused essentially the same phenotype (Figure 2.8C), and standard control MO was used as a negative control.

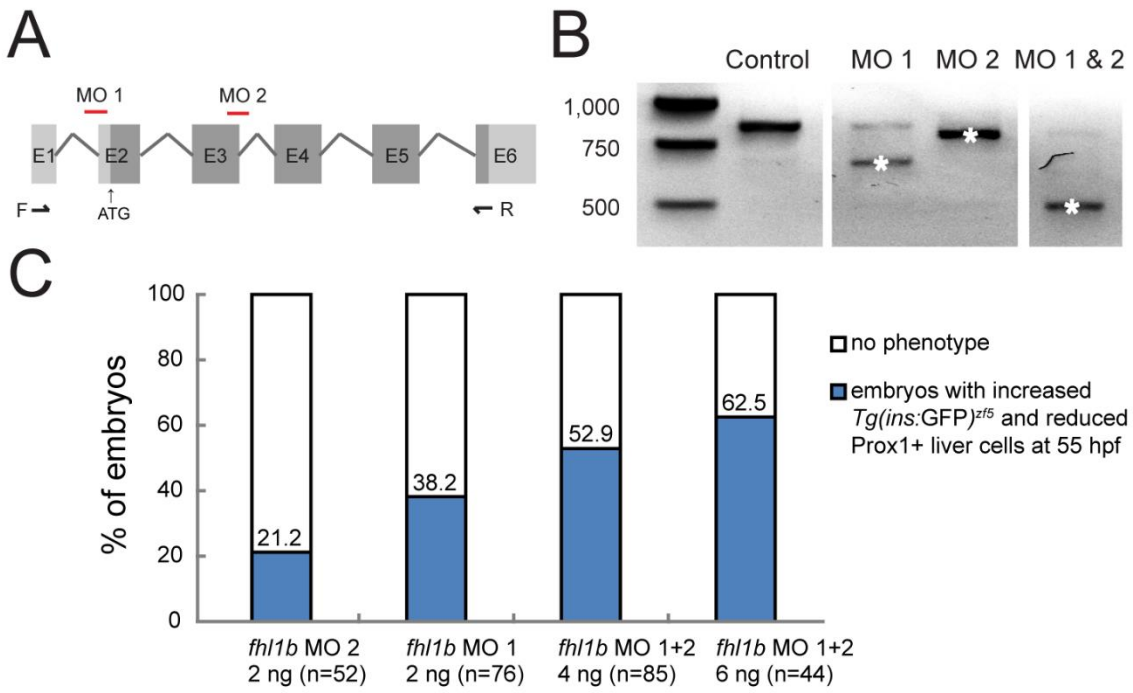

Figure 2.8 Specificity of *fhl1b* morpholinos.

(A) Schematic diagram of *fhl1b* genomic structure and targeting positions of *fhl1b* MOs (red lines). Black arrows indicate the position of primers (F and R) used for PCR amplification shown in (B). E1-E6: exon 1 to exon 6. Dark grey, coding regions; Light grey, untranslated regions. (B) RT-PCR analysis of *fhl1b* knockdown efficiency. Both MO 1 and MO 2 blocked the endogenous splice site of *fhl1b* and. As shown, a deletion of exon 2 (MO 1, white asterisk) or a formation of a cryptic splice form of exon 3 (MO 2, white asterisk) was detected, while a combination of MO 1 and 2 led to deletion of both exon 2 and 3 (MO 1 & 2, white asterisk). (C) The percentages of embryos are given for each single MO or combination of MOs based upon the expression domain of *Tg(ins:*GFP*)*^{zf5} in the pancreas and Prox1 in the liver at 55 hpf. The embryos were scored as having a "reduced" or "increased" expression domain when the expression area of each marker was distinctly (> 25%) smaller or larger than that of the control embryos based upon the calculation using ImageJ.

Next we performed more detailed phenotypic analysis on *fhl1b* morphants. At 30 hpf, morphants showed a decrease of the *hhex* (Ober et al., 2006) expression domain in the liver (Figure 2.9A-B, black arrows), whereas its expression appeared to be expanded in the early-forming dorsal pancreatic bud, which gives rise exclusively to the principal islet, a cluster of endocrine cells (Figure 2.9A-B, white dotted circles). The *pdx1* expression domain in morphants was also expanded in the dorsal pancreatic bud (Figure 2.9C-D, white dotted circles), whereas its expression in the intestinal bulb primordium appeared to be reduced (Figure 2.9C-D, black brackets).

Immunostaining with the antibodies recognizing Pdx1 and the early liver marker Prospero homeobox protein 1 (Prox1; (Field et al., 2003b)) in *Tg(sox17:GFP)*^{s870} embryos (Chung and Stainier, 2008) (Figure 2.10A-B') as well as Islet and Prox1 in *Tg(ins:GFP)*^{zf5} embryos ((Huang et al., 2001), Figure 2.10C-D'), respectively, showed an evident reduction of the Prox1 expression domain in the liver (Figure 2.10A-D'), an increase in the number of *Tg(ins:*GFP)^{zf5}-expressing and Islet-positive pancreatic endocrine cells (Figure 2.10C-D', white dotted circles), and an expansion of the Pdx1-expressing cell population in the dorsal pancreatic bud in morphants at 30-36 hpf (Figure 2.10A-B', white dotted circles). The Pdx1 expression domain in the intestinal primordium appeared to be decreased in morphants (Figure 2.10A-B', yellow brackets). At 55 hpf, morphants continuously exhibited an enlarged Insulin-expressing β-cell population (Figure 2.10E-G; 33.9±2.1 cells in controls vs. 57.8±3.6 cells in morphants; n=5 per condition; *P*=0.00003) with a reduced number of Prox1-positive cells in the liver (Figure 2.10E-G; 262.7±14.0 cells in controls vs. 148.0±15.2 cells in morphants; n=5 per condition; *P*=0.00003).

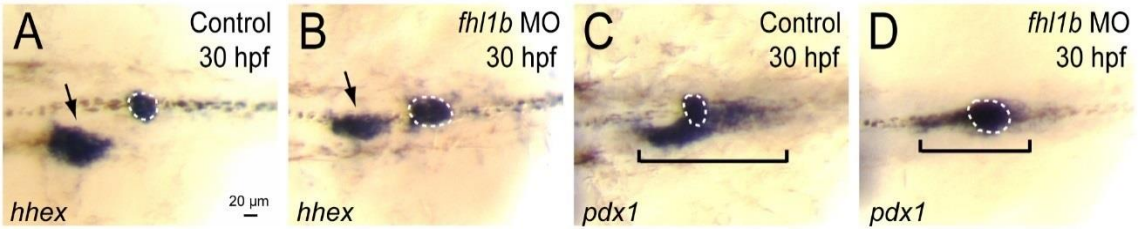

Figure 2.9 Loss of *fhl1b* activity expands expression of pancreatic gene domain and compromises expression of liver gene domain.

(A-D) Whole-mount *in situ* hybridization showing the expression of *hhex* (A and B) and *pdx1* (C and D), comparing control embryos (A and C) and *fhl1b* morphants (B and D) at 30 hpf. *hhex* is expressed in the liver (black arrows) and the dorsal pancreatic bud (white dotted circles). *pdx1* is expressed in the developing pancreas including the dorsal pancreatic bud (white dotted circles) and intestine (black brackets), but not in the liver. *hhex* expression was reduced in the liver of *fhl1b* morphants, while expanded in the dorsal pancreatic bud (B). *pdx1* expression in the dorsal pancreatic bud was also expanded, while its expression in the intestinal bulb primordium appeared to be reduced in *fhl1b* morphants (D) compared to that of control embryos (C). A-D, dorsal views, anterior to the left.

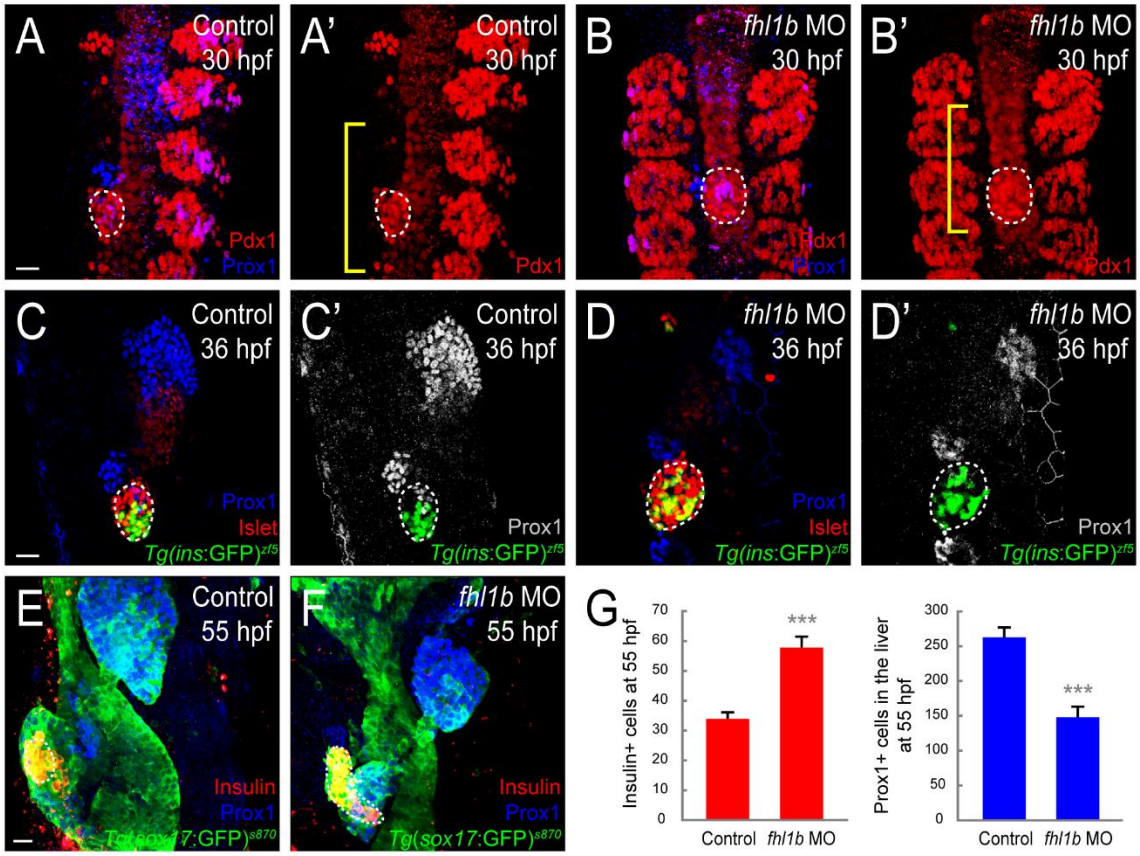

Figure 2.8 Loss of *fhl1b* activity enhances induction of pancreatic cells and compromises liver specification.

(A–B′) Confocal images of control embryos (A and A′) and *fhl1b* morphants (B and B′) at 30 hpf, stained for Pdx1 (red; expression in the dorsal pancreatic bud is outlined by white dotted circles) and Prox1 (blue). The somites are also Pdx1 positive. Compared to that of control embryos (A and A′), in *fhl1b* morphants (B and B′), the Pdx1 expression domain in the dorsal pancreatic bud was expanded, while the Prox1 expression domain was reduced. Note that the Pdx1 expression domain in the intestinal primordium (yellow brackets) appeared to be decreased in morphants (B'). (C-D') Confocal images of *Tg(ins:GFP)*^{zf5} control embryos (C and C′) and *fhl1b* morphants (D and D') at 36 hpf, stained for Islet (red; expression in the dorsal pancreatic bud is outlined by white dotted circles) and Prox1 (blue in C and D; grey in C' and D'). In *fhl1b* morphants (D and D'), the Prox1expression domain was greatly reduced, whereas the number of *Tg(ins:*GFP*)*^{zf5}- and Islet-expressing cells was increased. (E and F) Confocal images of *Tg(sox17:GFP)*^{s870} control embryos (E) and *fhl1b* morphants (F) at 55 hpf, stained for Insulin (red; outlined by white dotted circles) and Prox1 (blue). *fhl1b* morphants (F) continuously exhibited an enlarged Insulin-expressing β-cell population with a reduced number of Prox1-positive cells in the liver. (G) Quantification of the number (mean±SD) of Insulin-positive cells in the pancreas (red) and Prox1-positive cells in the liver (blue) at 55 hpf. Cells in 20 planes of confocal images from 5 individual larvae were counted. Asterisks indicate statistical significance: ***, $P < 0.001$. A-F, confocal projection images, ventral views, anterior to the top. Scale bars, 20 µm.

MO-mediated knockdown can often induce apoptosis mediated via aberrant p53 activation. Hence, we performed simultaneous knockdown of *tp53* and *fhl1b* to ameliorate apoptosis induced by MO off-targeting (Robu et al., 2007). We did not detect any differences in the phenotype of a small liver between single *fhl1b* (Figure 2.11B; white dotted circles) and double *fhl1b*/*tp53* MO-injected larvae (Figure 2.11C; white dotted circles) at 55 hpf. Consistently, no obvious difference in the phenotype of the increased Insulin-expressing β-cell population as well as pericardial edema between single *fhl1b* (Figure 2.11E; white squares and insets) and double *fhl1b*/*tp53* MO-injected larvae (Figure 2.11F; white squares and insets) at 5 dpf was detected.

Similarly, the reduced Prox1-expressing cell population in single *fhl1b* morphants (Figure 2.12B) was persistent to that in embryos co-injected with *fhl1b* and *tp53* MOs (Figure 2.12C). These data indicate that *fhl1b* knockdown phenotypes in the endoderm and heart are independent of the p53 pathway.

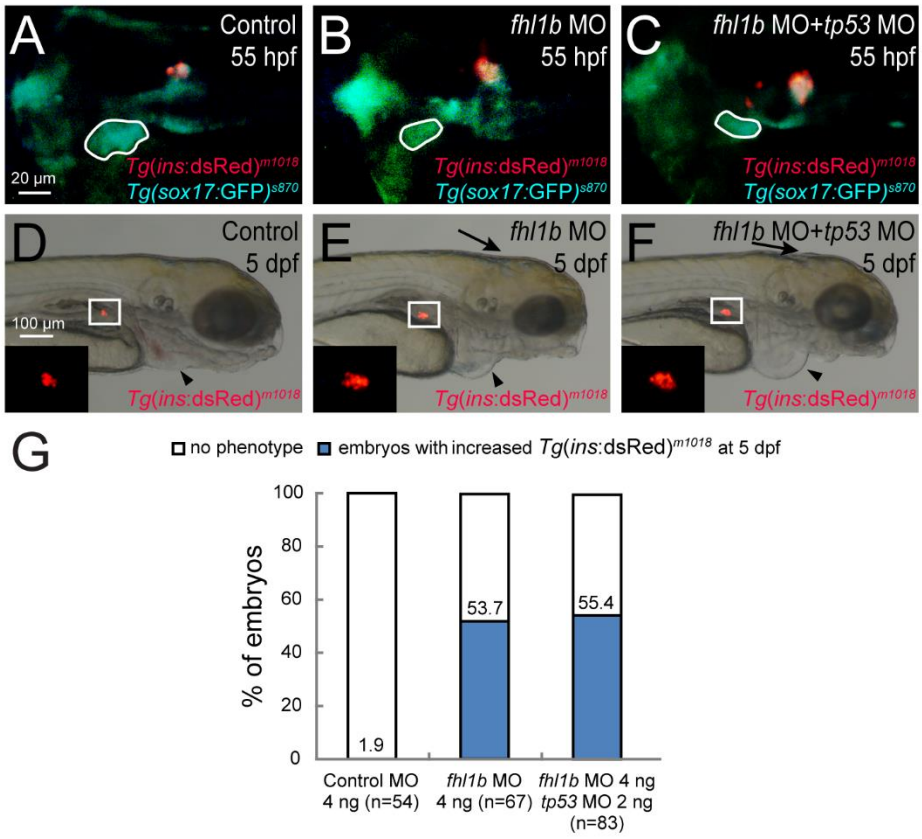

Figure 2.9 Loss of Fhl1b activity phenotypes are not caused by p53 induced apoptosis.

(A-C) Fluorescent images of *Tg(ins:*dsRed)^{m1018} and *Tg(sox17:*GFP)^{s870} expression showing that the developmental defects of the liver (white dotted circles) and β-cell formation in single *fhl1b* morphants (B) was comparable to double *fhl1b*/*tp53* morphants (C) at 55 hpf (n = 52, control; n = 64, single *fhl1b* morphants; n = 72, double *fhl1b*/*tp53* morphants). (D-F) Bright-field images combined with fluorescent images showing the overall morphology of embryos and *Tg(ins:*dsRed)^{m1018} expression (red) in control (D), single *fhl1b* morphants (E), and double *fhl1b*/*tp53* morphants (F) at 5 dpf. The enlarged *Tg(ins:*dsRed)^{m1018}-expressing cell population (white squares and insets) in single *fhl1b* morphants (E) was similar to that in embryos co-injected with *fhl1b* and *tp53* MOs (F). Note that potential off-target ventricle lumen inflation defects in the brain of single *fhl1b* morphants were attenuated by co-knockdown of *tp53* (black arrows), whereas pericardial edema persisted both in single *fhl1b* morphants and double *fhl1b*/*tp53* morphants (black arrowheads). (G) Quantification of the results in D-F. The embryos were scored as having an "increased" expression domain when the expression area of *Tg(ins:* dsRed)^{m1018} was distinctly (> 25%) larger than that of the control embryos based upon the calculation using ImageJ. A-C, dorsal views, anterior to the left. D-F, lateral views, anterior to the right. I-K, confocal projection images, ventral views, anterior to the top. Scale bars: A-C and I-K, 20 μm; D-F, 100 μm.

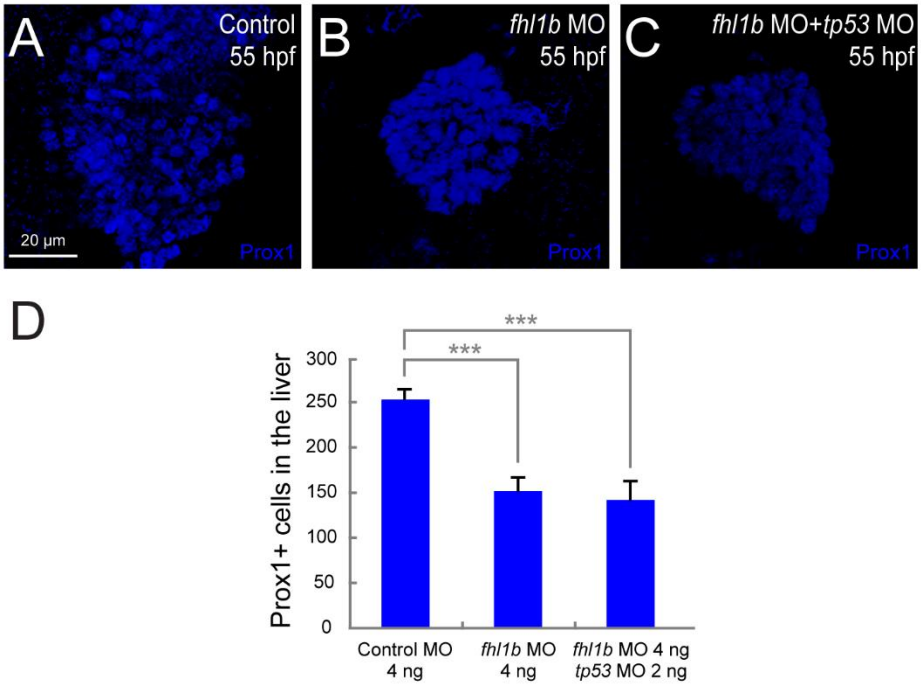

Figure 2.10 The reduced liver cell number in *fhl1b* depletion is not caused by p53 induced apoptosis.

(A-C) Confocal images of control embryos (A), single *fhl1b* morphants (B), and double *fhl1b*/*tp53* morphants (C) at 55 hpf, stained for Prox1 (blue). The reduced Prox1-expressing cell population in single *fhl1b* morphants (B) was similar to that in embryos co-injected with *fhl1b* and *tp53* MOs (C). (D) Quantification of the number (mean±SD) of Prox1-positive cells in the liver at 55 hpf. 252.6±11.5 cells were Prox1-positive in control embryos, while 151.3±16.2 and 142.3±17.4 cells expressed Prox1 in single *fhl1b* morphants and double *fhl1b*/*tp53* morphants, respectively (P = 0.0009 and P = 0007, respectively). Cells in 20 planes of confocal images from 5 individual embryos were counted. Asterisks indicate statistical significance: ***, P < 0.001. A-C, confocal projection images, ventral views, anterior to the top. Scale bars: A-C, 20 μm.

In addition, no TUNEL-positive liver cells were observed in *fhl1b* morphants at 48 hpf, suggesting that the small liver observed in morphants was not caused by enhanced cell death (Figure 2.13A-B).

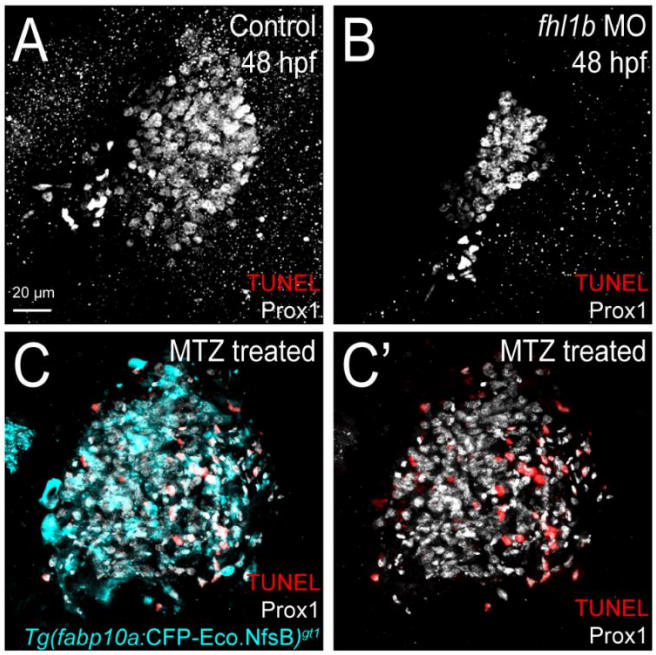

Figure 2.11 Cell death does not contribute to the reduction of liver size upon *fhl1b* depletion.

(A-B) TUNEL labeling (red) combined with anti-Prox1 immunostaining (grey) revealed that no TUNEL-positive liver cells were observed both in *fhl1b* morphants and control embryos at 48 hpf. (C-C') As a control, *Tg(fabp10a:CFP-NTR)*^{gt1} embryos were used. Treating metronidazole (MTZ) caused apoptosis in a large number of hepatocytes. A-C', confocal projection images, ventral views, anterior to the top. Scale bar, 20 μm.

To furthermore confirm that *fhl1b* MO specifically targets the endogenous *fhl1b* mRNA editing, we co-injected *in vitro* transcribed *fhl1b-P2A-mcherry* mRNA with *fhl1b* MO. Co-injection of *fhl1b* mRNA with a mixture of MO 1 and 2 successfully rescued the effect of *fhl1b* MO knockdown (Figure 2.14A-C'').

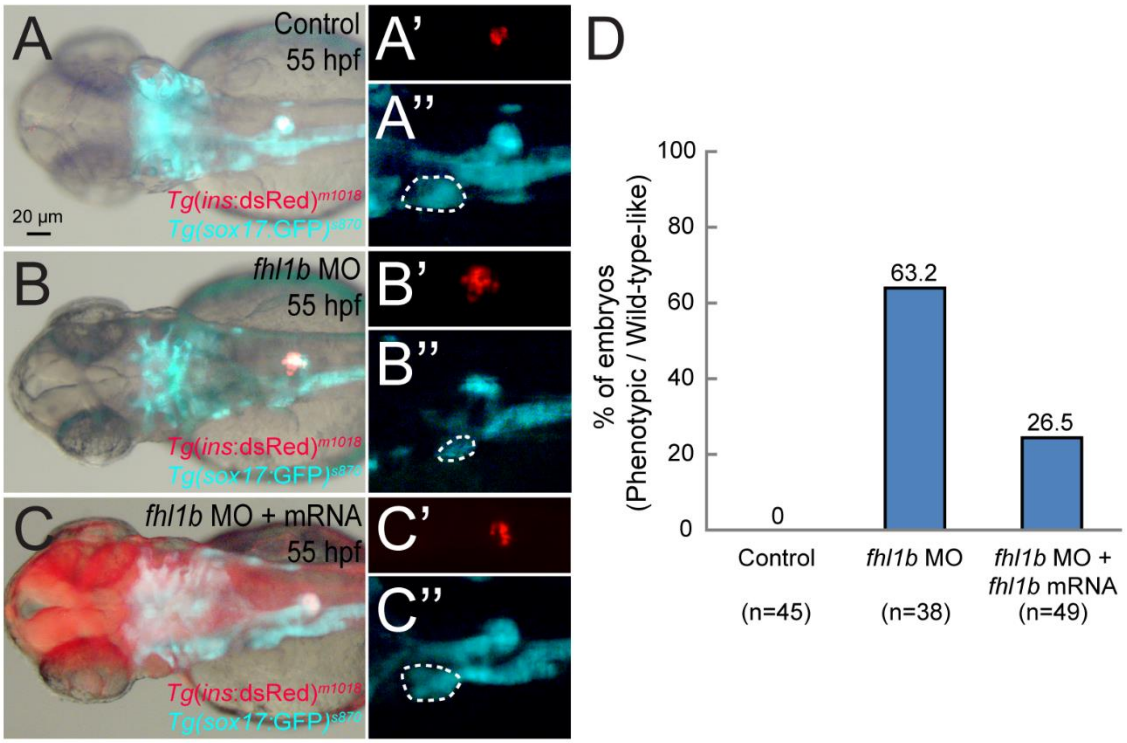

Figure 2.12 *fhl1b* mRNA injection rescues the effect of *fhl1b* MO knockdown.

(A-C'') The developmental defects of the liver (A-C and white dotted circles in A"-C") and β-cell formation (A-C and A'-C') in *fhl1b* morphants (B-B'') could be rescued by injection of *fhl1b-P2A-mcherry* mRNA (C-C''), restoring liver size and the β-cell population to a degree comparable to that of control embryos (A-A'') at 55 hpf. Fhl1b translation was monitored by mCherry expression as shown in C. (D) Quantification of the results in A-C''. The embryos were scored as having a "reduced" or "increased" expression domain when the expression area of *Tg(ins:*dsRed*)*^{m1018} and *Tg(sox17:*GFP*)*^{s870} was distinctly (> 25%) smaller or larger than that of the control embryos based upon the calculation using ImageJ. A-C, bright-field images combined with fluorescent images. A'-C'', fluorescent images. Dorsal views, anterior to the left. Scale bar, 20 μm.

To complement *fhl1b* MO knockdown studies, knockout of *fhl1b* was performed by applying the CRISPR/Cas9 nuclease targeting system (Hwang et al., 2013), which has been shown to lead to highly efficient biallelic conversion in somatic cells in zebrafish (Jao et al., 2013). We microinjected *cas9* mRNA and two guide RNAs (gRNAs), which were both designed to target overlapping regions in the exon 2 of *fhl1b* (Figure 2.15A), into one-cell stage embryos. We found that 11.62% of Cas9/gRNA-treated embryos (38 out of 327 embryos) showed an enlarged Insulin-expressing β-cell population (31.6±3.51 cells in controls vs. 45.3±6.0 cells in Cas9/gRNA-treated embryos; n=5 per condition; P=0.02) with a reduced number of Prox1-positive cells in the liver (265±18.6 cells in controls vs. 164±16.5 cells in Cas9/gRNA-treated embryos; n=5 per condition; P=0.002) as in *fhl1b* MO knockdown embryos at 55 hpf (Figure 2.15D-F). We randomly selected 4 embryos with these phenotypes and confirmed to contain insertions/deletions (indels) with the T7 endonuclease I (T7EI) assay and Sanger sequencing. T7EI assay revealed that the percent gene modification in the 4 tested embryos was between 21.75% and 31.58% (Figure 2.15B). Sanger sequencing of these 4 embryos (20-30 PCR amplicons were sequenced for each embryo) confirmed site-specific insertions/deletions (indels) including 2-17 bp deletions or 2-11 bp insertions (Figure 2.15C). Consistent with the report that Cas9 cuts the target DNA at six base pairs upstream of the protospacer adjacent motif (PAM) (Jinek et al., 2012), all mutations occurred at the 3′ end of the target sequence, further validating the sequence specificity of this targeting process. Taken together, these comparable MO knockdown and CRISPR/Cas9 knockout results suggest that Fhl1b is required for restraining endodermal progenitors from specifying to pancreatic endocrine cells and for the proper induction of the liver.

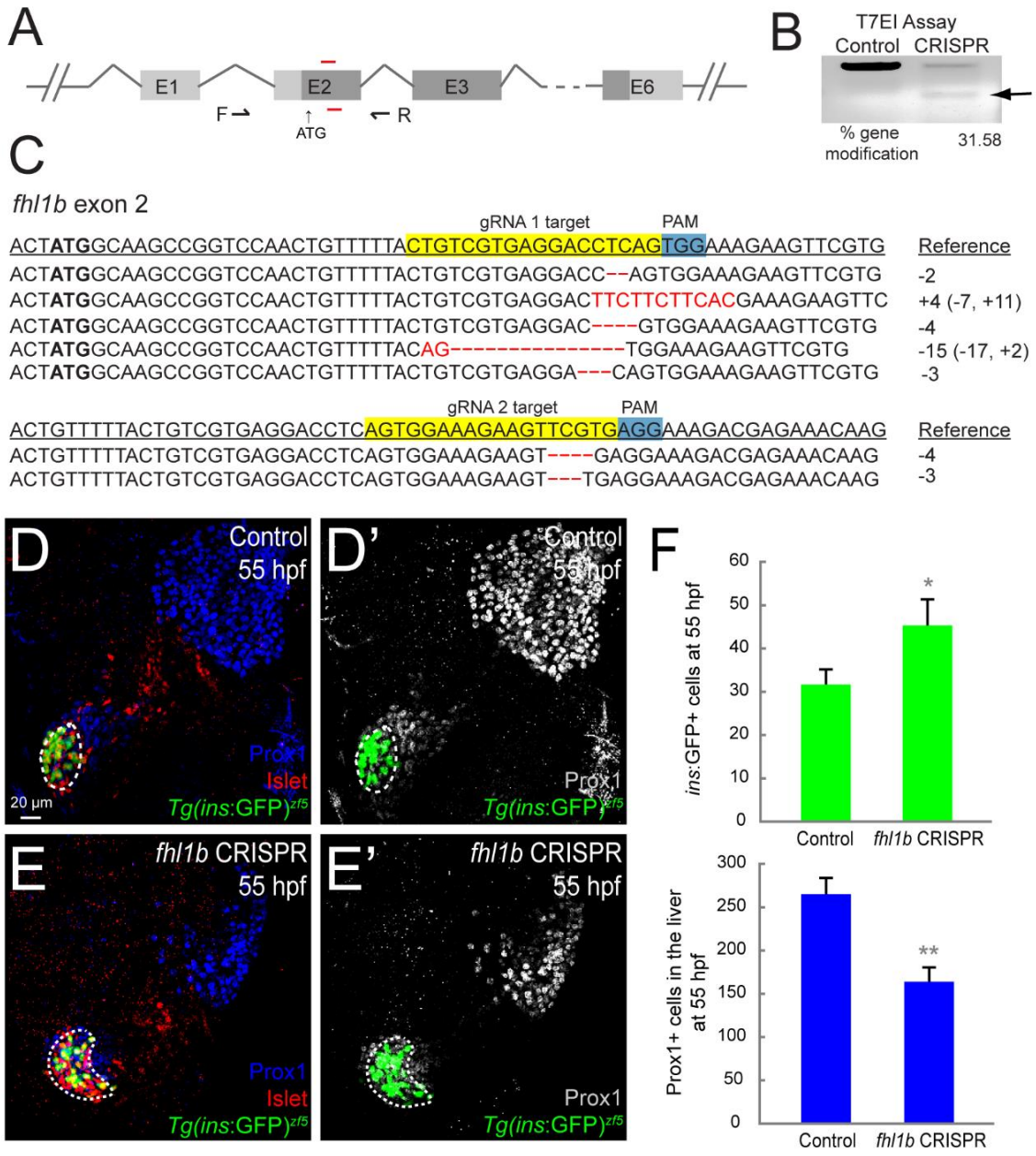

Figure 2.13 Cas9/gRNAs induces indels in the *fhl1b* locus in zebrafish.

(A) Illustration showing the position of each gRNA-targeting site in the *fhl1b* locus in zebrafish. Black arrows indicate the position of primers (F and R) used for sequencing to identify indels shown in (C). (B) Representative T7 assay showing the efficiency of Cas9-mediated cleavage in a single embryo at 55 hpf. (C) Representative Sanger sequencing results of the PCR amplicons of 4 individual embryos at 55 hpf, showing indels induced by Cas9/gRNA in the targeted *fhl1b* locus. Twenty to thirty clones were sequenced for each embryo. The wild-type sequence is shown at the top with the target sites highlighted in yellow and the PAM sequences (TGG and AGG) highlighted in blue.

Deletions are shown as red dashed lines and insertions are highlighted in red. The net change in length caused by each indel is to the right of each sequence (+, insertion; -, deletion). (D-E') Confocal images of *Tg(ins:GFP)^{zf5}* control embryos (D and D') and Cas9/gRNA-induced mutant embryos (E and E') at 55 hpf, stained for Prox1 (blue in D and E; grey in D' and E') and Islet (red; expression in the dorsal pancreatic bud is outlined by white dotted circles). Cas9/gRNA-induced mutant embryos exhibited an enlarged Insulin-expressing β-cell population with a reduced number of Prox1-positive cells in the liver, phenocopying that of the *fhl1b* MO knockdown embryos. (F) Quantification of the number (mean±SD) of Insulin-positive cells in the pancreas (green) and Prox1-positive cells in the liver (blue) at 55 hpf. 31.6±3.5 cells were Insulin-positive in control embryos, whereas 45.3±6.0 cells expressed Insulin in Cas9/gRNA-induced mutant embryos. 164±16.5 cells expressed Prox1 in Cas9/gRNA-induced mutant embryos, while 265±18.6 cells were Prox1-positive in control embryos. Cells in 20 planes of confocal images from 5 individual larvae were counted. Asterisks indicate statistical significance: *, $P < 0.05$, **, $P < 0.01$. D-E', confocal projection images, ventral views, anterior to the top. Scale bar, 20 μm.

.

2.4.2.2 Decreased *fhl1b* activity augments induction of pancreatic endocrine cells

The To further analyze which pancreatic cell types are induced in *fhl1b* morphants, we first examined the expression of *Tg(P0-pax6b:*GFP*)*^{ulg515}, a pan-endocrine progenitor reporter (Delporte et al., 2008). The number of *Tg(P0-pax6b:*GFP*)*^{ulg515}-expressing cells increased from 82.6±4.5 in controls to 103.2±2.0 in morphants at 30 hpf (Figure 2.16A-B, and 2.16I; n=5 per condition; *P*=0.0009). Next, we investigated which endocrine subpopulation was expanded in the morphants. The number of Insulin-expressing β-cells (Huang et al., 2001) was increased from 30.6±1.5 in controls to 44.6±2.0 in morphants at 30 hpf (Figure 2.16C-D, and 2.16I; n=5 per condition; *P*=0.0004). While the number of Somatostatin-expressing δ-cells was also increased in morphants (Figure 2.16E-F, and 2.16I; 20.7±0.8 cells in controls vs. 26.7±2.0 cells in morphants; n=5 per condition; *P*=0.0033), the number of Glucagon-expressing α-cells was slightly decreased in morphants (Figure 2.16G-H, and 2.16I; 26.5±0.7 cells in controls vs. 23.0±1.0 cells in morphants; n=5 per condition; *P*=0.02). As recently reported (Ye et al., 2015), Insulin and Glucagon, but not Insulin and Somatostatin, are co-expressed in both control embryos and *fhl1b* morphants at 30 hpf. The number of these dual-hormone expressing cells was decreased in *fhl1b* morphants at 30 hpf (10.0±1.4 cells in control vs. 6.3±0.5 cells in morphants; n=5 per condition; *P*=0.02).

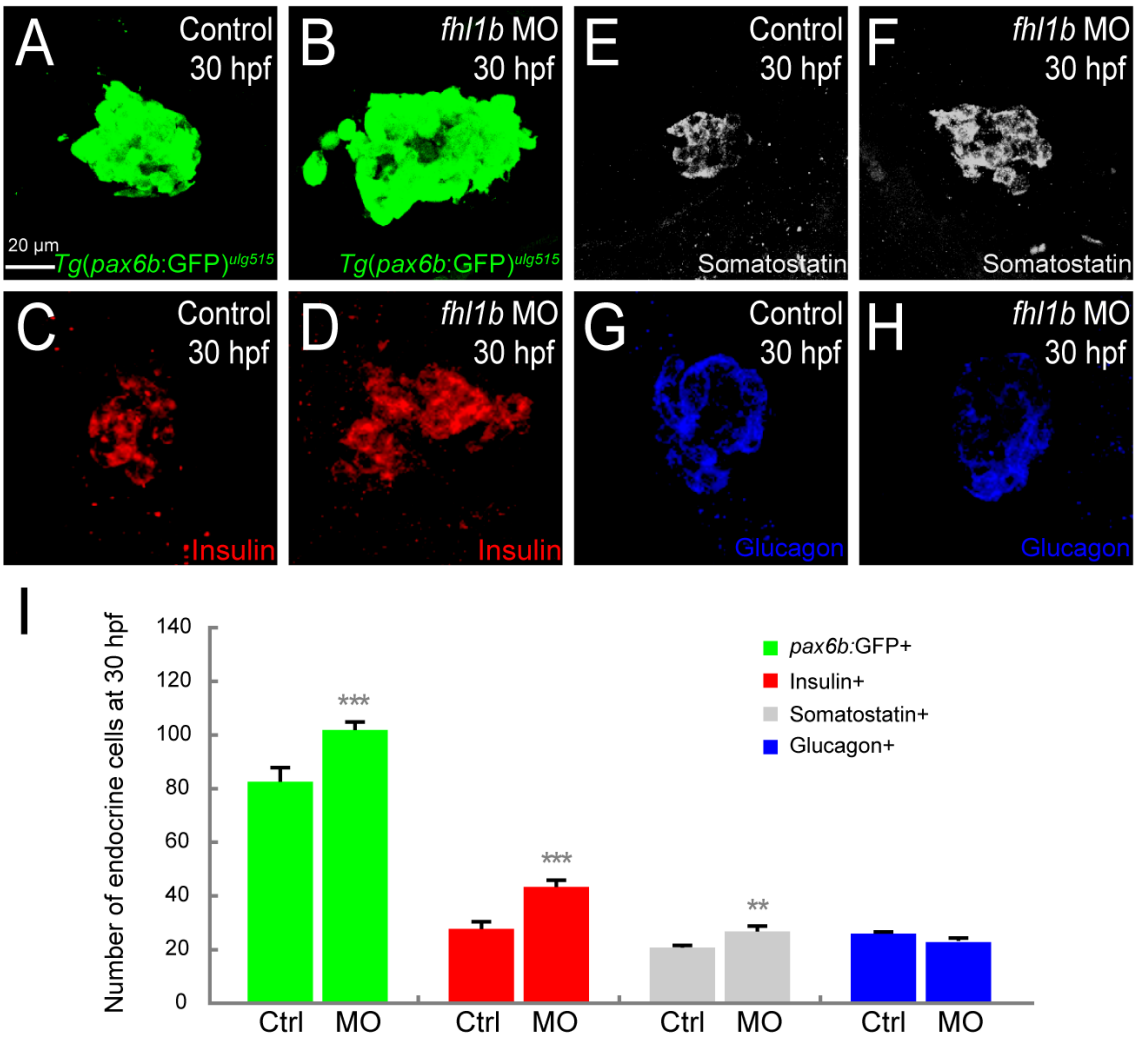

Figure 2.14 Decreased *fhl1b* activity augments induction of pancreatic endocrine cells.

(A-H) Confocal images showing *Tg(P0-pax6b:*GFP*)*^{ulg515} (A and B, green), Insulin (C and D, red), Somatostatin (E and F, grey), and Glucagon (G and H, blue) expression at 30 hpf, comparing control embryos (A, C, E, and G) and *fhl1b* morphants (B, D, F, and H). The number of *Tg(P0-pax6b:*GFP*)* (B)- and Insulin (D)-expressing cells was significantly increased in *fhl1b* morphants compared to that of control embryos (A and C, respectively). The number of Somatostatin-expressing cells was also increased (F), while that of Glucagon-expressing cells appeared slightly decreased in *fhl1b* morphants (H) compared to that of control embryos (E and G, respectively). (I) Quantification of the number (mean±SD) of total and individual pancreatic endocrine hormone-expressing cells, comparing that of control embryos and *fhl1b* morphants at 30 hpf. Cells in 20 planes of confocal images from 5 individual larvae were counted. Asterisks indicate statistical significance: **, $P < 0.01$; ***, $P < 0.001$.

A previous report showed that cell-autonomous suppression of Bmp signaling is critical for the induction of endocrine cells derived not only from the early-forming dorsal bud but also from the late-forming ventral bud (Chung et al., 2010). In zebrafish, the late-forming ventral pancreas, which mostly generates pancreatic exocrine cells (acinar and duct cells) as well as endocrine cells, subsequently encapsulates the early-forming dorsal pancreas, which gives rise exclusively to the endocrine cells and is also *pdx1*-positive, to establish the mature pancreatic structure (Field et al., 2003a). To test the role of Fhl1b in the induction of endocrine cells from the ventral bud specifically, we examined the numbers of the newly differentiated ventral bud-derived endocrine cells in *Tg(ins:GFP)*^{zf5}*;Tg(ins:dsRed)*^{m1018} double transgenic embryos. As dsRed takes 18-22 hours longer than GFP to mature, we can distinguish GFP only (ventral bud-derived) from GFP/dsRed double-positive (dorsal bud-derived) β-cells until at least 60 hpf (Hesselson et al., 2009). At 48 hpf, the number of GFP-only-positive β-cells increased in morphants compared to that of control embryos (Figure 2.17A-C; 5.0±0.7 cells in controls vs. 12.2±2.3 cells in morphants; n=5 per condition; P=0.0002), suggesting an augmented induction of β-cells from the ventral bud.

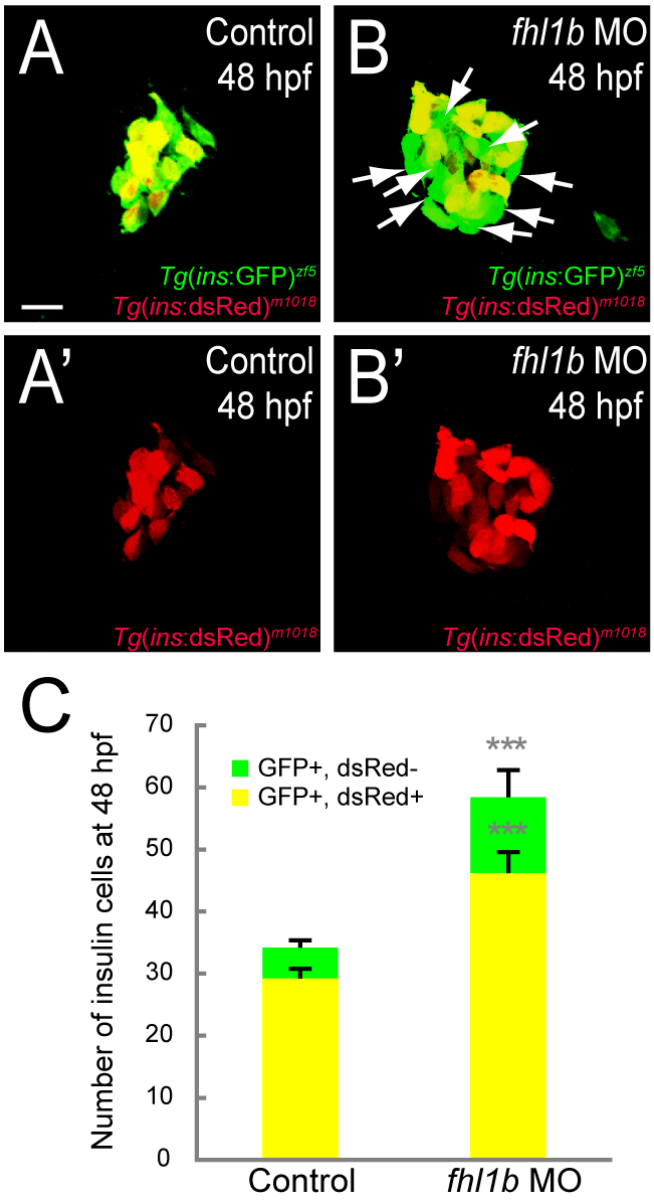

Figure 2.15 Decreased *fhl1b* activity augments induction of both dorsal and ventral insulin cells.

(A-B') Confocal images of *Tg(ins:GFP)^{zf5};Tg(ins:dsRed)^{m1018}* control embryos (A and A') and *fhl1b* morphants (B and B') at 48 hpf. Compared with the control embryos (A), *fhl1b* morphants showed an increased number of GFP-only-positive β-cells (B, white arrows). (C) Quantification of the number (mean±SD) of GFP- and dsRed-double positive (yellow) and GFP-only-positive (green) β-cells, comparing that of control embryos and *fhl1b* morphants at 48 hpf. 5.0±0.7 β-cells were GFP-only-positive in control embryos, while 12.2±2.3 β-cells were GFP-only-positive in *fhl1b* morphants. Cells in 20 planes of confocal images from 5 individual larvae were counted. Asterisks indicate statistical significance: ***, $P < 0.001$. Scale bars, 20 μm.

We further quantified total and subpopulations of pancreatic endocrine cells at 72 hpf. The number of *Tg(P0-pax6b:*GFP*)*^{ulg515}-, Insulin-, and Somatostatin-expressing cells was increased from 98.6±3.0, 32.3±2.0, and 28.7±1.4, respectively, in control embryos, to 132.0±5.2, 54.8±3.5, and 40.0±2.1, respectively, in morphants (Figure 2.18A-G; n=5 per condition; *P*=0.0003, *P*=0.0003, *P*=0.006, respectively), while the number of Glucagon-expressing cells was slightly decreased (Figure 2.18C, and 2.18F; 30.0±2.0 cells in controls vs. 25.3±2.0 cells in morphants; n=5 per condition; *P*=0.04). Altogether, these data suggest that Fhl1b is required for restricting the induction of pancreatic endocrine cells, specifically Insulin- and Somatostain-expressing cells, from endodermal progenitors.

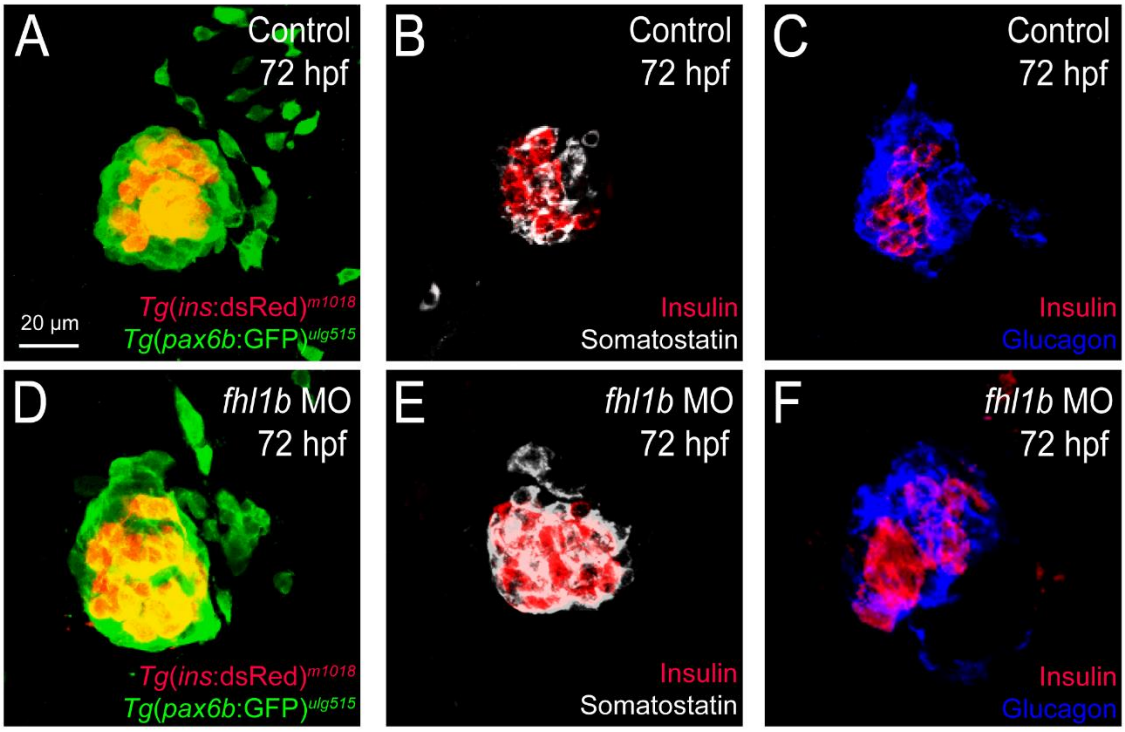

Figure 2.16 Decreased *fhl1b* activity increases the number of pancreatic endocrine cells.

(A-F) Confocal images showing *Tg(ins:*dsRed*)*^{m1018} (A and D) or Insulin (B-C, E-F, red) expression with *Tg(P0-pax6b:*GFP*)*^{ulg515} (A and D, green), Somatostatin (B and E, grey), or Glucagon (C and F, blue) expression at 72 hpf, comparing control embryos (A-C) and *fhl1b* morphants (D-F). The number of *Tg(ins:*dsRed*)*^{m1018}- or Insulin-expressing cells was significantly increased in *fhl1b* morphants (D-F) compared to that of control embryos (A-C). The number of *Tg(P0-pax6b:*GFP*)*- and Somatostatin-expressing cells was also increased (D and E, respectively), whereas that of *Tg(gcga:*GFP*)*^{ia1}-expressing cells appeared slightly decreased (F) in *fhl1b* morphants compared to control embryos (A, B, and C, respectively). A-F, confocal projection images, ventral views, anterior to the top. Cells in 20 planes of confocal images from 5 individual larvae were counted. Scale bar, 20 µm.

2.4.2.3 Increased *fhl1b* activity suppresses specification of pancreatic cells and induces liver

In a converse experiment, we assessed the effects of ectopic expression of *fhl1b* on liver and pancreas induction. We overexpressed *fhl1b* using a heat-inducible transgene, *Tg(hsp:fhl1b; hsp:GFP)*^{gt3}. In response to heat shock, robust ectopic expression of GFP was observed in a variety of tissues throughout the embryos without any discernible body phenotype. Concurrent expression of *fhl1b* all over the embryos was confirmed with whole-mount *in situ* hybridization. When *fhl1b* expression was induced at the 8-somite stage, the initial time point of *pdx1* expression in the pancreatic exocrine and intestinal progenitors and before the beginning of endogenous *fhl1b* expression, *hhex* expression domain was greatly expanded in the liver at 45 hpf (Figure 2.19A-B, black arrows). In these embryos, *pdx1* expression was significantly reduced in the intestinal bulb primordium and ventral pancreas, which gives rise mainly to the pancreatic exocrine cells, intestine cells, and a few endocrine cells (Fig 2.19C-D, black brackets). *pdx1* expression in the dorsal pancreatic bud appeared unaffected (Figure 2.19C-D, white dotted circles), consistent with the previous data that the lineage of this bud is specified primarily during the gastrulation stage (Chung et al., 2008).

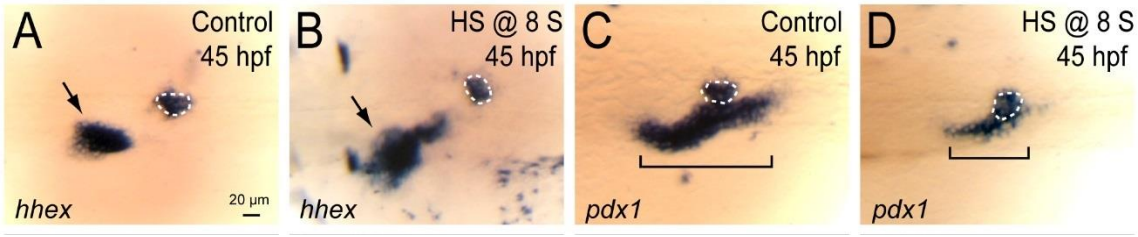

Figure 2.17 Ectopic Fhl1b induces the expression of liver gene domain and suppresses the expression of *pdx1* domain.

(A-D) Whole-mount *in situ* hybridization showing the expression of *hhex* (A and B) and *pdx1* (C and D), comparing control embryos (A and C) and *fhl1b*-overexpressing embryos (B and D, heat shock applied at the 8-somite stage). *hhex* is expressed in the liver (black arrows) and the dorsal pancreatic bud (white dotted circles). *pdx1* is expressed in the developing pancreas including the dorsal pancreatic bud (white dotted circles) and intestine (black brackets), but not in the liver. When *fhl1b* expression was induced at the 8-somite stage, *hhex* expression was greatly expanded in the liver (B, black arrow), while *pdx1* expression in the developing gut was reduced (D, black bracket). *hhex* and *pdx1* expression in the dorsal pancreatic bud in *fhl1b*-overexpressing embryos was comparable to that of control embryos. A-D, dorsal views, anterior to the left. Scale bars, 20 µm.

To determine whether specification of pancreatic exocrine cells is affected in *fhl1b*-overexpressing embryos, we examined the expression of *Tg(ptf1a*:GFP)^{jh1} (Godinho et al., 2005), which is largely restricted to the developing exocrine pancreas (Wang et al., 2015c), along with Prox1, which is highly expressed in the liver and developing exocrine pancreas at 50 hpf. Compared to control embryos, we found that in the embryos where *fhl1b* expression was induced at the 8-somite stage, *Tg(ptf1a*:GFP)^{jh1}expression was almost completely eliminated whereas the Prox1 expression domain was markedly expanded, suggesting that virtually all Prox1-expressing cells are liver cells (Figure 2.20A-B'). Quantification showed that while 235.5±7.3 cells were Prox1-positive in control embryos, 306.5±12.6 cells expressed Prox1 in *fhl1b*-overexpressing embryos (Figure 2.20C; n=5 per condition; *P*=0.000067). In contrast, the number of *Tg(ptf1a:*GFP)^{jh1}-expressing cells was decreased from 82.2±6.4 in controls to 16.0±5.2 in *fhl1b*-overexpressing embryos (Figure 2.20D; n=5 per condition; *P*=0.000004). These results suggest that Fhl1b is sufficient to inhibit specification of pancreatic exocrine cells and induce the liver.

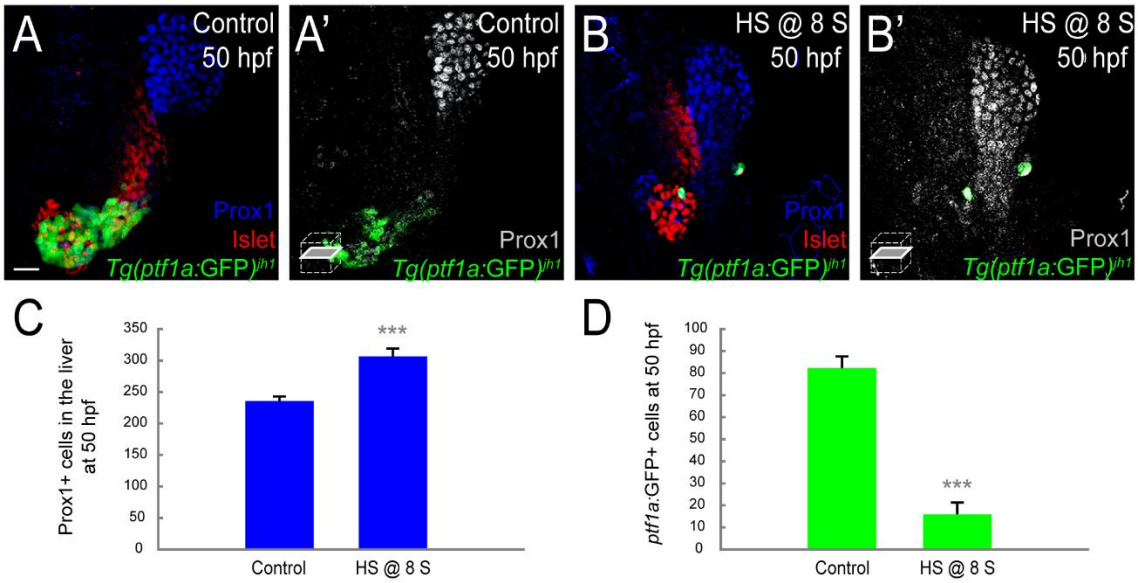

Figure 2.18 Ectopic Fhl1b suppresses specification of pancreatic cells and induces liver.

(A-B') Confocal images showing Islet (red), Prox1 (blue in A and B; grey in A' and B'), and *Tg(ptf1a:*GFP*)*^{jh1} (green) expression at 50 hpf, comparing control embryos (A and A') and *fhl1b*-overexpressing embryos (B and B', heat shock applied at the 8-somite stage). When *fhl1b* expression was induced at the 8-somite stage (B and B'), the Prox1 expression domain was expanded, whereas *Tg(ptf1a:*GFP*)*^{jh1} expression was drastically reduced. (C) Quantification of the number (mean±SD) of Prox1-positive cells in the liver at 50 hpf. 235.5±7.3 cells were Prox1-positive in control embryos, while 306.5±12.6 cells were Prox1-positive in fhl1b-overexpressing embryos (heat shock applied at the 8-somite stage). (D) Quantification of the number (mean±SD) of *Tg(ptf1a:*GFP*)*^{jh1}-expressing cells in the exocrine pancreas at 50 hpf. The number of these cells decreased from 82.2±6.4 in control embryos to 16.0±5.2 in *fhl1b*-overexpressing embryos (heat shock applied at the 8-somite stage). Cells in 20 planes of confocal images from 5 individual larvae were counted. Asterisks indicate statistical significance: ***, $P < 0.001$. A and B, confocal projection images; A' and B', confocal single-plane images, ventral views, anterior to the top. Scale bars, 20 µm.

2.4.3 Fhl1b as a major effector of Bmp signaling determines the fate of the endodermal progenitors into liver versus pancreas

2.4.3.1 Fhl1b regulates the patterning and subsequent fate of the medial and lateral endodermal progenitors

To determine the role of Fhl1b in the M-L patterning of endodermal progenitors, which is essential for the fate decision of liver versus pancreas (Chung et al., 2008), we first examined the *pdx1* gradient in the endodermal sheet of *fhl1b*-depleted embryos. From the 14-somite stage onwards, morphants showed a dramatic lateral expansion of the *pdx1* expression domain (Figure 2.21A-B). The expression domain of *neurod*, which marks pancreatic endocrine progenitor cells that express high levels of *pdx1* (corresponding to the cells with white asterisks in Figure 2.21A-B; (Chung et al., 2008; Soyer et al., 2010)), was markedly expanded (Figure 2.21C-D). Furthermore, multiple *TgBAC(neurod:*EGFP*)*^{nl1}-expressing cells were found even in the lateral part of the endodermal sheet, which normally gives rise to the liver, exocrine pancreas, and intestine (Figure 2.21E-F) (Chung et al., 2008).

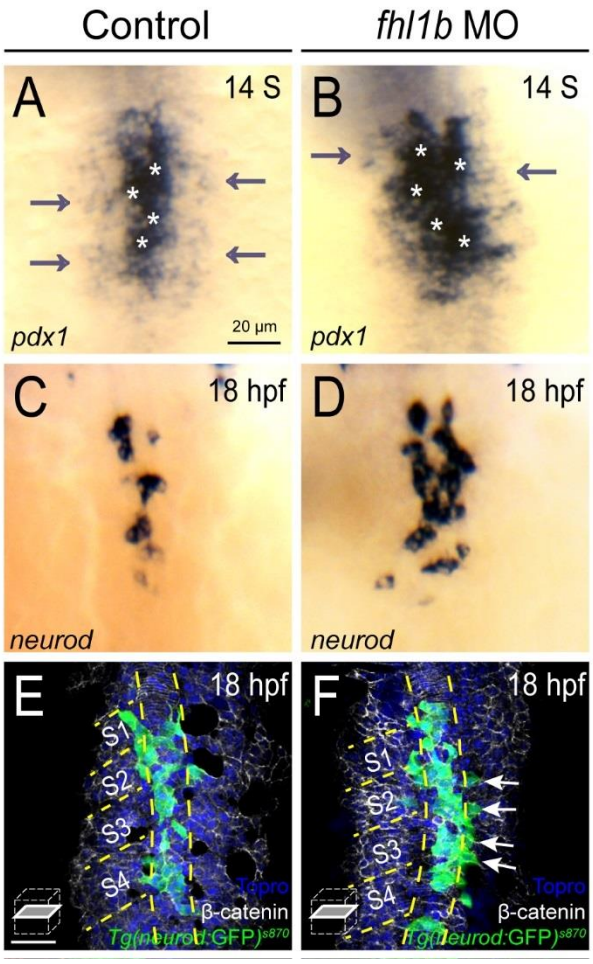

Figure 2.19 Fhl1b regulates the patterning of the medial and lateral endodermal progenitors.

(A-D) Whole-mount *in situ* hybridization showing the expression of *pdx1* (A and B) and *neurod* (C and D), comparing that of control embryos (A and C) and *fhl1b* morphants (B and D) at the 14-somite stage (A and B) and 18 hpf (C and D). *pdx1* is expressed at high levels in the most medial cells (white asterisks) and at low levels in the lateral cells (white arrows). *neurod* is expressed in the high-level *pdx1*-expressing cells. In *fhl1b* morphants, high levels of *pdx1* (white asterisks) and *neurod* expression were expanded laterally (B and D). (E-F) Ventral confocal images showing *TgBAC(neurod:*EGFP*)*^{nl1}, β-catenin (white), and Topro (blue) at 18 hpf (the notochord is outlined by yellow dashed lines). Somites are numbered from anterior to posterior (S1-S4). (E) In control embryos, *TgBAC(neurod:*EGFP*)*^{nl1}-expressing cells are located close to the notochord. (F) Ectopic *TgBAC(neurod:*EGFP*)*^{nl1}-expressing cells were found in lateral endodermal regions in *fhl1b* morphants (white arrows).

Next, we performed single-cell lineage tracing experiments to examine possible cell fate changes caused by modulation of *fhl1b* activity. *Tg(sox17:GFP)*^{s870} embryos were injected at the one-cell stage with the photoactivatable lineage tracer CMNB-caged fluorescein dextran conjugate, and single endodermal cells at 3 different M-L positions (medial, lateral 1, and lateral 2) at the level of somite 2 were uncaged using a 405nm laser at the 6–8 somite stage. In Consistent with earlier data (Chung et al., 2008), in control embryos, lateral 2 cells at the level of somite 2 predominantly gave rise to the exocrine pancreas, intestine, and liver, but rarely to the endocrine pancreas (Figure 2.22A and 2.26C-E, 2.26F (as L2), 2.26H; in 1 out of 10 control embryos lateral 2 cells gave rise to the endocrine pancreas). In every *fhl1b*-depleted embryo, lateral 2 cells contributed to the pancreatic endocrine cells (Figure 2.22B and 2.26D, 2.26F (as fhl1b MO L2), 2.26H; n = 10).

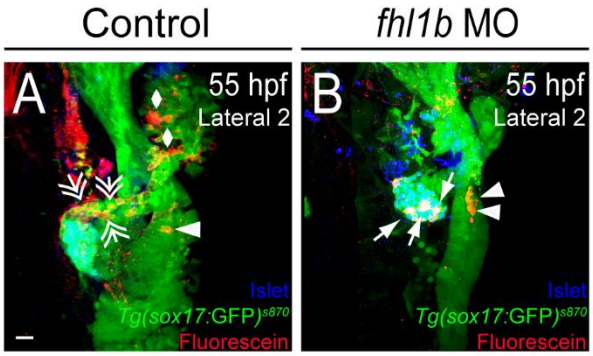

Figure 2.20 Fhl1b regulates the fate of the medial and lateral endodermal progenitors.

(A and B) Confocal images of *Tg(sox17:GFP)*^{s870} embryos at 55 hpf, stained for uncaged-Fluorescein (red) and Islet (blue). In control embryos (A), lateral 2 (L2) cells gave rise to the liver (white rhombi), intestine (white arrowhead), and exocrine pancreas (white double arrows), but rarely gave rise to the endocrine pancreas. In *fhl1b* morphants (B), L2 cells contributed to the Islet-positive pancreatic endocrine cells (white arrows), but not to the liver or exocrine pancreas.

Assessment of exocrine pancreas development and differentiation by analyzing the expression of *Tg(ptf1a:*GFP*)*^{jh1}, which labels developing exocrine pancreatic cells, as well as that of *Tg*(*fabp10a*:DsRed;*ela3l*:EGFP)^{gz15} (Farooq et al., 2008), which marks differentiated hepatocytes and pancreatic acinar cells, showed a reduced number of pancreatic exocrine cells at 72 and 96 hpf (Figure 2.23A-D). These data suggest that depletion of Fhl1b function results in the conversion from no/low to high *pdx1*-expressing cells, leading to a significant increase in the number of pancreatic endocrine cells along with a concomitant compromise of the development of liver and pancreatic exocrine cells, which are derivatives of no and low *pdx1*-expressing cells (Chung et al., 2008).

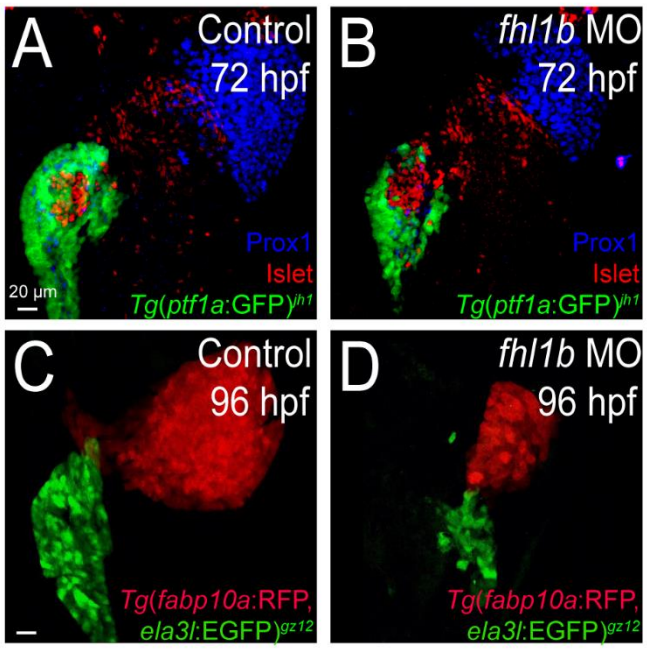

Figure 2.21 Decreased *fhl1b* activity inhibits liver and exocrine pancreas differentiation.

(A and B) Confocal images of *Tg(ptf1a:GFP)*^{jh1} control embryos (A) and *fhl1b* morphants (B), stained for Prox1 (grey). The expression domain of the Prox1 and *Tg(ptf1a:GFP)*^{jh1} was reduced in *fhl1b* morphants (B) compared to that of control embryos (A). (C and D) Confocal images of *Tg(fabp10a:RFP, ela3l:EGFP)*^{gz12} control embryos (C) and *fhl1b* MO-injected larvae (D) at 96 hpf. The expression domain of the *Tg(fabp10a:*RFP, *ela3l:*EGFP*)*^{gz12} was reduced both in the liver and exocrine pancreas in *fhl1b* MO-injected larvae (D) compared to that of control larvae (C). A-D, confocal projection images, ventral views, anterior to the top. Scale bars, 20 µm.

Conversely, we examined the *pdx1* gradient in *fhl1b*-overexpressing embryos. In *Tg(hsp:fhl1b; hsp:GFP)*^{gt3} embryos in which *fhl1b* expression was induced at the 8-somite stage, medial cells, as their counterpart in control embryos, exhibited high levels of *pdx1* (Figure 2.24A-B, white asterisks). Consistently, *neurod* expression appeared unaffected (Figure 2.24C-D). In contrast, lateral cells exhibited greatly reduced levels of *pdx1* compared to that of control embryos (Figure 2.24A-B, white arrows), demonstrating that *fhl1b* overexpression during the post-gastrulation stage led to a decrease of *pdx1* expression in the pancreatic exocrine and intestinal progenitors.

Next, a single lateral 1 cell in *Tg(hsp:fhl1b; hsp:GFP)*^{gt3} embryos was heat-shocked and uncaged at the 6-8 somite stage. In every embryo where *fhl1b* expression was induced at the 6-8 somite stage, lateral 1 cells contributed to the liver (Figure 2.25B and 2.26D, 2.26G (as HS @ 8s L1), 2.26H; n=11); However, in most control embryos lateral 1 cells only gave rise to the pancreas and intestine, but not to the liver (Figure 2.25A and 2.26B, 2.26D-E, 2.26G (as L1), 2.26H; 1 out of 10 control embryos showed contribution of lateral 1 cells to the liver). These results indicate that augmentation of Fhl1b activity decreases *pdx1* expression levels in pancreatic exocrine and intestinal progenitor cells, leading them to become liver cells.

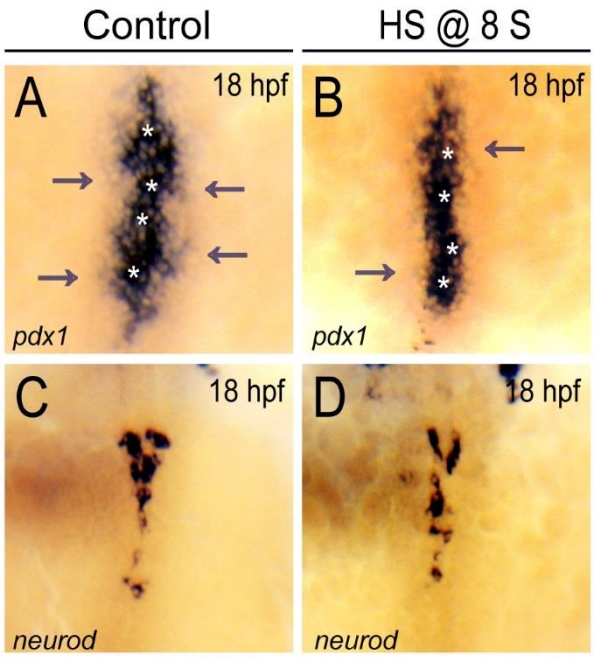

Figure 2.22 Fhl1b regulates the patterning of the medial and lateral endodermal progenitors.

(A-D) Whole-mount *in situ* hybridization showing the expression of *pdx1* (A and B) and *neurod* (C and D) at 18 hpf, comparing control embryos (A and C) and *fhl1b*-overexpressing embryos (B and D, heat shock applied at the 8-somite stage). In embryos induced to overexpress *fhl1b* at the 8-somite stage (B and D), *neurod* and high levels of *pdx1* expression (white asterisks in B) were maintained, while low levels of *pdx1* expression (white arrows) were reduced. Scale bars, 20 µm.

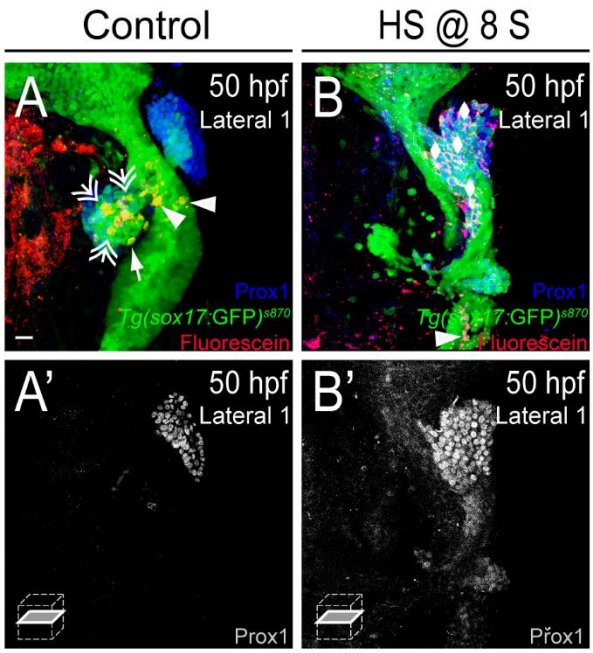

Figure 2.23 Fhl1b regulates the fate of the medial and lateral endodermal progenitors.

(A-B') Confocal images of *Tg(sox17:GFP)*^{s870} embryos at 50 hpf, stained for uncaged-Fluorescein (red) and Prox1 (blue in A and B; grey in A' and B'). In control embryos (A and A'), lateral 1 (L1) cells gave rise to the exocrine pancreas (white double arrows) and the intestine (white arrowheads), but not to the liver. In embryos induced to overexpress *fhl1b* at the 8-somite stage (B and B'), L1 cells mostly contributed to the Prox1-positive liver cells (white rhombi). Scale bars, 20 µm.

As previously reported (Chung et al., 2008), the medial cells at the 6-8 somite stage, which express high levels of *pdx1*, give rise mostly to pancreatic endocrine cells (Figure 2.26A, 2.26D-E, 2.26H; n=11), indicating an early fate restriction of these cells primarily during the gastrulation stage. Taken together, these results suggest that Fhl1b plays an essential role in determining the precise patterning of medial and lateral endodermal progenitors by modulating the levels of *pdx1* expression for proper fate choice of liver versus. pancreas.

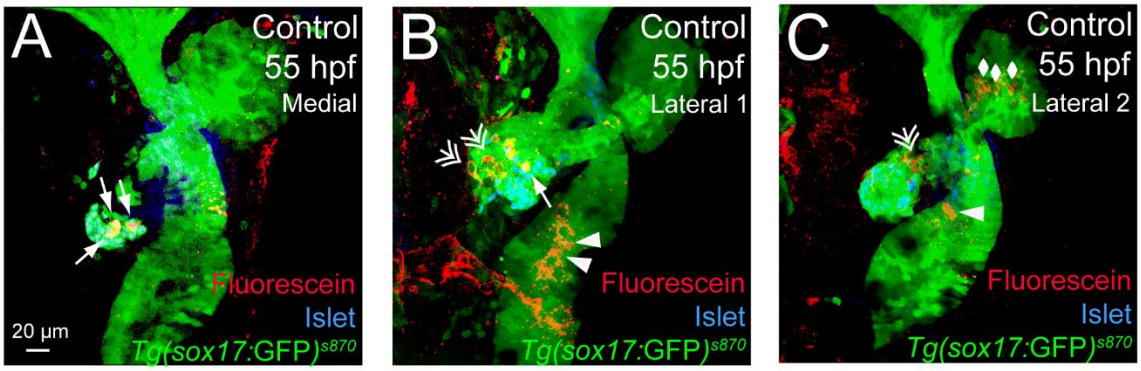

D

	Meidial-Lateral Position	Endocrine Pancreas (%)	Exocrine Pancreas (%)	Intestine (%)	Liver (%)
Control	Medial (M)	11/11 (100)	0/11 (0)	4/11 (36.4)	0/11 (0)
	Lateral 1 (L1)	10/10 (100)	9/10 (90)	10/10 (100)	1/10 (10)
	Lateral 2 (L2)	1/10 (10)	10/10 (100)	10/10 (100)	9/10 (90)
Treatment	*fhl1b* MO L2	10/10 (100)	3/10 (30)	8/10 (80)	1/10 (10)
	HS @ 8 S L1	1/11 (9.1)	2/11 (18.2)	8/11 (72.7)	11/11 (100)

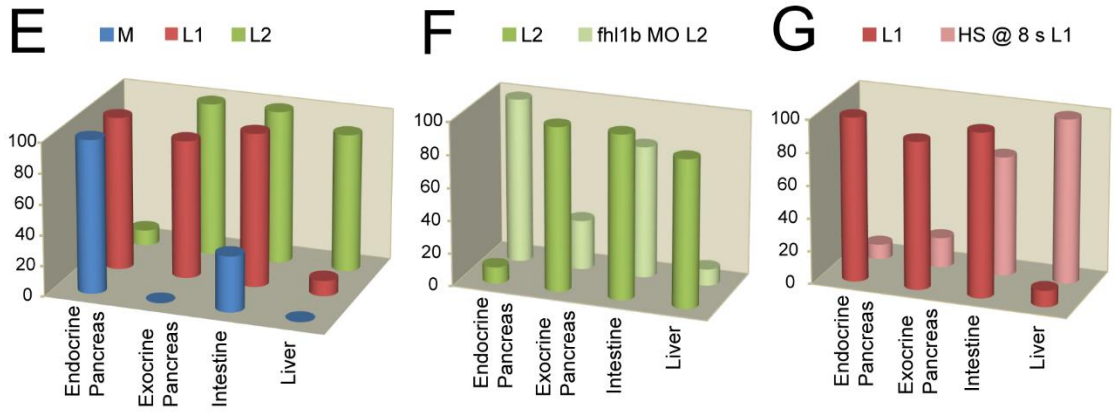

H

Meidial-Lateral Position	Endocrine Pancreas	Exocrine Pancreas	Intestine	Liver	number of embryos (%)
Medial (M)	+				7 (63.6)
n=11	+		+		4 (36.4)
Lateral 1 (L1)	+	+	+		8 (80)
	+		+		1 (10)
n=10	+	+	+	+	1 (10)
Lateral 2 (L2)		+	+	+	8 (80)
		+	+		1 (10)
n=10	+	+	+	+	1 (10)
fhl1b MO L2	+		+		5 (50)
	+				2 (20)
n=10	+	+	+		2 (20)
	+	+	+	+	1 (10)
HS @ 8 S L1			+	+	6 (54.5)
				+	3 (27.3)
n=11		+	+	+	1 (9.1)
	+	+	+	+	1 (9.1)

Figure 2.24 Endodermal progenitors contribute to distinct endodermal tissues based on their M-L position and the activity of *fhl1b*.

(A-C) Confocal images of *Tg(sox17:GFP)*^{s870} embryos at 55 hpf, stained for Islet (blue) and uncaged-Fluorescein (red), showing the progeny of the medial (A), lateral 1 (B) and lateral 2 (C) cells. Medial cells (A) mostly gave rise to pancreatic endocrine cells (white arrows). Lateral 1 cells (B) gave rise to pancreatic exocrine (white double arrows), endocrine (white arrow), and intestinal (white arrowheads) cells. Lateral 2 cells (C) gave rise to liver (white rhombi), intestine (white arrowhead), and pancreatic exocrine cells (white double arrow). (D-H) The numbers and the percentages of embryos that showed incorporation into a given tissue type in each specific position, comparing control embryos (D, E, F (as L2), G (as L1), and H) as well as *fhl1b* morphants and embryos induced to overexpress *fhl1b* at the 8-somite stage (D, F (as fhl1b MO L2), G (as HS @ 8s L1), and H). In every *fhl1b*-depleted embryo, lateral 2 cells contributed to the pancreatic endocrine cells (D, F (as fhl1b MO L2), and H), while in control embryos, most of the lateral 2 cells gave rise to the exocrine pancreas, intestine, and liver, but seldom gave rise to the endocrine pancreas (D, E, F (as L2), and H). In control embryos, lateral 1 cells mostly gave rise to pancreatic and intestinal cells, but not to liver cells (D, E, G (as L1), and H), whereas in every *fhl1b*-overexpressing embryo, lateral 1 cells contributed to the liver (D, G (as HS @ 8s L1), and H). Data in each 3-D column (%) in E-G were obtained by summing the number of embryos that showed incorporation into a given tissue type and normalizing it to the total number of embryos examined in each specific position: M, L1 and L2. Colored rectangles in H highlight the most dominant pattern in *fhl1b* morphants (red) and *fhl1b*-overexpressing (blue) embryos. A-C, confocal projection images, ventral views, anterior to the top. Scale bar, 20 μm.

2.4.3.2 Relationship between Bmp2b, Fhl1b, and Id2a in fate choice of liver versus pancreas

Our data indicate that Fhl1b is a novel physiological effector of Bmp2b signaling that regulates the adequate fate choice for liver and pancreas. To investigate the epistatic relationship between Bmp2b signaling and Fhl1b, we induced *bmp2b* expression at the 8-somite stage in the presence or absence of *fhl1b*. As previously reported (Chung et al., 2008), in *bmp2b*-overexpressing embryos, the Prox1 expression domain in the liver was significantly expanded (Figure 2.27B), whereas the number of Islet-positive pancreatic endocrine cells appeared unaffected (red; dorsal pancreatic bud is outlined by white dotted circle; Figure 2.27B). We found that the majority of *bmp2b*-overexpressing *fhl1b* morphants exhibited an enlarged Islet-positive pancreatic endocrine cell population (red; dorsal pancreatic bud is outlined by white dotted circle; Figure 2.27D, 80%) with a reduced number of Prox1-positive cells in the liver (Figure 2.27D, 80%) as in *fhl1b* morphants (Figure 2.27C), whereas a small portion of *bmp2b*-overexpressing *fhl1b* morphants restored the developmental defects of the liver and pancreatic endocrine formation (Figure 2.27D, 20%). These results suggest that Fhl1b is a critical mediator of Bmp2b signaling in governing the liver versus pancreas fate decision.

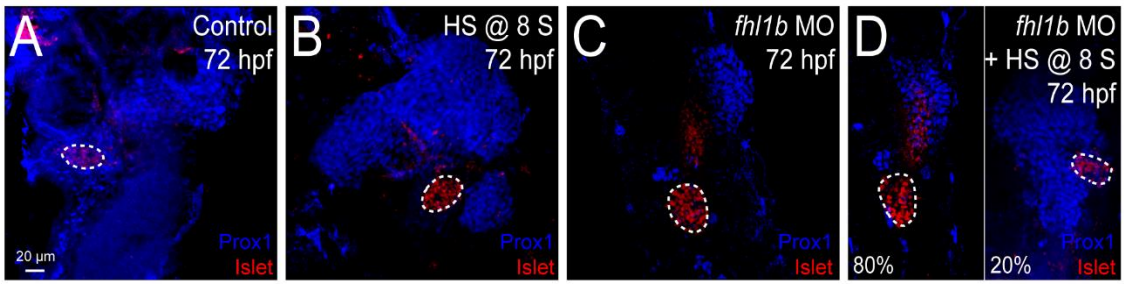

Figure 2.25 Fhl1b is an essential mediator of Bmp2b signaling directing liver versus pancreas fate decision.

(A-D) Confocal images of control embryos (A), *bmp2b*-overexpressing embryos (B), *fhl1b* morphants (C), and *bmp2b*-overexpressing *fhl1b* morphants (D) at 72hpf, stained for Islet (red; expression in the dorsal pancreatic bud is outlined by white dotted circles) and Prox1 (blue). (B) Prox1 expression in the liver was greatly expanded when *bmp2b* expression was induced at the 8-somite stage, whereas Islet expression in the mesenchymal cells surrounding the HPD system as well as in the pancreatic endocrine cells appeared unaffected. As in *fhl1b* morphants (C), the majority of *bmp2b*-overexpressing *fhl1b* morphants exhibited an enlarged Islet-positive pancreatic endocrine cell population with a reduced number of Prox1-positive cells in the liver (D, 80% (22 out of total 28 embryos analyzed)). A small portion of *bmp2b*-overexpressing *fhl1b* morphants restored the developmental defects of the liver and pancreatic endocrine formation (D, 20% (6 out of total 28 embryos analyzed)). A-D, confocal projection images, ventral views, anterior to the top. Scale bars, 20 μm.

Furthermore, these data raise the possibility of other effector(s) of Bmp2b signaling that may act in concert with Fhl1b in this process. Hence, we analyzed the function of Id2, which has been implied in suppressing the function of Neurod (Hua et al., 2006) and an immediate target of Bmp signaling (Miyazono and Miyazawa, 2002). Zebrafish have two *id2* genes: *id2a* and *id2b* (Khaliq et al., 2015). Only *id2a* is restrictively expressed in the liver from 30 hpf onwards (Khaliq et al., 2015). We conducted loss-of-function analyses using published *id2a* MO (Uribe and Gross, 2010). While *id2a* morphants showed a decrease of the *hhex* expression domain in the liver (Figure 2.28B, black arrow), its expression in the dorsal pancreas appeared unaffected at 30 hpf (Figure 2.28B, white dotted circle). Consistently, the *pdx1* expression domain in *id2a* morphants was comparable to that of control embryos (Figure 2.28F). Double *id2a*/*fhl1b* morphants exhibited synergistically more severe defects in liver formation (Figure 2.28D, black arrow) than that of single *id2a* (Figure 2.28B, black arrow) or single *fhl1b* morphants (Figure 2.28C, black arrow), whereas the dorsal pancreas of double morphants (Figure 2.28D and 2.28H, white dotted circles) phenocopied that of single *fhl1b* morphants (Figure 2.28C and 2.28G, white dotted circles). The expression of *id2a* in *fhl1b* morphants in the liver biliary epithelial cells was comparable to that of control embryos at 72 hpf (Figure 2.28I-J). Taken together, these data indicate that Fhl1b is an essential mediator of Bmp2b signaling in determining the proper fate decision of liver versus. pancreas. These results further suggest that an unknown effector of Bmp2b signaling may play a role in regulating this process, while Id2a is primarily necessary for regulating liver development (Figure 2.28K).

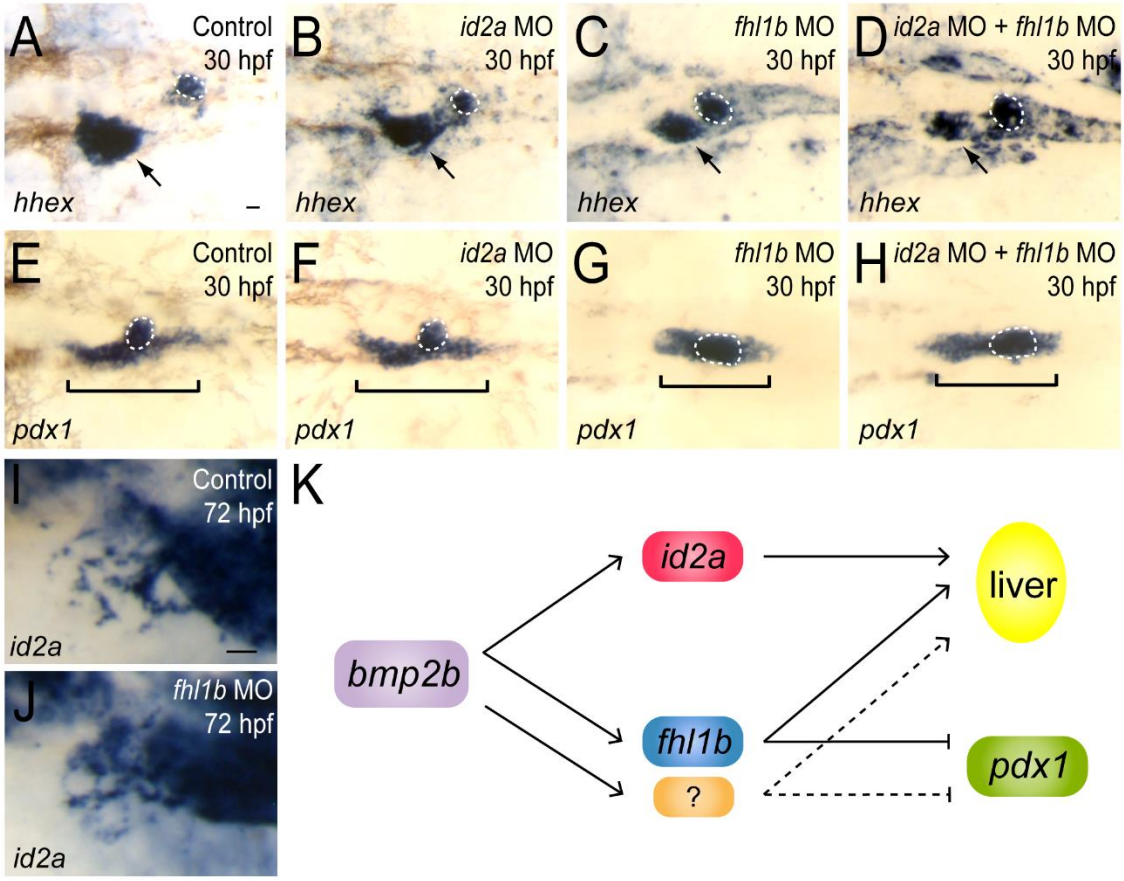

Figure 2.28 Fhl1b, but not Id2a, is an essential mediator of Bmp2b signaling directing liver versus pancreas fate decision.

(A-H) Whole-mount *in situ* hybridization showing the expression of *hhex* (A-D) and *pdx1* (E-H), comparing control embryos (A and E), *id2a* morphants (B and F), *fhl1b* morphants (C and G), and double *fhl1b*/*id2a* morphants (D and H) at 30 hpf. *hhex* is expressed in the liver (black arrows) and the dorsal pancreatic bud (white dotted circles). *pdx1* is expressed in the developing pancreas including the dorsal pancreatic bud (white dotted circles) and intestine (black brackets), but not in the liver. The *hhex* expression domain was reduced in the liver of *id2a* morphants (B, black arrow) but appeared unaffected in the dorsal pancreatic bud (B, white dotted circle). *fhl1b* morphants showed a reduced *hhex* expression domain in the liver (C, black arrow) with a concomitant expansion of its expression domain in the dorsal pancreatic bud (C, white dotted circle). Double *fhl1b*/*id2a* morphants showed a more severe reduction of *hhex* expression domain in the liver (D, black arrow), whereas its expression domain in the dorsal pancreatic bud was comparable to that in single *fhl1b* morphants (compare C and D, white dotted circles). *pdx1* expression in *id2a* morphants was comparable to that in control embryos (F). *pdx1* expression domain in double *fhl1b*/*id2a* morphants in the dorsal pancreatic bud was expanded (H, white dotted circle), whereas its expression in the intestinal bulb primordium appeared to be reduced (H, black bracket), and was comparable to that in

fhl1b morphants (G, white dotted circle and black bracket, respectively). (I-J) Whole-mount *in situ* hybridization showing the expression of *id2a*. The expression of *id2a* in *fhl1b* morphants in the liver biliary epithelial cells (J) was comparable to that in control embryos (I) at 72 hpf. (K) Schematic model of the relationship between Bmp2b, Fhl1b, and Id2a in liver versus pancreas fate decision. Fhl1b is essentially required for suppressing *pdx1* expression to keep progenitors competent to differentiate into the liver, while Id2a is required primarily for liver development. Solid lines indicate connections supported by the data presented in this study, while dashed lines indicate potential connections by an unknown effector. A-J, dorsal views, anterior to the left (n=20 per each condition). Scale bars, 20 μm.

2.5 Conclusion

We identified and analyzed the role of a novel Bmp2b downstream effector Fhl1b in the liver versus pancreas fate decision. In bipotential hepatopancreatic progenitors from the 12-somite stage onwards, Fhl1b regulates the proper cell fate choice by modulating the levels of *pdx1* expression (Figure 2.29). The portion of the progenitor population that express high *pdx1* level mainly differentiate into pancreatic endocrine cells, while the portion in which *pdx1* expression is suppressed mostly develop into liver cells after fate decision window.

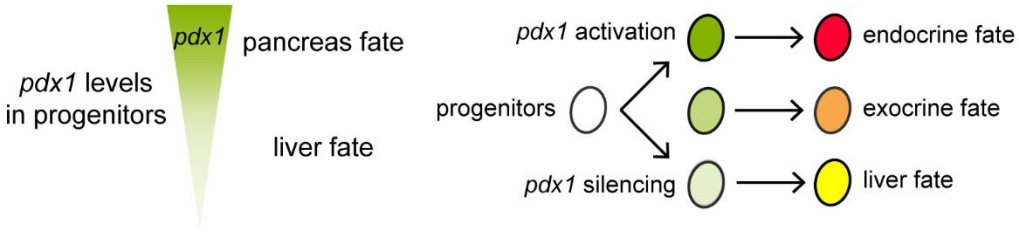

Figure 2.29 *pdx1* levels are associated to the cell fate of progenitors.

Endodermal progenitors experience different levels of *pdx1* regulating their fates as pancreatic endocrine (high levels of *pdx1*), pancreatic exocrine (low levels of *pdx1*), or liver (*pdx1* silencing) cells. The expression of *pdx1* is color-coded as green.

fhl1b depletion compromised liver specification and enhanced induction of pancreatic cells, causing a hepatic-to-pancreatic endocrine fate switch. Conversely, *fhl1b* overexpression promoted liver specification and inhibited induction of pancreatic cells, redirecting pancreatic progenitors to become liver cells (Figure 2.30).

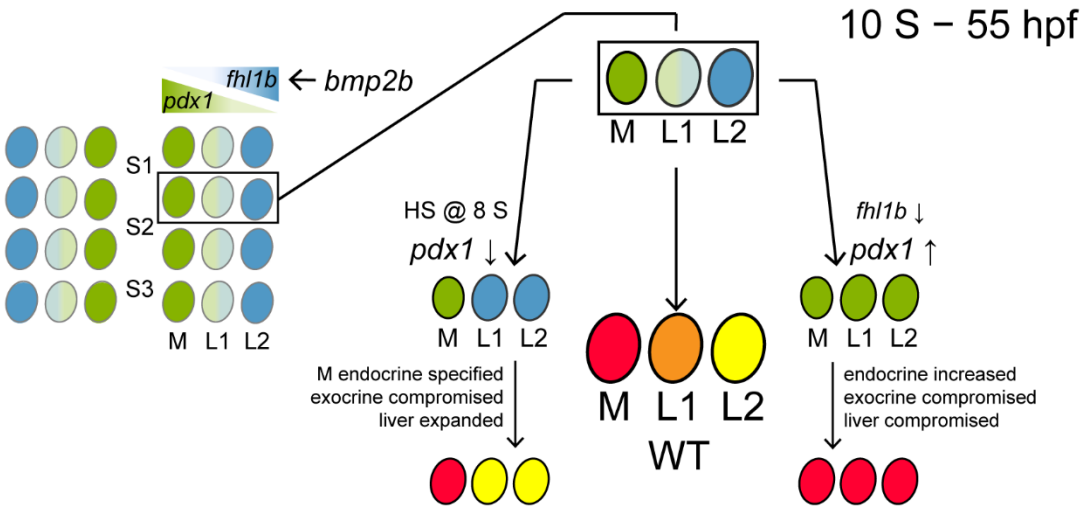

Figure 2.30 Fhl1b is essential for regulating the cell fate choice of liver versus pancreas.

From the 12-somite stage onwards, single endodermal cells in the lateral 2 position (L2) between somites 1 and 3 in the endodermal sheet give rise not only to pancreatic exocrine cells and intestinal cells, but also to liver cells, functioning as bipotential hepatopancreatic progenitors. *bmp2b*, which is expressed in the lateral plate mesoderm, induces *fhl1b* expression in the prospective liver anlage. This may form a reciprocal gradient of *fhl1b*-*pdx1*. Decreased *fhl1b* function leads to an increase in levels of *pdx1* expression in lateral 1 and 2 cells, causing a hepatic and pancreatic exocrine to a pancreatic endocrine fate switch. Conversely, augmentation of *fhl1b* activity at the initial time point of *pdx1* expression in the pancreatic exocrine and intestinal progenitors (HS @ 8 S) causes a decrease in levels of *pdx1* expression in pancreatic exocrine and intestinal progenitor cells, leading them to become liver cells. The lineage of the most medial cells, which express high levels of *pdx1* and subsequently give rise to pancreatic endocrine cells, is specified primarily during the gastrulation stage.

2.6 Discussion

Previously, it's showed that there is a medial-lateral *pdx1* "gradient" in the endodermal sheet in zebrafish (Chung et al., 2008). The most medial cells with high levels of *pdx1* mainly gave rise to pancreatic endocrine cells, whereas lateral 1 cells with low levels of *pdx1* gave rise to pancreatic exocrine cells and intestinal cells, as well as a few pancreatic endocrine cells. Some lateral 2 cells without *pdx1* expression populate the liver. Consistently, in mice, it was suggested that the level of *Pdx1* gene activity is differentially required for the proper development of the pancreas and subsequent lineage allocation of the pancreatic endocrine cells (Fujitani et al., 2006). While homozygous mutants of the *Pdx1* enhancer region deletion resulted in severe impairment of endocrine maturation but normal formation of acinar tissue, heterozygous mice showed an islet size similar to that of wild type mice with abnormally more α- and pancreatic polypeptide-producing PP cells but fewer differentiated β-cells. These findings support the possibility that conversion of common endocrine precursors to β-cells relies on a high-level of *Pdx1* expression. Our studies show that depletion of *fhl1b* resulted in the conversion from no/low to high *pdx1*-expressing cells, which is marked by *neurod* expression. This conversion led to a significant increase in the number of pancreatic endocrine cells, especially β-cells and compromised the development of liver and pancreatic exocrine cells, which are derivatives of no and low *pdx1*-expressing cells. In these embryos, lateral 2 cells contributed frequently to pancreatic endocrine cells. Conversely, *fhl1b* overexpression at the post-gastrulation stage (i.e. 8-somite stage) caused a decrease in the number of low *pdx1*-expressing cells, leading to the induction of the liver at the expense of the exocrine pancreas. In these embryos, lateral 1 cells contributed primarily to liver cells. When *fhl1b* was overexpressed during the gastrulation stage, the number of cells

expressing low and high levels of *pdx1* decreased with a subsequent decrease in the number of pancreatic exocrine cells and Insulin-expressing β-cells, thus, confirming the critical role of Fhl1b in the modulation of *pdx1* levels to coordinate the medio-lateral patterning of the endodermal sheet for proper induction of the liver and pancreas. Intriguingly, the numbers of β- and δ-cells were increased, whereas the number of α-cells was slightly decreased in *fhl1b* morphants. These results are consistent with previous data that Bmp receptor *alk8* MO-injected donor cells mainly gave rise to β- and δ-cells, but rarely to α-cells (Chung et al., 2010). It has been shown that β/δ-cell versus α-cell fate is differentially regulated by Pax4 and Arx, respectively (Collombat et al., 2003). Moreover, overexpression of *Pdx1* eliminated glucagon mRNA and protein and promoted the expression of β-cell specific genes, while induction of dominant-negative *Pdx1* resulted in differentiation of β-cells into α-cells in the rat insulinoma cell line (Wang et al., 2001). Hence, it is plausible to speculate that Fhl1b is an essential mediator of Bmp signaling to regulate the discrete levels of *pdx1* expression for precise lineage allocation of the pancreatic endocrine progenitors. Interestingly, we found that in a portion of embryos, *fhl1b* is also expressed in the *TgBAC(neurod:*EGFP*)*^{nl1}-expressing cells. Therefore, it is possible to hypothesize that after serving as an essential effector for the hepatic versus pancreatic fate decision, Fhl1b may function further to fine-tune the lineage allocation of the specified pancreatic endocrine cells. As LIM proteins often function as molecular adaptors or scaffolds to support the assembly of multimeric protein complexes (Chang et al., 2003), it will be intriguing to determine whether Fhl1b modulates *pdx1* expression by facilitating the formation of a novel protein complex that is involved in either mediator-or chromatin-mediated gene expression control.

Our findings of Bmp regulation of Fhl1b suggest a new paradigm of how Bmp signaling regulates the cell fate choice of liver versus pancreas and β-cell mass. Despite the long-standing focus on the active role of Bmp signaling on the liver gene program through both genetic and epigenetic regulation (Rossi et al., 2001; Shin et al., 2007; Xu et al., 2011), the link between Fhl1b and *pdx1* expression shown in this study suggests that Bmp may function actively to suppress the pancreas gene program to properly modulate liver induction. Hence, our data elucidates why effective Bmp suppression is critical for the induction of *PDX1* and the subsequent generation of β-cells from the human pluripotent stem cells (Kroon et al., 2008; Nostro et al., 2011; Rezania et al., 2012) and from zebrafish endodermal progenitors (Chung et al., 2010). A comprehensive understanding of how lineage-specific multipotent progenitors make a developmental choice will shed light on the programming and reprogramming of stem/progenitor cells into specific cell lineages, enabling us to generate functionally relevant cells for clinical utility.

CHAPTER 3
SIGNALING PATHWAYS PROMOTING β-CELL REGENERATION

The work in this chapter contributes to the following publication:

Xu, J., et al. (2016). *PLOS Genetics*.

Xu, J., et al. (2017). *Under review*.

3.1 Abstract

Fhl1b as a novel Bmp2b signaling downstream target, regulates regeneration of insulin-secreting β-cells by modulating *pdx1* and *neurod* expression in the HPD system. Loss of *fhl1b* enhances neogenesis of new β-cells from the progenitor cell population residing in the HPD system. While overexpression of *fhl1b* blocked the endogenous neogenesis of β-cells during regeneration. In addition, we identified inhibitors of non-canonical IκB kinases (IKKs), TANK-binding kinase 1 (TBK1) and IκB kinase ε (IKKε) as enhancers of β-cell regeneration. TBK1/IKKε inhibitors stimulated β-cell-specific proliferation. TBK1/IKKε inhibitors augmented function and proliferation of β-cells in mammalian islets including human islets. TBK1/IKKε inhibitor treatment improved glycemic control in streptozotocin (STZ)-induced diabetic mice with increase in β-cell proliferation, and total insulin content. Therefore, our work suggests a new paradigm of how Bmp signaling regulates β-cell regeneration through its novel target Fhl1b. Our data also shows an

evolutionarily conserved and critical role of TBK1/IKKε suppression in expanding functional β-cell mass, providing a potential candidate pathway for clinical practice.

3.2 Introduction

It has been reported that β-cell regeneration can occur via the proliferation of residual β-cells (Dor et al., 2004) or the neogenesis of β-cells from non-β-cells (Ye et al., 2015). Non-β-cells could be progenitor cells residing in the pancreatic ductal systems (Xu et al., 2008) or other mature cell types including glucagon-expressing α-cells (Thorel et al., 2010). It's also been suggested that a progenitor cell population in the HPD system can be activated and undergo differentiation in later stages. In addition, *pdx1* is expressed in the HPD system, and may play a role in guiding the fate choice of the progenitors (Field et al., 2003a; Kimmel et al., 2011; Spence et al., 2009). Intriguingly, Id2, a Bmp signaling marker, is excluded in the endocrine pancreas, and HPD system (Chung et al., 2010). However, from our expression data, *fhl1b*, a novel Bmp2b target, is expressed in HPD system in later stages. Nonetheless, the underlying mechanisms of how Bmp signaling orchestrates the proper lineage choice of the progenitors in the HPD system await further investigation.

Islet inflammation has emerged as a key contributor to the loss of functional β-cell mass in both type 1 diabetes (T1DM) and type 2 diabetes (T2DM) (Esser et al., 2014; Imai et al., 2013). In T1DM, β-cells are the target of an autoimmune assault. Chronic low-grade inflammation and activation of the immune system are major factors in obesity-induced insulin resistance and T2DM. Therefore, immunotherapies designed to block β-cell apoptosis may stand as a unifying target for diabetes treatment. Despite this rationale, the slow rate of β-cell regeneration in adult humans (Meier et al., 2008; Wang et al., 2015b) limits the efficacy of immune-intervention trials. Accordingly, among multiple small mitogenic molecules identified (Aamodt et al., 2016; Andersson et al.,

2012; Annes et al., 2012; Boerner et al., 2015; El Ouaamari et al., 2016; Shen et al., 2015; Shen et al., 2013; Walpita et al., 2012; Wang et al., 2015a; Wang et al., 2009; Zhao et al., 2014), several of them have either not shown or shown minor functional effects in human β-cells (Andersson et al., 2012; Annes et al., 2012; Boerner et al., 2015; Shen et al., 2013; Zhao et al., 2014). Thus, identifying β-cell regenerating agents that increase residual functional β-cells and coupling them with immunomodulators represent an auspicious treatment for T1DM and T2DM (Pozzilli et al., 2015).

Non-canonical IκB kinases (IKKs), TANK-binding kinase 1 (TBK1) and IKKε, have high sequence homology with comparable phosphorylation profiling of substrate(s) (Clement et al., 2008). These kinases regulate inflammatory reactions primarily through their action on the interferon regulatory factor (IRF) pathway (Caillaud et al., 2005; Chau et al., 2008). Upon induction in response to obesity-dependent inflammation, TBK1/IKKε directly phosphorylate phosphodiesterase (PDE) 3B (Mowers et al., 2013), a major cyclic AMP (cAMP) hydrolyzing PDE isoform in adipocytes (Zmuda-Trzebiatowska et al., 2006). Consequently, genetic deletion of IKKε and pharmacological inhibition of TBK1/IKKε with amlexanox, a small molecule inhibitor of these kinases, increased cAMP levels in adipocytes (Mowers et al., 2013). This led to the secretion of interleukin-6 (IL-6) and the activation of the hepatic Signal Transducer and Activator of Transcription 3 (STAT3) (Inoue et al., 2004), resulting in reduced gluconeogenesis and reversal of metabolic dysfunctions in obese mice (Reilly et al., 2015). In addition, IKKε was shown to be among putative targets of diarylamide WS6, a small molecule that promoted human β-cell proliferation *in vitro* (Boerner et al., 2015; Shen et al., 2013). Despite these data suggesting a role for suppression of TBK1/IKKε in ameliorating

defective glucose handling and in expanding β-cells, the key question of how TBK1/IKKε function in β-cells remains elusive. Furthermore, validation of TBK1/IKKε inhibitors as mitogens for β-cells has yet been reported.

Intracellular cAMP levels are essential for β-cell replication, survival, and function (Inada et al., 2004; Xie et al., 2007; Zhao et al., 2014), and they are modulated by their rate of synthesis via adenylyl cyclase and their rate of degradation via PDEs (Conti and Beavo, 2007). Adenosine receptors A2a and A2b, which are G-protein coupled receptors (GPCRs), were shown to increase β-cell proliferation during homeostatic control and regeneration of the β-cell mass by activating $G_{\alpha s}$ and stimulating production of cAMP (Andersson et al., 2012; Annes et al., 2012). Several of PDEs including PDE3B (Pyne and Furman, 2003) and PDE3A (Byun et al., 2014) are highly expressed in β-cells. Inhibition of PDE3 with cilostamide was reported to reduce streptozotocin (STZ)-induced islet cell death in mice (Byun et al., 2014) and augment β-cell proliferation and regeneration in rat islets and zebrafish (Andersson et al., 2012; Zhao et al., 2014), underscoring a critical role of cAMP in β-cells.

Using small molecules in disease treatment has been in favor for several obvious advantages. Normally, small molecules are relatively simple and economical for massive manufacture. They also remain stable and effective for reasonable periods. Furthermore, small molecules are easy to access desired target locations, with or without additional delivery carriers. Unlike peptide hormonal factors, which affect a multitude of cellular processes and need to be administered by injection, small molecules can be selective and taken orally (Vetere et al., 2014). For diabetes treatment, small molecules can be taken orally, facilitating to increase residual functional β-cells in patients, or to be applied *in*

vitro to expand β-cell pools in isolated culture from cadaveric donors for transplantation (Wang et al., 2015b). Despite all the advantages, specificity and potency are still two of the biggest concerns when using small molecules for treatment. So far, multiple small mitogenic molecules identified have failed to either show functional effects in human β-cells or yield reproducible findings (Andersson et al., 2012; Annes et al., 2012; Shen et al., 2013; Vetere et al., 2014).

In this study, using the zebrafish model of type I diabetes, we identified TBK1/IKKε inhibitors (TBK1/IKKε-Is) as enhancers of β-cell regeneration. Pharmacological and genetic loss- and gain-of-function analyses in zebrafish indicate that TBK1/IKKε-Is augmented β-cell-specific proliferation by increasing cyclic AMP (cAMP) levels via PDE3. TBK1/IKKε inhibitors improved function and replication of mammalian β-cells including primary human β-cells. Furthermore, TBK1/IKKε inhibitors improved glycemic control and induced β-cell proliferation with increase in cAMP levels in streptozotocin (STZ)-induced diabetic mice.

3.3 Methods

3.3.1 Zebrafish strains

To generate the *Tg(hsp*:*pde3a; hsp*:*GFP)*^{gt4}, *pde3a* coding sequence was amplified (forward: 5'- GACGAATTCGTGACCGATGGCACTGGAAT-3', reverse: 5'-GACCTCGAGTCATTCTGGATCTTTCTGGTCTTCG-3') and cloned into a vector containing a multimerized minimal heat shock promoter, which drives *gfp* and *pde3a* transcription bi-directionally in response to a heat shock (Bajoghli et al., 2004). Tol2-mediated transgenesis was achieved as described (Kawakami et al., 1998).

3.3.2 Chemical treatment

The following compounds and the concentrations are used in zebrafish: 100 µM amlexanox, 50 µM BX795, 20 µM (E)-3-(3-phenylbenzo[c]isoxazol-5-yl)acrylic acid (PIAA), and 20 µM PIAA-1, PIAA-2, and PIAA-3.

3.3.3 Immunohistochemistry

Immunohistochemistry on whole-mount zebrafish larvae was performed using the following antibodies: mouse anti-Glucagon (1:100; Sigma), chicken anti-GFP (1:1000; Aves Labs), rabbit anti-Somatostatin (1:100; MP Biomedicals), rabbit anti-Prox1 (1:100; GeneTex), and fluorescently conjugated Alexa antibodies (1:200; Molecular Probes). Nuclei were visualized with TOPRO (1:10000; Molecular Probes). To assess cell proliferation, zebrafish larvae were incubated with 7µM 5-ethynyl-2'-deoxyuridine (EdU) and DMSO at 1.7% final concentration for the indicated time period. EdU

incorporation was revealed for 30 minutes using Click-iT EdU Imaging Kit (Invitrogen), prior to primary antibody staining. Larvae were mounted in Vectashield (Vector Laboratories) and imaged on a Zeiss LSM 700-405 confocal microscope. Rabbit anti-Ki67 (1:100; Abcam) and guinea pig anti-Insulin (1:100; Sigma) antibodies were additionally used for immunohistochemistry on rat INS-1 cells, mammalian islet culture, and mice pancreata. Nuclei were visualized with TOPRO (1:2000; Molecular Probes). Rat INS-1 cells and islet samples were directly imaged in plates on a Zeiss LSM 700-405 confocal microscope. Mice pancreata were dissected, fixed in 4% PFA, treated with a 30% sucrose solution, then embedded in Tissue-Tek OCT compound (Sakura Finetek). 8 µm cryostat sections were obtained by using a cryostat microtome (CryoStar NX70 Cryostat), stained with antibodies, mounted in Vectashield (Vector Laboratories), and imaged on a Zeiss LSM 700-405 confocal microscope. Two 8 µm pancreas sections (separated by 400 µm) per mouse were used to assess β-cell area. Images were taken after Insulin staining using a Zeiss LSM 700-405 confocal microscope, and islet size/area and the total areas of the sections were determined using the ZEN software (Zeiss). The percentage of β-cell area in each section was calculated by dividing the area of all insulin-positive cells in one section by the total area of this section.

3.3.4 Glucose and cAMP measurements

For free glucose measurements, the zebrafish larvae were collected in 2 mL microcentrifuge tubes and frozen on crushed dry ice after removal of excess egg water. Upon thawing, 200 µL of PBS were added and the larvae were homogenized using a hand-held mechanical homogenizer. To measure glucose in larval extracts, 15 µL of

supernatant was used and mixed for each reaction, and incubated for 30 minutes at 37°C in the dark. Fluorescence (excitation, 535 nm; emission, 590 nm) was measured using Biotek Synergy H4 Multi-Mode Plate Reader. Each sample was measured in triplicate. For cAMP content measurements, treated zebrafish larvae were collected (10 larvae were pooled per condition), homogenized in 100 μL 0.1 M HCl, and centrifuged at 6,000 *g* for 10 min at 4°C.

The rat INS-1 cells were cultured in RPMI 1640 (Gibco) supplemented with 10% FBS, 1% Penicillin/Streptomycin, 25mM HEPES (Invitrogen), and 50 μM β-mercaptoethanol and used for experiments between passages 6-10. INS-1 cells were seeded in 6-well plates at $5x10^5$ cells per well and starved for 18 hours in serum-free RPMI with 2.5 mM glucose prior to exposure to PIAA for 1 hour. After treatment, cells were lysed in 200 μL 0.1 M HCl and centrifuged. For mice, 2-3 hours after PIAA treatment, the relevant organs were harvested and homogenized in 0.1 M HCl. Supernatants from all samples were collected and stored at −80°C until cAMP content measurements.

3.3.5 Mammalian *ex vivo* islet culture

Male Lewis rats were housed on a 12-hour light/dark cycle in a controlled climate according to Georgia Institute of Technology regulations. Pancreatic islets were isolated from rats by collagenase digestion (Liberase TL, Roche Diagnostics) and gradient purification, and then hand-picked and pooled. Islets were cultured overnight in CMRL-1066 (Invitrogen) supplemented with 10% FBS, 1% Penicillin/Streptomycin, and 25mM HEPES (Invitrogen). The next day, islets were either directly treated with PIAA for 4 days or dissociated with 0.05% trypsin-EDTA (Invitrogen) for 3-5 minutes with gentle

agitation to aid cell cluster disruption. Single cells obtained from islet dissociation were plated in 96-well plates and allowed 48 hours to attach prior to treatment with PIAA for 4 days. Human islets were cultured in Human Islet Media (Prodo Labs) supplemented with 1% Penicillin/Streptomycin and 10% human serum for 24-48 hours prior to experimentation.

3.3.6 Glucose tolerance tests

For glucose tolerance tests, after a twelve-hour fast, mice were given an intraperitoneal injection of glucose at a dose of 2 g per kg. We measured blood glucose at basal, 30, 60, 90, and 120 minutes from tail blood using the OneTouch Ultra glucometer (Lifescan).

3.3.7 Assessment of insulin content

For insulin content measurements, isolated mice pancreata were placed in acid-ethanol mixture (0.18 M HCl, 75% EtOH), incubated overnight (−80°C), and then homogenized; the tissue levels of insulin extracted by centrifugation (2,000 rpm, 15 min, 4 °C) were then determined by mouse insulin ELISA kit (Mercodia) and normalized to total pancreatic protein content determined by Pierce BCA protein assay kit (Thermo Fisher).

3.3.8 Reverse transcription quantitative real-time polymerase chain reaction

Total RNA was extracted using the Trizol Reagent (Invitrogen). cDNA synthesis was performed using ImProm-II Reverse Transcription System (Promega). PCR was

conducted using iTaq Universal SYBR Green Supermix in triplicate (Bio-Rad). Optimized primers targeting each gene were designed using Primer3 (Untergasser et al., 2012). The StepONE Plus PCR System (Applied Biosystems) was used to obtain the *C*t value. The relative gene expression of each sample was determined using the comparative *C*t method with *β-actin* or *Gapdh* as an internal control (Schmittgen and Livak, 2008). The following primers were used: mouse *Ikbke*: forward 5'-ACAAGGCCCGAAACAAGAAAT-3', reverse 5'- ACTGCGAATAGCTTCACGATG -3'; mouse *Tbk1*: forward 5'- ACTGGTGATCTCTATGCTGTCA-3', reverse 5'-TTCTGGAAGTCCATACGCATTG-3'; mouse *Gapdh*: forward 5'-TCGTCCCGTAGACAAAATGGT-3', reverse 5'- TGGCAACAATCTCCACTTTGC-3'; zebrafish *β-actin*: forward 5'-CGAGCTGTCTTCCCATCCA-3', reverse 5'-TCACCAACGTAGCTGTCTTTCTG-3'; zebrafish *ikbke*: forward 5'-CAGCAAACGTCTACAAAGCCA-3', reverse 5'- TGAGGAACTCGGACTCAGGA-3'; zebrafish *tbk1*: forward 5'- GAAAACAGGCGATCTGTACGC-3', reverse 5'-GCACCTTATGACGTGTGTTCG-3'; zebrafish *pde3a*: forward 5'-TGCTGGAGAATCATCACGCT-3', reverse 5'- TCATTGGTCCAGTCGATCCC-3'.

3.3.9 Glucose stimulated insulin secretion from *ex vivo* islet culture

Human and rat islets were evaluated for glucose stimulated insulin secretion using standard methods. Cultured islets with 4-5 days treatment with DMSO or 40-80 μM PIAA were equilibrated within a column in the center of a 1 mL sandwich of Sephadex beads using 3 mM glucose in Krebs buffer for one hour. After

equilibration, 3-4 replicates per group were subjected to 1 hour sequential incubations with Krebs low (3 mM glucose), high (16 mM glucose), and low again. Secreted insulin was monitored using a human or rat ELISA kit (Mercodia) and normalized to total DNA (PicoGreen, Invitrogen).

3.3.10 Mice experiments

All mice studied were 6–8-wk old males on the C57BL/6 background (Jackson Laboratory). Only mice that had fed blood glucose values of >300 mg glucose/dL were used. Mice were given daily intraperitoneal injections of vehicle (dimethylsulphoxide final 6.7% formulated in 1% methylcellulose) or PIAA (12.5 mg per kg body weight; formulated in 1% methylcellulose). Mice were housed in pathogen-free facilities and maintained in the Animal Care Facilities at Parker H. Petit Institute for Bioengineering and Bioscience, Atlanta, GA. Studies conducted and protocols used were approved by the Institutional Animal Care and Use Committees of Georgia Institute of Technology and were in accordance with National Institute of Health guidelines.

3.4 Results

3.4.1 Modulation of *fhl1b* activity regulates the capacity of β-cell regeneration

Given the critical role of Fhl1b in restricting the induction of pancreatic endocrine cells, we investigated whether altering Fhl1b activity changes β-cell regeneration efficiency. Using *Tg*(*ins*:*CFP-NTR*)^{s892} (Curado et al., 2007) together with *Tg(ins:Kaede)*^{jh6} (Pisharath et al., 2007), we compared the β-cell regeneration efficiency in control vs. *fhl1b* MO-injected larvae. We first converted the fluorescence of the Kaede protein from green to red by exposing the larvae to UV light. This conversion permanently marked all β-cells that were present before the ablation step. We then treated the larvae from 84−108 hpf with metronidazole (MTZ) to ablate the β-cells. In this set-up, newly formed β-cells express green-fluorescent Kaede only, whereas β-cells that survive the ablation co-express red- and green-fluorescent Kaede. The ablated control islets exhibited recovery of green-only β-cells during the washout period (Figure 3.1A, 3.1C and 3.4A; 3.8±1.3 cells per islet; n=10). In recovering *fhl1b* MO-injected larvae, we observed that a greater number of green-only β-cells regenerated (Figure 3.1B-C and 3.4A; 9.6±1.4 cells per islet; n=10; *P*=0.00000005).

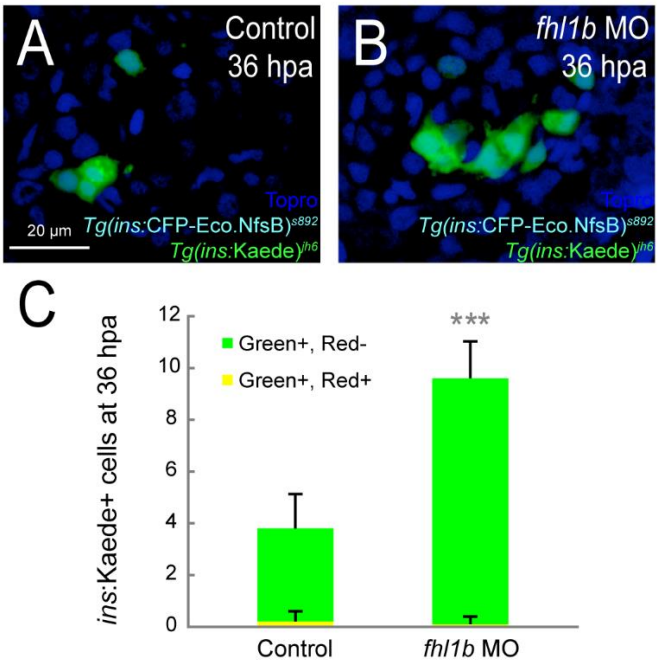

Figure 3.1 Reduction of *fhl1b* activity enhances the capacity of β-cell regeneration.

(A and B) Confocal images of [*Tg(ins:CFP-NTR)*^{s892}; *Tg(ins:Kaede)*^{jh6}] control larvae (A) and *fhl1b* MO-injected (B) larvae at 36 hours-post-ablation (hpa) stained with Topro (blue). A greater number of β-cells regenerated in recovering *fhl1b*-MO injected larvae (B) compared to that of control larvae (A). (C) Quantification of the number (mean±SD) of regenerating and surviving β-cells. After photoconversion and ablation, the surviving β-cells are red and green (yielding a combined color of yellow), whereas the newly formed β-cells are green only. 3.8±1.3 β-cells were green-only-positive in control regenerating larvae, while 9.6±1.4 β-cells expressed as green-only in *fhl1b*-MO injected regenerating larvae. Almost no β-cells survived the ablation in both the control and *fhl1b*-MO injected regenerating larvae. Cells in 20 planes of confocal images from 10 individual larvae were counted. Asterisks indicate statistical significance: ***, $P < 0.001$.

Conversely, we overexpressed *fhl1b* using *Tg(hsp:fhl1b; hsp:GFP)*^{gt3} in conjunction with *Tg*(*ins*:*CFP-NTR*)^{s892} and *Tg(ins:Kaede)*^{jh6} to measure the regenerative efficiency of β-cells in control vs. *fhl1b*-overexpressing larvae. We found that the number of regenerated β-cells significantly decreased when *fhl1b* was induced at 50 hpf (Figure 3.4A; 3.8±1.3 cells per islet in control vs. 1.5±0.5 cells per islet in *fhl1b*-overexpressing larvae; n=10 per each condition; *P*=0.0008). We further examined the underlying mechanism of how Fhl1b modulates the efficiency of β-cell regeneration. At 72 hpf, the number of Islet-positive cells in or adjacent to the hepatopancreatic ductal (HPD) system dramatically decreased after inducing *fhl1b* at 50 hpf even in the presence of Fgf inhibitor SU5402, which induces ectopic Islet1-positive cells in the HPD system (Chung et al., 2010) (Figure 3.2A-C').

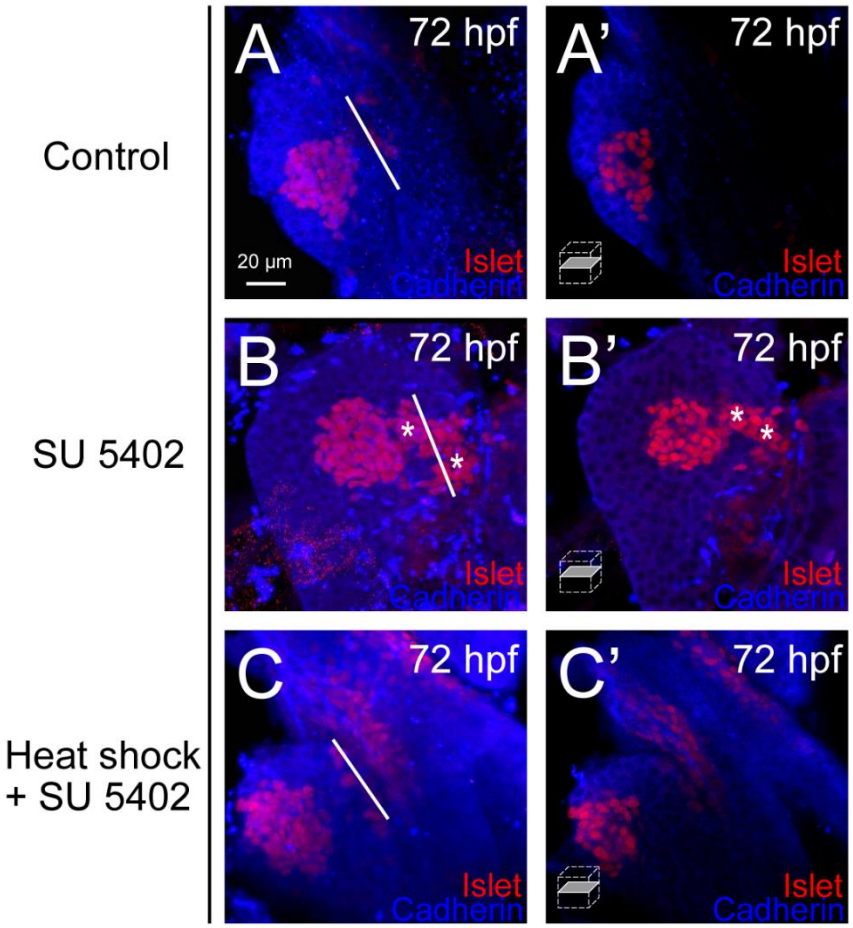

Figure 3.2 Fhl1b blocks induction of late-forming ventral bud-derived endocrine cells.

(A-C') Confocal images of control embryos without SU5402 (A and A') and with SU5402 (B and B') treatment as well as *fhl1b*-overexpressing embryos with SU5402 treatment (C and C', heat shock applied at 50 hpf) at 72 hpf, stained for Islet (red) and Cadherin (blue). Upon treatment of Fgf receptor inhibitor SU5402, ectopic Islet-positive endocrine cells appeared in the hepatopancreatic ductal system (HPD) (B and B', white asterisks). This effect was blocked by overexpression of *fhl1b* (C and C'). The white lines depict the junction between the pancreas and the HPD. A-C, confocal projection images; A'-C', confocal single-plane images, ventral views, anterior to the top. Scale bar, 20 µm.

Conversely, at 72 hpf, *fhl1b* morphants showed a dramatic increase of *pdx1* and *neurod* expression in the principal islet (Figure 3.3A-B, white dotted circles) and in the HPD system (Figure 3.3C-D, white brackets). Intriguingly, *fhl1b* and *pdx1* exhibit a reciprocal expression pattern in control embryos at 3 dpf. The level of *fhl1b* expression is high in the liver (Figure 3.3F, black arrow) and in patches of cells in the distal intestine (Figure 3.3F, white dotted lines), low in the HPD system (Figure 3.3F, white bracket), and absent in most pancreatic cells except for a few cells in the principal islet (Figure 3.3F, yellow arrow). The *pdx1* level of expression is high in the proximal intestine (Figure 3.3E, white dotted lines) and in most pancreatic cells, moderate in the HPD system (Figure 3.3E, white bracket), and absent in the liver (Figure 3.3E).

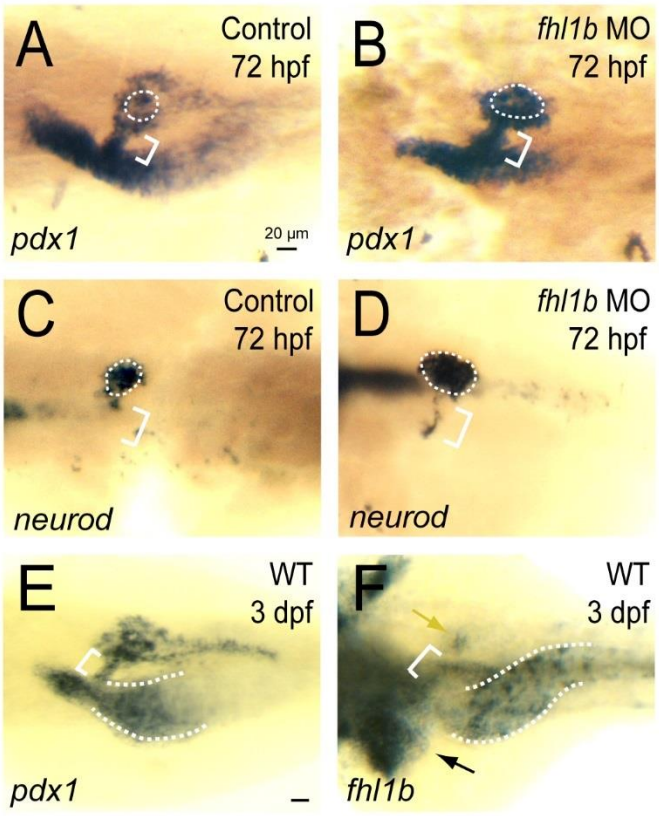

Figure 3.3 Reduction of *fhl1b* activity enhances the expression of *pdx1* and *neurod*.

(A-D) Whole-mount *in situ* hybridization showing the expression of *pdx1* (A and B) and *neurod* (C and D) at 72 hpf, comparing control embryos (A and C) and *fhl1b* morphants (B and D). *pdx1* is expressed in the pancreas including the principal islet (white dotted circles), the HPD system (white brackets), and the proximal intestine, but not in the liver. *neurod* is expressed mainly in the principal islet (white dotted circles) with slight expression in the HPD system (white brackets). *pdx1* (B) and *neurod* (D) expression in the principal islet and the HPD system was greatly increased in *fhl1b* morphants. (E-F) Whole-mount *in situ* hybridization showing the expression of *pdx1* (E) and *fhl1b* (F) in wild-type embryos at 3 days-post-fertilization (dpf). (E) *pdx1* is expressed in the pancreas including the principal islet, the HPD system (white bracket), and the proximal intestine (white dotted line), but not in the liver. (F) *fhl1b* is expressed at high levels in the liver cells (black arrow), which never express *pdx1*, whereas the HPD system (white bracket) expresses low levels of *fhl1b*. Most pancreatic cells except for a few cells in the principal islet (yellow arrow) do not express *fhl1b*. The distal intestine also expresses *fhl1b* (white dotted lines). A-F, dorsal views, anterior to the left. Scale bars, 20 µm.

In line with these expression data, in recovering *fhl1b* MO-injected larvae, multiple regenerating β-cells were found at the junction between the pancreas and the HPD system marked with 2F11 (Zhang et al., 2014) (Figure 3.4B-C; white arrowheads).

A

	Green+ (regenerated β-cells)	Yellow+ (survived β-cells)
Control	3.80±1.33	0.20±0.40
fhl1b MO	9.60±1.43	0.10±0.30
p-value	0.00000005	
HS @ 50 hpf	1.50±0.58	0.20±0.42
p-value	0.000815	

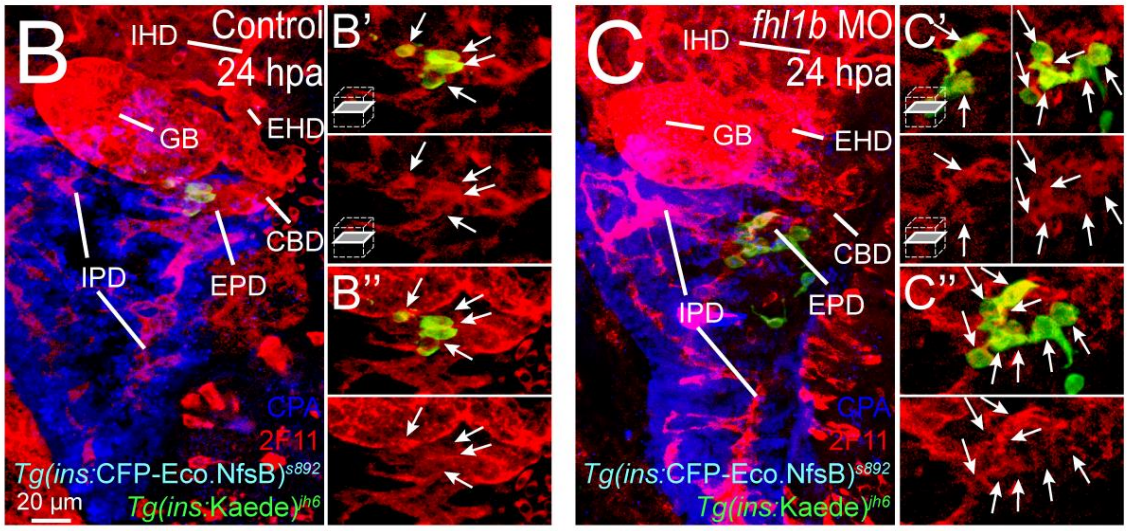

Figure 3.4 Fhl1b enhances neogenesis of β-cell during regeneration.

(A) Quantification of the number (mean±SD) of regenerating (Green^{+}) and surviving cells (Red^{+}) in control, *fhl1b* MO-injected, and *fhl1b*-overexpressing larvae at 36 hours-post-ablation (hpa). Cells in 20 planes of confocal images from 10 individual larvae were counted. (B-C") Confocal single images and projections of [*Tg(ins:CFP-NTR)*^{s892}; *Tg(ins:Kaede)*^{jh6}] control (B-B") and *fhl1b* MO-injected (C-C") larvae at 24 hours-post-ablation (hpa) stained with 2F11 (red) and Carboxypeptidase (blue). A greater number of regenerated β-cells in fhl1b-MO injected larvae were mainly located at the junction between the pancreas and the HPD system, specifically at the EPD (C-C"). While upper insets in B', B", C', and C" show the enlarged images of EPD with white arrows pointing the regenerated β-cells, lower insets in B', B", C', and C" only display the magnified images of EPD with white arrows. Abbreviations: GB, gallbladder; CBD, common bile duct; EHD, extrahepatic duct; EPD, extrapancreatic duct; IHD, intrahepatic duct; IPD, intrapancreatic duct. n = 10 per condition.

Double antibody and in situ hybridization staining in *Tg(ins:GFP)*^{zf5} embryos at 3 dpf showed that in the principal islet, *fhl1b* expression is confined to the peripheral boundary and does not overlap with the centrally located β-cells (Figure 3.5A, yellow arrow) nor does with the δ-cells (Figure 3.5B, black arrowheads) but partially with a small number of α-cells (Figure 3.5C, black arrowheads).

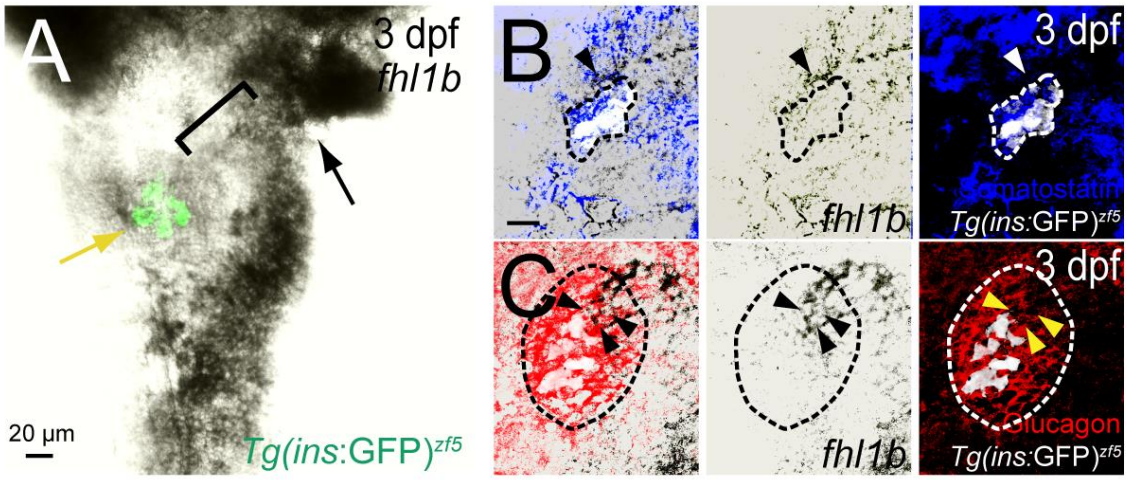

Figure 3.5 *fhlb* expression in the principal islet.

(A) Double antibody and in situ hybridization staining of *fhl1b* at 3 dpf in *Tg(ins:*GFP)^{zf5} embryos. At 3 dpf, the level of *fhl1b* expression is high in the liver (black arrow) and in the distal intestine, low in the HPD system (black bracket), and absent in most pancreatic cells except for a few cells in the principal islet (yellow arrow). In the principal islet, *fhl1b* expression is confined to the peripheral boundary and does not significantly overlap with the core β-cells marked by *Tg(ins:*GFP)^{zf5} expression. n = 10. (E-F) Double antibody and in situ hybridization staining of *fhl1b* with Somatostatin (E) and Glucagon (F) at 3 dpf in *Tg(ins:*GFP)^{zf5} embryos. In the principal islet, *fhl1b* expression (black arrowheads in E and F) does not overlap with the Somatostatin-expressing δ-cells (E) but partially with a small number of Glucagon-expressing α-cells (F). *Tg(ins:*GFP)^{zf5} expression is pseudo colored as white, whereas Somatostatin (E) and Glucagon (F) expression is outlined by both white and black dotted circles. The relative position of *fhl1b*-expressing cells to the Somatostatin (E) and Glucagon (F) expression are indicated by white (E) and yellow (F) arrowheads. Merged views of the middle and right panels are shown in the left panels. n = 10 per condition.

Previous studies showed that glucose is crucial for β-cell differentiation and regeneration (Guillemain et al., 2007; Ye et al., 2015) and acts as a potent β-cell mitogen (Alonso et al., 2007; Bonner-Weir et al., 1989; Porat et al., 2011). To test the possibility of whether Fhl1b regulates β-cell regeneration by affecting liver-derived glucose production, we measured free glucose levels. At 3 dpf, prior to MTZ treatment, there was no significant difference in free glucose levels between control/WT, *fhl1b*-MO injected, and *fhl1b*-overexpressing larvae (Figure 3.6). Free glucose levels were dramatically elevated after β-cell ablation, but were recovered to a great extent from 5-7 dpf in MTZ-treated, MTZ/*fhl1b* MO-injected, and MTZ/*fhl1b*-overexpressing larvae (Figure 3.6). Importantly, normal levels of free glucose were recovered significantly faster in the MTZ/*fhl1b* MO-injected larvae (Figure 3.6, green line) than in the MTZ-treated (Figure 3.6, red line) or MTZ/*fhl1b*-overexpressing larvae (Figure 3.6, purple line). Furthermore, MTZ/*fhl1b*-overexpressing larvae still had increased levels of free glucose at 7 dpf (Figure 3.6, purple line) compared to MTZ-treated (Figure 3.6, red line) or MTZ/*fhl1b* MO-injected larvae (Figure 3.6, green line). Taken together, these data suggest that the activity of Fhl1b on the HPD system, rather than the liver-derived glucose production, can modulate the efficiency in restoration of functional β-cells.

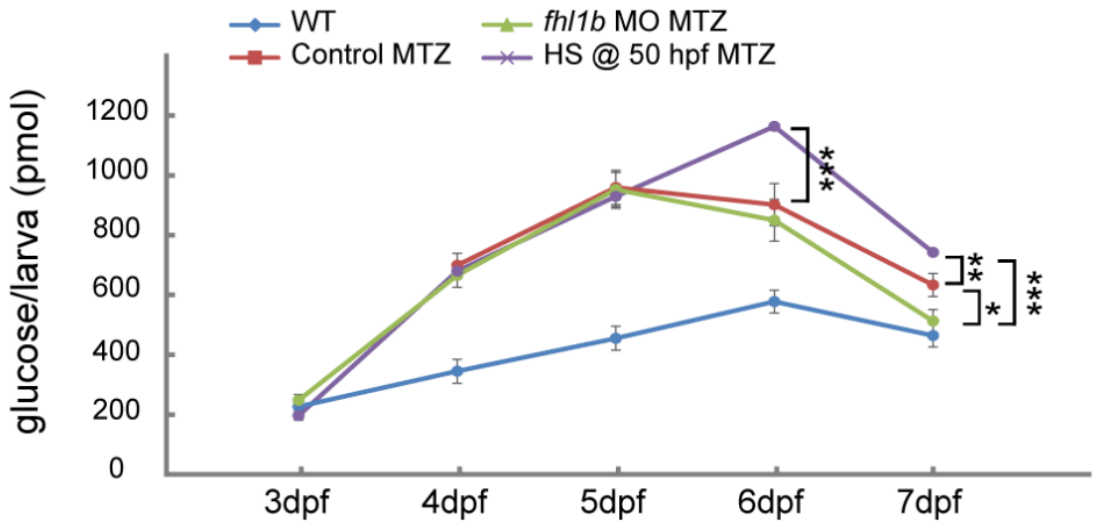

Figure 3.6 Fhl1b enhances the restoration of β-cell function.

Free-glucose levels were measured during β-cell regeneration in wild-type, MTZ-treated, MTZ/*fhl1b* MO-injected, and MTZ/*fhl1b*-overexpressing embryos/larvae. At 7 dpf, free-glucose levels were significantly lower in MTZ/*fhl1b* MO-injected larvae (green line, 512 pmol/larva) than MTZ-treated (red line, 633 pmol/larva) or MTZ/*fhl1b*-overexpressing (purple line, 742 pmol/larva) larvae. *, $P < 0.05$; **, $P < 0.01$; ***, $P < 0.001$. n = 30 larvae (3 pools of 10 larvae) per data point.

3.4.2 Identification of TBK1/IKKε inhibitors as enhancers for β-cell regeneration in zebrafish

Considering inhibition of TBK1/IKKε pathway improves insulin sensitivity in obese mice (Reilly et al., 2013), and the potential regulatory effect of TBK1/IKKε on cAMP via PDE3 (Mowers et al., 2013), we investigated whether TBK1/IKKε pathway is directly involved in pancreatic β-cell regeneration. We tested several TBK1/IKKε inhibitors in the *Tg*(*ins*:*CFP-NTR*)^{s892} line, with *Tg(ins:Kaede)*^{jh6}. MTZ was added at 3 dpf for 24 hours to induce β-cell apoptosis, followed by washing out of MTZ at 4 dpf, and subsequent recovery in the presence or absence of chemical compounds for 48 hours (4-6 dpf, corresponding to 0-48 hpa). Interestingly, we observed that the compound BX795 can approximately double the number of regenerated β-cells at 48 hpa (Figure 3.7B and 3.7E). In addition, biologically well-known TBK1/IKKε inhibitor amlexanox (Reilly et al., 2013), and a cinnamic acid derivative (E)-3-(3-phenylbenzo[c]isoxazol-5-yl)acrylic acid (abbreviated as PIAA), identified using a positional scanning peptide library (PSPL) technology (Hutti et al., 2012) (originally described as (E)-3-(3-phenylbenzo[c]isoxazol-6-yl)acrylic acid (*iso*-PIAA; Figure 3.9A-C)), augmented the number of regenerated β-cells even more drastically (Figure 3.7C-E). Among all, PIAA showed the highest efficiency (Figure 3.7D-E). These results suggest that inhibition of TBK1/IKKε panthway enhances β-cell regeneration.

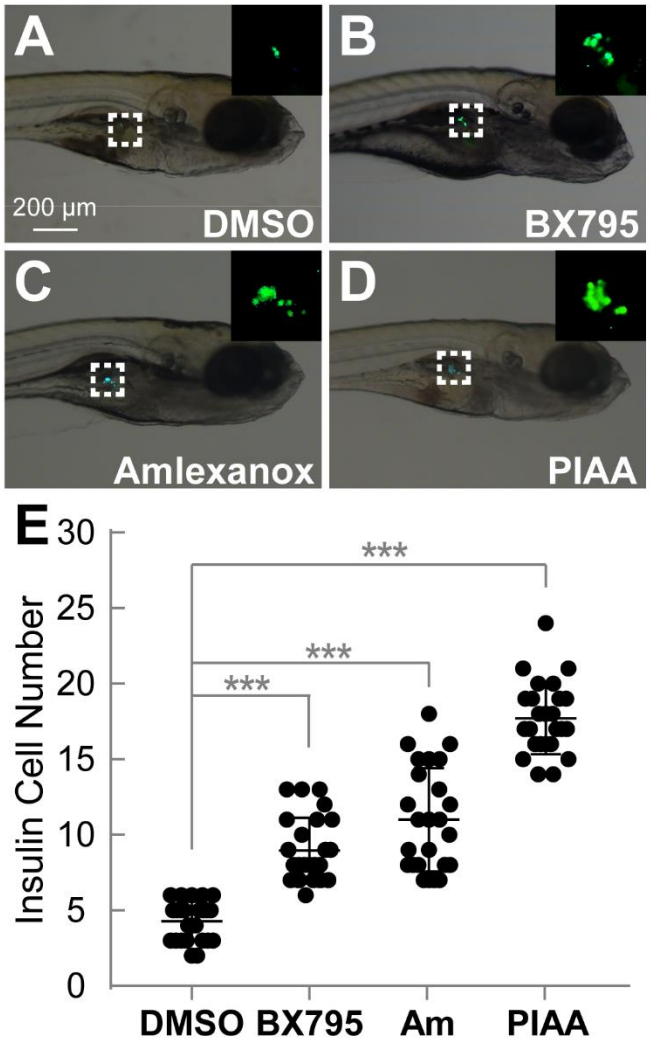

Figure 3.7 TBK1/IKKε inhibition augments β-cell regeneration in zebrafish.

(A-D) Bright-field images combined with fluorescent images showing the overall morphology and [*Tg(ins*:CFP-NTR)^{s892}; *Tg(ins*:Kaede)^{jh6}] expression (green) of larvae at 48 hpa treated with DMSO (A), BX795 (B), amlexanox (C), and PIAA (D), respectively. TBK1/IKKε inhibitors substantially expanded [*Tg(ins*:CFP-NTR)^{s892}; *Tg(ins*:Kaede)^{jh6}]-expressing cell population (white squares and insets) during regeneration (B-D) compared to DMSO (A). (E) Quantification of the number (mean±SD) of total regenerated β-cells at 48 hpa (in A-D; 4.3±1.3 (DMSO), 9.0±2.2 (BX795), 11.0±3.4 (amlexanox), and 17.7±2.4 (PIAA). n=25 larvae per condition. ***, $P < 0.001$.

To further elucidate the direct involvement of TBK1/IKKε pathway in β-cell regeneration, we examined the expression levels of *ikbke* and *tbk1* in various tissues in wild-type and β-cell-ablated larvae. mRNA levels of *ikbke* and *tbk1* are substantially and specifically elevated in the pancreas upon β-cell ablation (Figure 3.8A-B), suggesting that TBK1/IKKε may repress an adaptive regenerative response to β-cell injury.

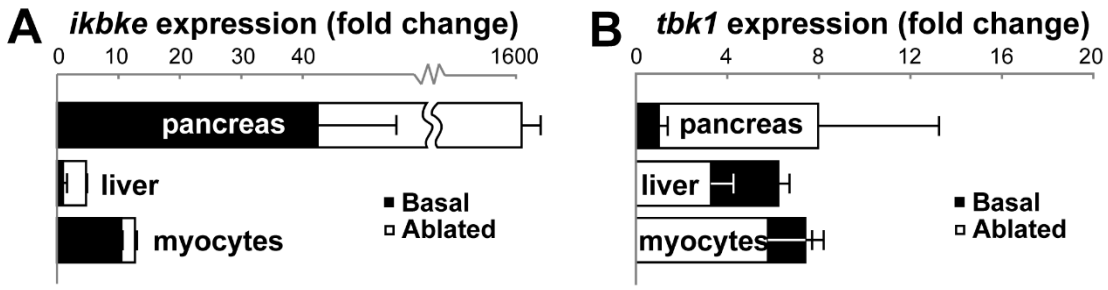

Figure 3.8 Specific expression of TBK1/IKKε in zebrafish pancreas.

(A-B) qRT-PCR results of *ikbke* (A) and *tbk1* (B) in wild-type or β-cell ablated larvae, comparing the fold changes of their expression in relevant tissues/organs. The expression levels of *ikbke* and *tbk1* are significantly and specifically elevated in the pancreas upon β-cell ablation.

To confirm the interactions between TBK1/IKKε and inhibitors, we performed molecular docking simulations in collaboration with Oyelere lab, using the well-characterized TBK1 crystal structure in complex with BX795 (PDB entry 4EUT) (Ma et al., 2012). We observed that amlexanox and PIAA adapt docking poses that closely mimic the crystallographically obtained structure of BX795 by forming multiple hydrogen bonds (H-bonds) with key residues within the kinase domain of TBK1 (Figure 3.9E-G). The core aromatic moieties, the carboxylate of amlexanox and PIAA, and the thiophene amide of BX795 all bound within an unvaried region of the kinase domain (Figure 3.9E-G), while BX795, being a longer molecule, used its urea moiety to extend toward the outer rim of the kinase domain through interaction with the carbonyl group of Pro-90 (Figure 3.9F-G).

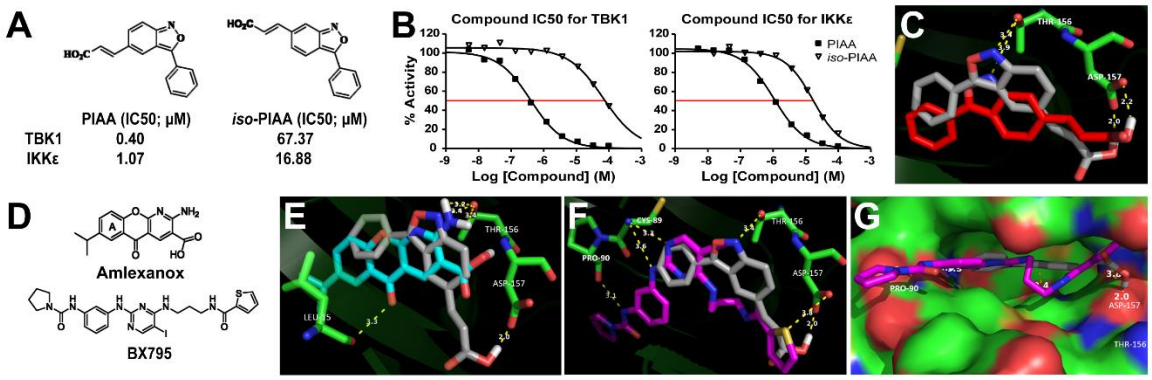

Figure 3.9 Kinase profiling, and molecular docking analyses reveal selectivity of the TBK1/IKKε inhibitors (images C, and E-G provided by Tapadar, S).

(A-B) Chemical structures and kinase profiling of PIAA and *iso*-PIAA. Dose responses of PIAA and *iso*-PIAA were generated to determine the potency of the inhibitors (IC_{50}). (C) Ball and stick model of PIAA (grey) and *iso*-PIAA (red) docked into the binding pocket of TBK1. PIAA adapts a docked pose that has its isoxazole nitrogen and carboxylate moieties engaged in stronger interactions, relative to the same moieties on *iso*-PIAA, with THR-156 and ASP-157 at the active site of TBK1. (D) Chemical structures of amlexanox and BX795. (E-G) Molecular docking simulations showing interactions of TBK1/IKK□-Is and TBK1. Ball and stick model of PIAA (grey), amlexanox (blue), and BX795 (purple) docked into the binding pocket of TBK1 (E and F). Space filling model of PIAA (grey) and BX795 (purple) docked into the binding pocket of TBK1 (G). The core moieties of PIAA, amlexanox, and BX795 all bound within an unvaried region of the kinase domain of TBK1, while the urea moiety of BX795 extends toward the outer rim of the TBK1 kinase domain and interacts with the carbonyl group of Pro-90. Specifically, the carboxylate moieties of PIAA and amlexanox are placed next to the carboxylate side chain of ASP-157 buried in the TBK1 active site, forming a strong low-barrier H-bonding between these two carboxylate groups.

To corroborate the docking simulations, we further performed structure-activity relationship (SAR) studies of PIAA, the most potent β-cell regeneration enhancer among those tested. We synthesized three analogs: PIAA-1 (an analog lacking the carboxylate group), PIAA-2 (a methyl ester analog of PIAA), and PIAA-3 (an analog with an open isoxazolyl ring) (Figure 3.10A-C). The carboxylate group and the intact isoxazolyl ring were both required in enhancing β-cell regeneration, since analogs lacking either group were inactive (Figure 3.10D). Thus, the SAR data and modeling of TBK1 and inhibitor interactions delineate the molecular basis of the selectivity of the TBK1/IKKε inhibitors used in *in vivo* chemical screens. Taken together, these results indicate that suppression of TBK1/IKKε augments β-cell regeneration in the zebrafish model of type I diabetes.

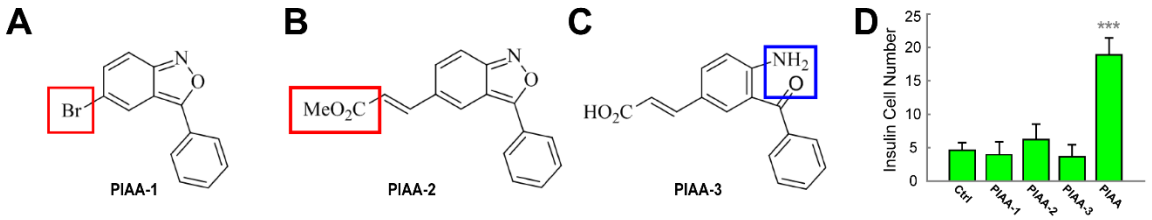

Figure 3.7 Structure-activity relationship analysis reveals selectivity of the TBK1/IKKε inhibitors (images A-C provided by Tapadar, S).

(A-C) Chemical structures of three PIAA analogs. The moieties that were replaced and different from the original PIAA structure are marked in red (PIAA-1 and PIAA-2) or blue (PIAA-3). (D) Quantification of the number (mean±SD) of total regenerated β-cells at 48 hpa treated with DMSO, PIAA 1, PIAA 2, PIAA 3, and PIAA, respectively (4.8±0.8 (DMSO), 4.2±1.3 (PIAA 1), 6.2±1.3 (PIAA 2), 4.0±1.2 (PIAA 3), and 18.6±3.4 (PIAA)). Cells in 20 planes of confocal images from 10 individual larvae were counted. ***, $P < 0.001$.

3.4.3 TBK1/IKKε inhibitors specifically promote β-cell proliferation

3.4.3.1Repression of TBK1/IKKε increases β-cell regeneration by primarily promoting their proliferation

To exclude a substantial contribution of pre-existing β-cells to regeneration of β-cells, we converted the fluorescence of the Kaede protein from green to red by exposing the [*Tg*(*ins*:*CFP-NTR*)^{s892}; *Tg(ins:Kaede)*^{jh6}] larvae to UV light at 3 dpf immediately after MTZ treatment (Figure 3.11A). We found that 48 hpa islets contained only unconverted green-only β-cells both in DMSO- or TBK1/IKKε inhibitor-treated recovering larvae with a greater number of green-only β-cells in TBK1/IKKε inhibitor-treated larvae (Figure 3.11B). These results demonstrate that essentially all β-cells were ablated by MTZ treatment and that TBK1/IKKε inhibitors augment the number of the newly formed β-cells.

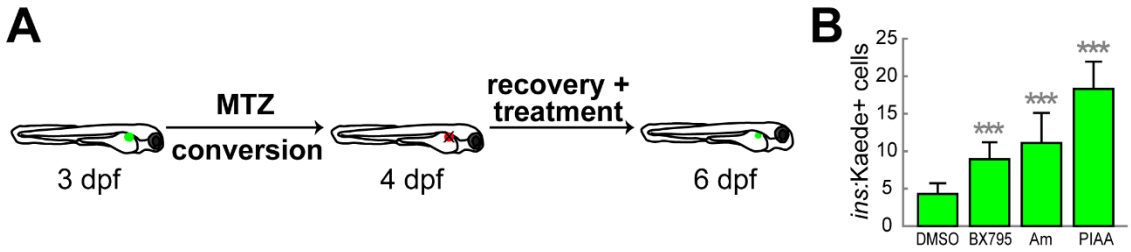

Figure 3.8 TBK1/IKKε inhibition augments β-cell regeneration in zebrafish.

(A) Schematic diagram for assessment of ablation efficiency of β-cells. (B) Quantification of the number (mean±SD) of newly regenerated (Green^{+}) β-cells at 48 hpa (4.4±1.6 β-cells were green-only-positive in DMSO-treated larvae, while 9.3±2.2 (BX795), 11.1±4.4 (amlexanox), and 18.1±3.6 (PIAA) β-cells expressed as green-only in TBK1/IKKε inhibitor-treated recovering larvae). Cells in 20 planes of confocal images from 10 individual larvae were counted. ***, $P < 0.001$.

The TBK1/IKKε inhibitor-induced increase in the number of newly regenerated β-cells could result from enhanced proliferation of β-cells, stimulation of neogenesis from non-β-cells, or both (Baeyens et al., 2014; Dor et al., 2004; Thorel et al., 2010; Xu et al., 2008). Hence, we determined the effect of TBK1/IKKε suppression on β-cell proliferation by performing cell cycle analysis with the replication marker 5-ethynyl-2'-deoxyuridine (EdU). [*Tg*(*ins*:*CFP-NTR*)^{s892}; *Tg(ins:Kaede)*^{jh6}] larvae were treated with MTZ from 3–4 dpf to ablate the β-cells, and subsequently treated with EdU and DMSO or TBK1/IKKε inhibitors for 48 hours (4-6 dpf, corresponding to 0-48 hpa). The number of β-cells that incorporated EdU was significantly greater in TBK1/IKKε inhibitor-treated larvae than in DMSO-treated larvae (Figure 3.12).

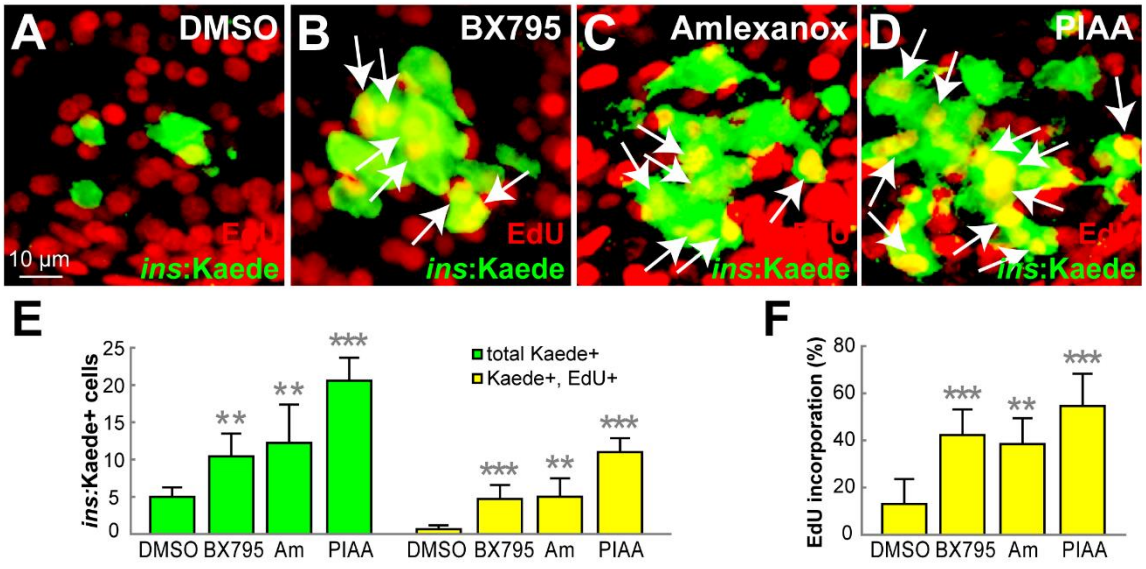

Figure 3.9 TBK1/IKKε inhibitors promote β-cell replication.

(A-D) Confocal images of [*Tg(ins*:*CFP-NTR)*^{s892}; *Tg(ins*:*Kaede)*^{jh6}] larvae at 48 hpa, concurrently treated with EdU and DMSO (A), BX795 (B), amlexanox (C), or PIAA (D), respectively, from 0-48 hpa. The number of β-cells that incorporated EdU (white arrows) was substantially increased in TBK1/IKKε inhibitor-treated recovering larvae (B-D) compared to DMSO-treated larvae (A). (E) Quantification of the number (mean±SD) of total regenerated β-cells (green bars) and regenerated β-cells that incorporated EdU (yellow bars) at 48 hpa (in A-D; 5.0±1.3 total regenerated β-cells, of which 0.7±0.5 (DMSO), 11.0±3.4, of which 4.6±1.8 (BX795), 12.8±4.8, of which 5.2±2.8 (amlexanox), and 20.6±3.1, of which 11.0±1.9 (PIAA) incorporated EdU). (F) The percentage (mean±SD) of regenerated β-cells that incorporated EdU at 48 hpa (in A-D; 13.0±11.0% (DMSO), 42.0±5.0% (BX795), 39.0±7.0% (amlexanox), and 55.0±14.0% (PIAA)). Cells in 20 planes of confocal images from 10 individual larvae were counted. **, $P < 0.01$; ***, $P < 0.001$.

A previous study showed that β-cell neogenesis occurs through both α-to-β-cell transdifferentiation and ductal progenitor-to-β-cell conversion during the initial stages of regeneration in zebrafish (Ye et al., 2015). Administering TBK1/IKKε inhibitors, specifically amlexanox and PIAA, for 24 hours (from 4-5 dpf) rather than for 48 hours (from 4-6 dpf), caused a slight increase in the number of cells that co-express Insulin and Glucagon (Figure 3.13E-H). There was minimal enhancement of the number of β-cells in/adjacent to the hepatopancreatic ductal (HPD) system and that of cells co-expressing Insulin and Somatostatin (Figure 3.13A-D). These results indicate that TBK1/IKKε repression does not primarily affect β-cell neogenesis.

To further test whether these compounds increase proliferation of newly formed β-cells, we introduced a transitional day between β-cell ablation and TBK1/IKKε inhibitor treatment. This time lag allowed MTZ-induced ablation to conclude and the default neogenesis to begin before the compounds were added. Amlexanox and PIAA both potently increased the number of EdU incorporated β-cells with the transitional day (Figure 3.14A-B). Taken together, these data suggest that TBK1/IKKε suppression enhances β-cell proliferation to promote regeneration of β-cells.

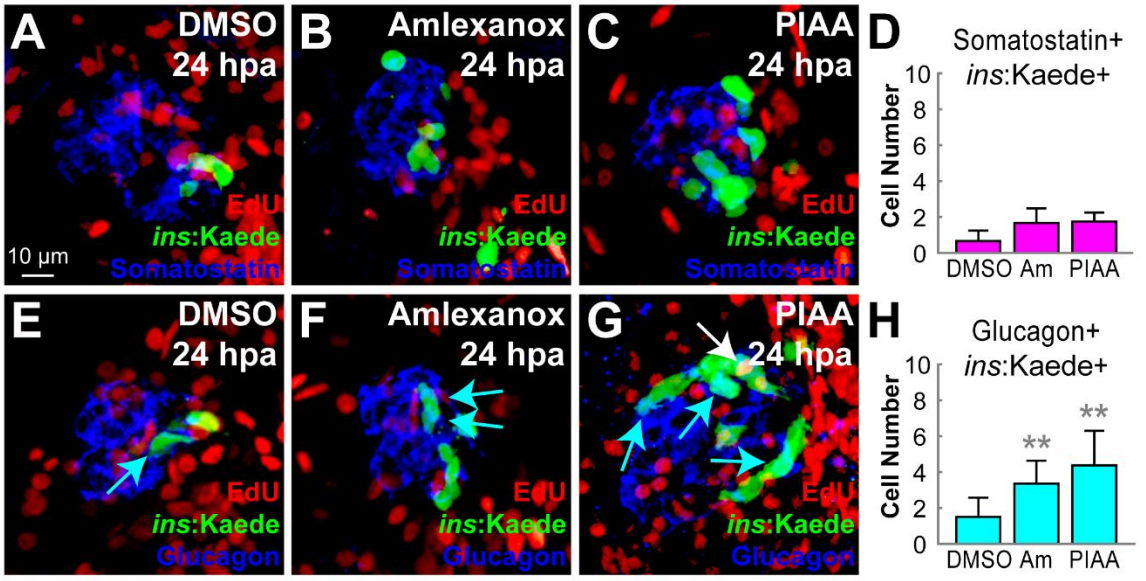

Figure 3.10 TBK1/IKKε inhibitors have modest effects on α-to-β-cell transdifferentiation.

(A-C) Confocal images of [*Tg(ins:CFP-NTR)*^{s892}; *Tg(ins:Kaede)*^{jh6}] larvae at 24 hpa, concurrently treated with EdU and DMSO (A), amlexanox (B), or PIAA (C), respectively, from 0-24 hpa, stained for Somatostatin (blue). (D) Quantification of the number (mean±SD) of Insulin and Somatostatin-double positive cells at 24 hpa (in A-C; 0.7±0.6 (DMSO), 1.7±0.8 (amlexanox), and 1.8±0.5 (PIAA)). (E-G) Confocal images of [*Tg(ins:CFP-NTR)*^{s892}; *Tg(ins:Kaede)*^{jh6}] larvae at 24 hpa, concurrently treated with EdU and DMSO (E), amlexanox (F), or PIAA (G), respectively, from 0-24 hpa, stained for Glucagon (blue). Note that the number of Insulin and Glucagon-double positive cells (blue arrows) was increased in TBK1/IKKε inhibitor-treated recovering larvae (F and G) compared to DMSO-treated larvae (E). PIAA-treated larvae also showed an EdU-incorporated β-cell (white arrow) (G). (H) Quantification of the number (mean±SD) of Insulin and Glucagon-double positive cells at 24 hpa (in E-G; 1.5±1.1 (DMSO), 3.4±1.3 (amlexanox), and 4.4±1.9 (PIAA)). Cells in 20 planes of confocal images from 10 individual larvae were counted. **, $P < 0.01$.

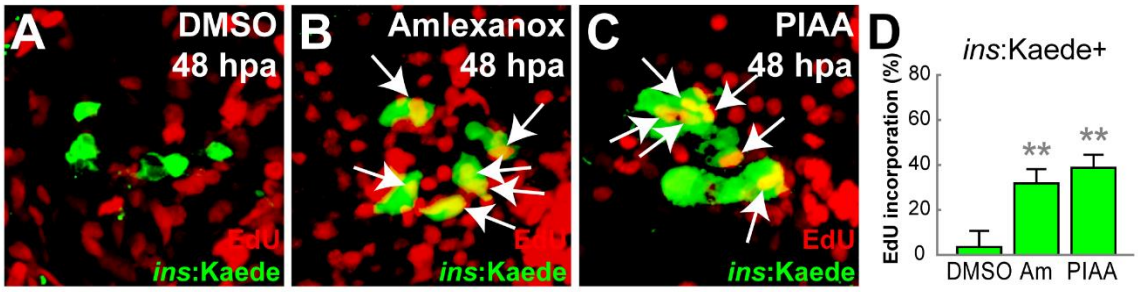

Figure 3.11 TBK1/IKKε inhibitors strongly enhance β-cell proliferation.

(A-C) Confocal images of [*Tg(ins*:*CFP-NTR)*^{s892}; *Tg(ins*:*Kaede)*^{jh6}] larvae at 48 hpa, concurrently treated with EdU and DMSO (A), amlexanox (B), or PIAA (C), respectively, from 24-48 hpa. The number of β-cells that incorporated EdU (white arrows) was significantly increased in TBK1/IKKε inhibitor-treated recovering larvae (B and C) compared to DMSO-treated larvae (A). (B) The percentage (mean±SD) of regenerated β-cells that incorporated EdU at 48 hpa (in A-C; 4.0±7.0% (DMSO), 32.0±6.0% (amlexanox), and 39.0±6.0% (PIAA)). Cells in 20 planes of confocal images from 10 individual larvae were counted. **, $P < 0.01$.

3.4.3.2 TBK1/IKKε inhibition selectively accelerates proliferation of β-cells

To determine whether TBK1/IKKε inhibitors increase proliferation of β-cells specifically or whether they trigger a general increase in cell proliferation, we assessed the replication rate of other pancreatic endocrine cells and tissues, specifically Somatostatin-producing δ-cells, Glucagon-producing α-cells, and liver cells. Inhibition of TBK1/IKKε led to minimal increase of EdU incorporation in δ-cells, whereas it enhanced proliferation of β-cells in the regenerating pancreas (Figure 3.15A-D). TBK1/IKKε inhibitors also displayed no significant effects on α-cell replication (Figure 3.15E-H).

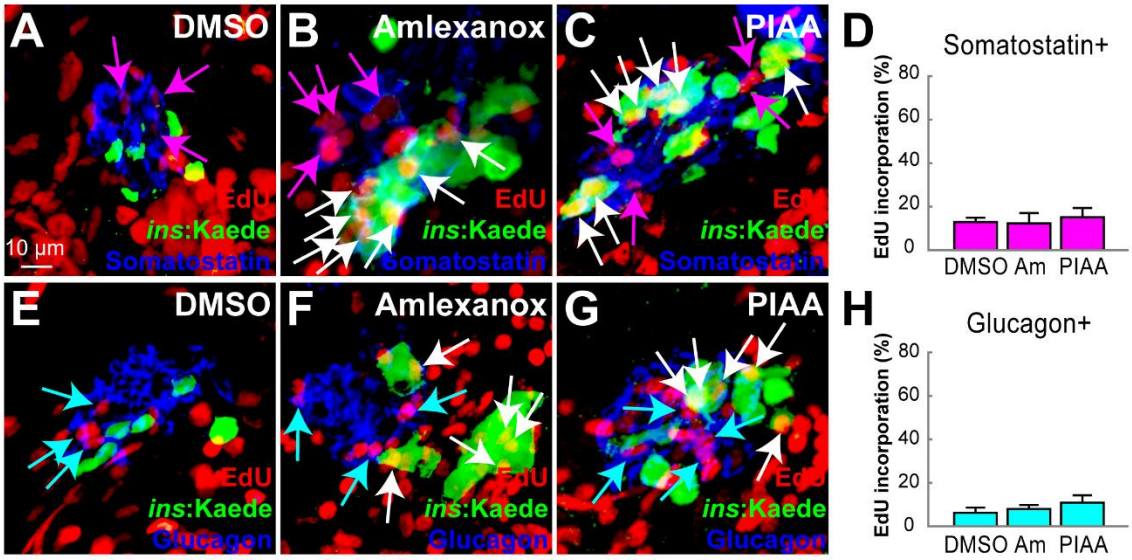

Figure 3.12 TBK1/IKKε inhibitors selectively increase the number of β-cells.

(A-C) Confocal images of [*Tg(ins*:*CFP-NTR)*^{s892}; *Tg(ins*:*Kaede)*^{jh6}] larvae at 48 hpa, concurrently treated with EdU and DMSO (A), amlexanox (B), or PIAA (C), respectively, from 0-48 hpa, stained for Somatostatin (blue). The number of Somatostatin-expressing δ-cells that incorporated EdU (purple arrows) did not increase in TBK1/IKKε inhibitor-treated recovering larvae (B and C) compared to DMSO-treated larvae (A). (D) The percentage (mean±SD) of δ-cells that incorporated EdU at 48 hpa (in A-C; 12.9±2.0% (DMSO), 12.4±4.7% (amlexanox), and 15.1±4.3% (PIAA)). Cells in 20 planes of confocal images from 10 individual larvae were counted. (E-G) Confocal images of [*Tg(ins*:*CFP-NTR)*^{s892}; *Tg(ins*:*Kaede)*^{jh6}] larvae at 48 hpa, concurrently treated with EdU and DMSO (E), amlexanox (F), or PIAA (G), respectively, from 0-48 hpa, stained for Glucagon (blue). The number of Glucagon-expressing α-cells that incorporated EdU (blue arrows) did not increase in TBK1/IKKε inhibitor-treated recovering larvae (F and G) compared to DMSO-treated larvae (E). (H) The percentage (mean±SD) of α-cells that incorporated EdU at 48 hpa (in E-G; 6.2±2.4% (DMSO), 8.0±1.9% (amlexanox), and 10.9±3.4% (PIAA)). Cells in 20 planes of confocal images from 10 individual larvae were counted.

Furthermore, there was no considerable difference between DMSO- and TBK1/IKKε inhibitor-treated larvae on the number of liver cells that incorporated EdU (Figure 3.16).

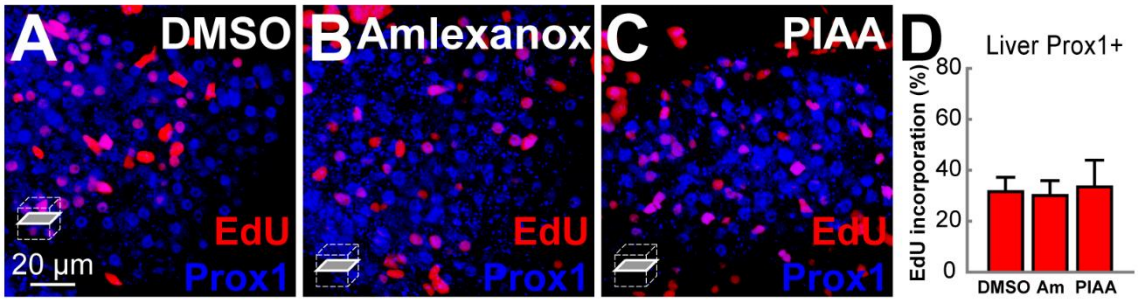

Figure 3.13 TBK1/IKKε inhibitors do not increase proliferation of liver cells.

(A-C) Confocal single-plane images of [*Tg(ins*:*CFP-NTR)*^{s892}; *Tg(ins*:*Kaede)*^{jh6}] larvae at 48 hpa, concurrently treated with EdU and DMSO (A), amlexanox (B), or PIAA (C), respectively, from 0-48 hpa, stained for Prox1 (blue). The number of Prox1-positive cells in the liver that incorporated EdU did not significantly increase in TBK1/IKKε inhibitor-treated recovering larvae (B and C) compared to DMSO-treated larvae (A). (D) The percentage (mean±SD) of Prox1-positive liver cells that incorporated EdU at 48 hpa (in A-C; 31.6±5.6% (DMSO), 30.1±5.8% (amlexanox), and 33.5±10.5% (PIAA)). Cells in 10 planes of confocal images from 5 individual larvae were counted.

A longer treatment with TBK1/IKKε inhibitors, for 96 hours after β-cell ablation, showed that TBK1/IKKε inhibitor treatment did not lead to an overshoot in β-cell number (Figure 3.17). These results suggest that suppression of TBK1/IKKε enhances β-cell proliferation during the most dynamic period of β-cell regeneration without inducing a general increase in proliferation of other cell types and tissues.

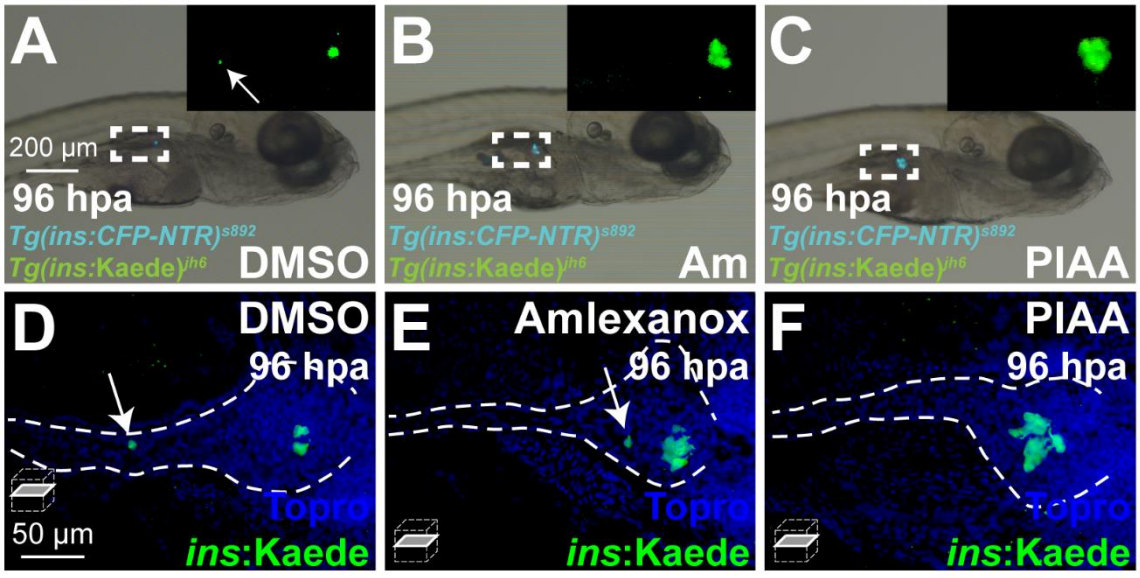

Figure 3.14 TBK1/IKKε inhibitors do not lead to an overshoot in β-cell number.

(A-C) Bright-field images combined with fluorescent images showing the overall morphology of embryos and [*Tg(ins*:CFP-NTR)^{s892}; *Tg(ins*:Kaede)^{jh6}] expression (green) in larvae at 96 hpa treated with DMSO (A), amlexanox (B), and PIAA (C), respectively. While TBK1/IKKε inhibitors treatment expanded [*Tg(ins*:CFP-NTR)^{s892}; *Tg(ins*:Kaede)^{jh6}]-expressing cell population (white squares and insets) during regeneration (B and C) compared to DMSO (A), a longer treatment (0-96 hpa) did not result in overproliferation of β-cells. (D-F) Confocal single-plane images of [*Tg(ins*:*CFP-NTR)*^{s892}; *Tg(ins*:*Kaede)*^{jh6}] larvae at 96 hpa (in A-C), stained with Topro (blue). White arrows indicate β-cells located in secondary islets.

Next, we examined the ability of TBK1/IKKε inhibitors to restore normoglycemia. Free glucose levels were elevated after β-cell ablation, but declined from 24-72 hpa (corresponding to 5-7 dpf) in DMSO- and TBK1/IKKε inhibitor-treated larvae. Importantly, normal levels of free glucose were recovered significantly faster in TBK1/IKK□-I-treated, especially PIAA-treated, larvae than in DMSO-treated larvae (Figure 3.18). Altogether, these data suggest that inhibition of TBK1/IKKε induces selective increase in β-cell number that accelerates restoration of sufficient overall β-cell function.

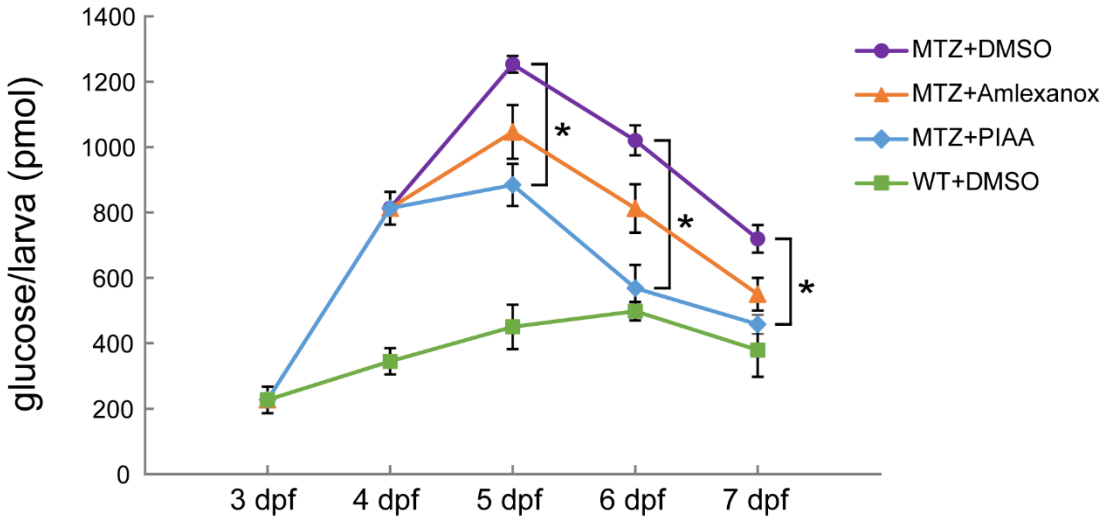

Figure 3.15 TBK1/IKKε inhibitors accelerate restoration of β-cell function.

Free-glucose levels (mean±SD) during β-cell regeneration in non-ablated wild type, DMSO-treated recovering, and TBK1/IKKε inhibitor-treated recovering larvae. At 7 dpf, free-glucose levels were significantly lower in PIAA-treated recovering larvae (blue line, 457.7±28.8 pmol/larva) than in DMSO-treated larvae (purple line, 719.3±42.2 pmol/larva). *, $P < 0.05$. n = 30 larvae (3 pools of 10 larvae) per data point.

3.4.3.3 Repression of TBK1/IKKε enhances β-cell replication via cAMP activation

Given the previous studies showing increased cAMP levels in adipocytes induced by inhibition of TBK1/IKKε (Mowers et al., 2013), and direct phosphorylation and activation of PDE3B *in vitro* by TBK1 and IKKε (Mowers et al., 2013), we hypothesized that inhibition of TBK1/IKKε induces the activity of the cAMP for β-cell regeneration via suppression of a TBK1/IKKε-PDE3 signaling axis (Figure 3.19A). To test this hypothesis, we first measured the cellular cAMP levels in the PIAA-treated regenerating larvae. Treatment with PIAA led to pronounced increases in cAMP levels (Figure 3.19B). Furthermore, we assessed the effects of ectopic expression of *pde3a* on mitogenic potential of inhibition of TBK1/IKKε using a heat-inducible transgene *Tg(hsp*:*pde3a; hsp*:*GFP)*^{gt4}. Pde3a is the only PDE3 isoform in zebrafish and its expression is significantly and specifically elevated in the pancreas upon β-cell ablation (Figure 3.19C).

When *pde3a* expression was induced during recovery period in the presence of PIAA, the proportion of new β-cells that proliferate was decreased compared to PIAA-only-treated larvae (Figure 3.20B-D). These data suggest that suppression of TBK1/IKKε bestows an increase in β-cell number by regulating cAMP activity through PDE3 in the zebrafish model of type I diabetes.

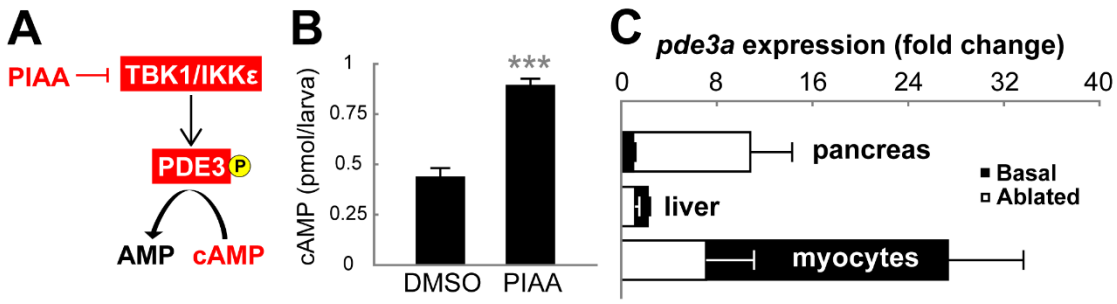

Figure 3.16 The TBK1/IKKε-PDE3-cAMP signaling axis during β-cell regeneration.

(A) Schematic of the TBK1/IKKε-PDE3 signaling that modulates cAMP levels. (B) Quantification of cAMP levels (mean±SD) at 48 hpa (0.4±0.1 pmol/larva (DMSO) and 0.9±0.0 pmol/larva (PIAA)). (C) qRT-PCR results of *pde3a* in wild-type or β-cell ablated larvae, comparing the fold changes of their expression in relevant tissues/organs. The expression levels of *pde3a* are significantly and specifically elevated in the pancreas upon β-cell ablation. n=20 larvae per condition. ***, $P < 0.001$.

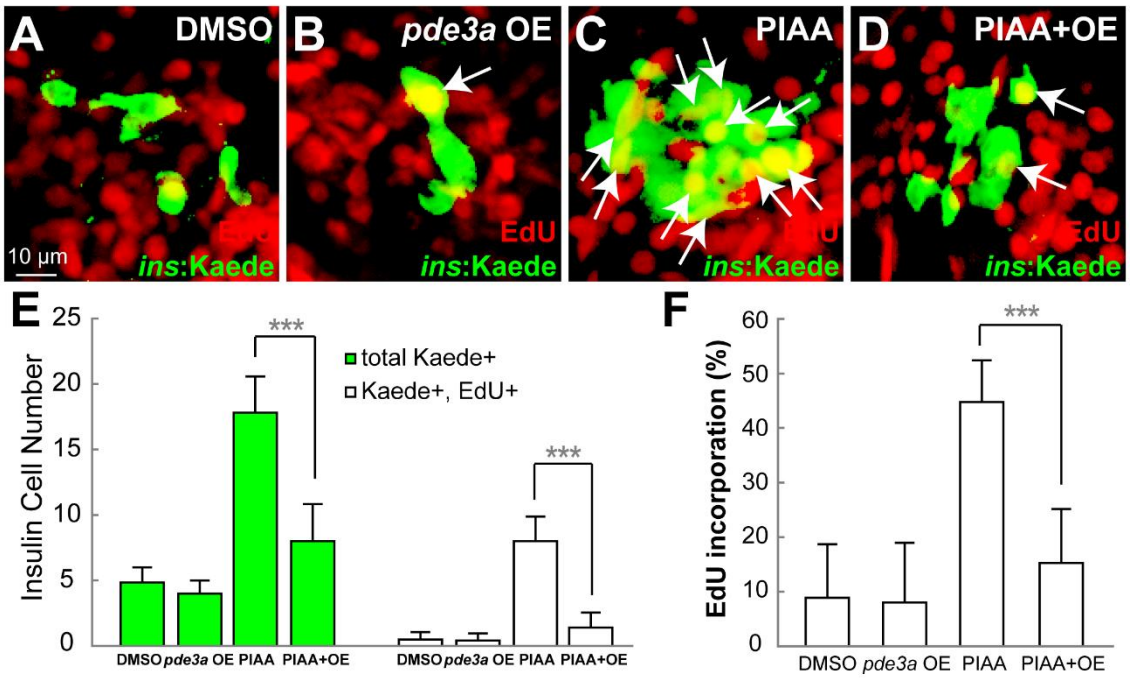

Figure 3.17 Suppression of the TBK1/IKKε-PDE3 signaling axis promotes β-cell proliferation.

(A-D) Confocal images of EdU-administered [*Tg(ins:CFP-NTR)*^{s892}; *Tg(ins:Kaede)*^{jh6}] larvae at 48 hpa, treated with DMSO (A) and PIAA (C), respectively, or induced *pde3a* expression upon β-cell ablation (B) and *pde3a* expression upon β-cell ablation in the presence of PIAA (D), respectively, from 0-48 hpa. The number of EdU-incorporated (white arrows) β-cells was increased in recovering larvae treated with PIAA (C) compared to DMSO-treated larvae (A). When *pde3a* expression was induced upon β-cell ablation, PIAA-dependent increases in the number of EdU-incorporated β-cells were suppressed (D). (E) Quantification of the number (mean±SD) of total regenerated β-cells (green bars) and regenerated β-cells that incorporated EdU at 48 hpa (in A-D; 4.8±1.2 total regenerated β-cells, of which 0.6±0.6 (DMSO), 4.0±1.0, of which 0.5±0.5 (*pde3a* overexpressing), 17.8±2.8, of which 8.9±2.0 (PIAA), and 8.0±2.8, of which 1.7±1.2 (*pde3a* overexpressing in the presence of PIAA)). (F) The percentage (mean±SD) of regenerated β-cells that incorporated EdU at 48 hpa (in A-D; 9.4±10.5% (DMSO), 8.8±11.6% (*pde3a* overexpressing), 46.5±8.3% (PIAA), and 16.1±10.5% (*pde3a* overexpressing in the presence of PIAA)). Cells in 20 planes of confocal images from 10 individual larvae were counted. ***, $P < 0.001$.

3.4.4 TBK1/IKKε inhibition augments β-cell function and proliferation in mammalian systems

To determine whether the effects of TBK1/IKKε suppression on β-cells are conserved across species, we collaborated with Garcia lab and first performed glucose-stimulated insulin release (GSIR) assay in primary rat and human islets as elevation of cAMP levels has shown to lead to both improved insulin secretion and enhanced replication of β-cells (Inada et al., 2004; Xie et al., 2007; Zhao et al., 2014). PIAA treatment significantly increased glucose stimulation indices in rat and human islets (Figure 3.22D and 3.23D). Next, we investigated mitogenic effect of TBK1/IKKε inhibition by analyzing the ability of TBK1/IKKε inhibitors to increase β-cell proliferation in INS-1 rat pancreatic β-cells. Treating INS-1 cells with PIAA resulted in increased percentage of proliferating Insulin-positive cells (co-expressed Ki-67) (Figure 3.21A-C), and cAMP levels (Figure 3.21D), suggesting that suppression of TBK1/IKKε promotes replication of β-cells via activation of the cAMP in mammalian systems.

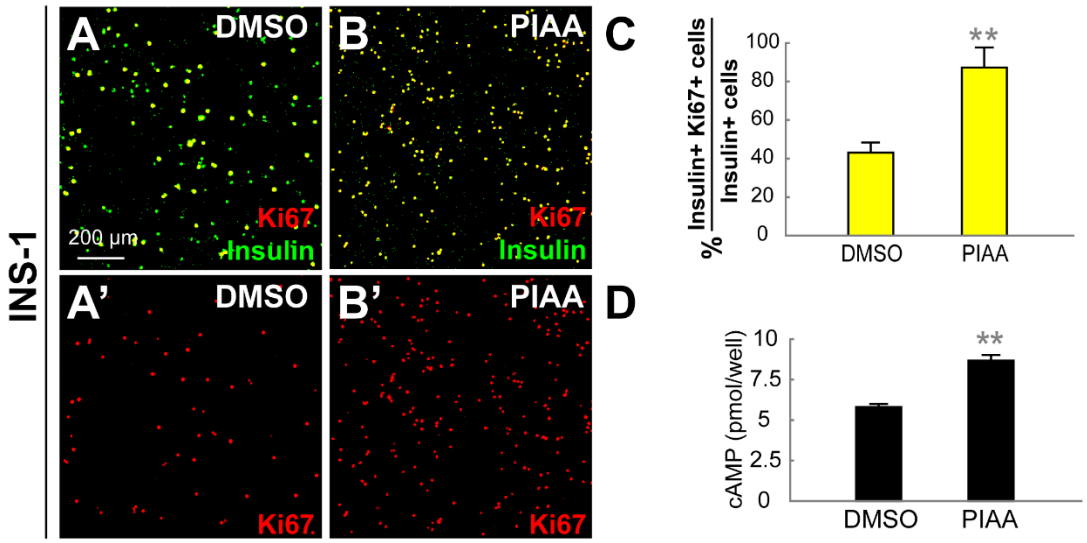

Figure 3.18 PIAA induces proliferation of cultured rat β-cells.

(A-B') Confocal images of rat INS-1 β-cells treated with DMSO (A-A') and PIAA (B-B'), respectively, stained for Ki67 (red) and Insulin (green). (C) The percentage (mean±SD) of Ki67 and Insulin-double positive cells (in A-B'; 43.1±5.2% (DMSO) and 87.3±10.4% (PIAA)). (D) Quantification of cAMP levels (mean±SD) (5.8±0.2 pmol/well (DMSO) and 8.7±0.4 pmol/well (PIAA)). **, $P < 0.01$.

PIAA increased β-cell proliferation in whole rat islets in a dose-dependent manner (Figure 3.22A-C). Importantly, treatment of PIAA on primary human β-cells using islets obtained from 3 cadaveric organ donors caused a notable, dose-dependent induction of β-cell proliferation (Figure 3.23A-C).

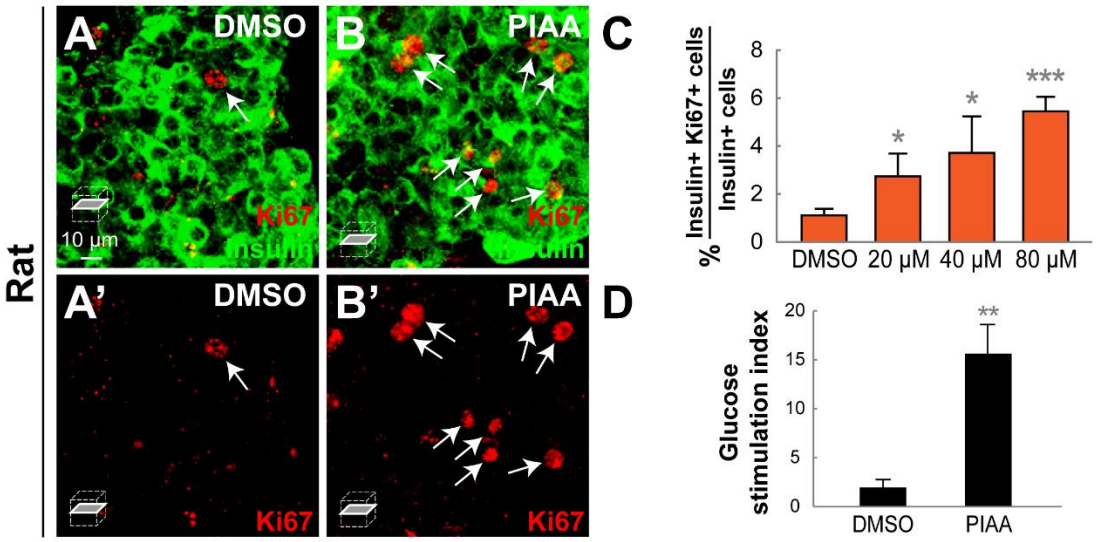

Figure 3.19 PIAA induces proliferation of cultured rat islets (image D provided by Weaver, J).

(A-B') Confocal single-plane images of whole rat islets treated with DMSO (A-A') and PIAA (B-B'), respectively, stained for Ki67 (red, white arrows) and Insulin (green). (C) The percentage (mean±SD) of Ki67 and Insulin-double positive cells in whole rat islets increased in a dose-dependent manner with treatment of PIAA (1.1±0.3% (DMSO), 2.7±0.9% (20 µM), 3.7±1.5% (40 µM), and 5.5±0.6% (80 µM)). n=5 replicates per condition. (D) Glucose stimulation indices of rat islets treated with DMSO or PIAA (300 islet equivalents per column, triplicate). *, $P < 0.05$; **, $P < 0.01$; ***, $P < 0.001$.

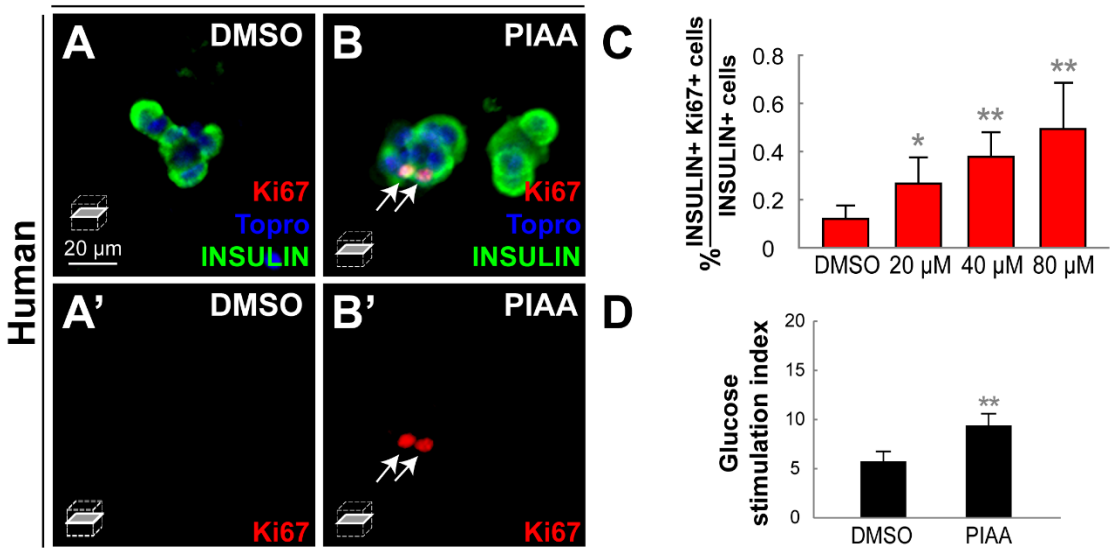

Figure 3.20 PIAA induces proliferation of cultured human islets (image D provided by Weaver, J).

(A-B') Confocal single-plane images of human islets treated with DMSO (A-A') and PIAA (B-B'), respectively, stained for Ki67 (red, white arrows), Topro (blue), and INSULIN (green). (C) The percentage (mean±SD) of Ki67 and Insulin-double positive cells in human islets increased in a dose-dependent manner with treatment of PIAA (0.1±0.0% (DMSO), 0.3±0.1% (20 μM), 0.4±0.1% (40 μM), and 0.5±0.2% (80 μM)). n=5 replicates per condition from 3 cadaveric donors. (D) Glucose stimulation indices of human islets treated with DMSO or PIAA (300 islet equivalents per column, triplicate). *, $P < 0.05$; **, $P < 0.01$; ***, $P < 0.001$.

We further investigated whether PIAA could increase β-cell regeneration in the streptozotocin (STZ)-induced mouse model of type I diabetes. First we checked if TBK1/IKKε exhibit distinct expression pattern in mouse tissues. Indeed, *Ikbke* and *Tbk1* show prominent basal and induced expression in the pancreas and white adipose tissue (WAT) upon STZ treatment (Figure 3.24A-B).

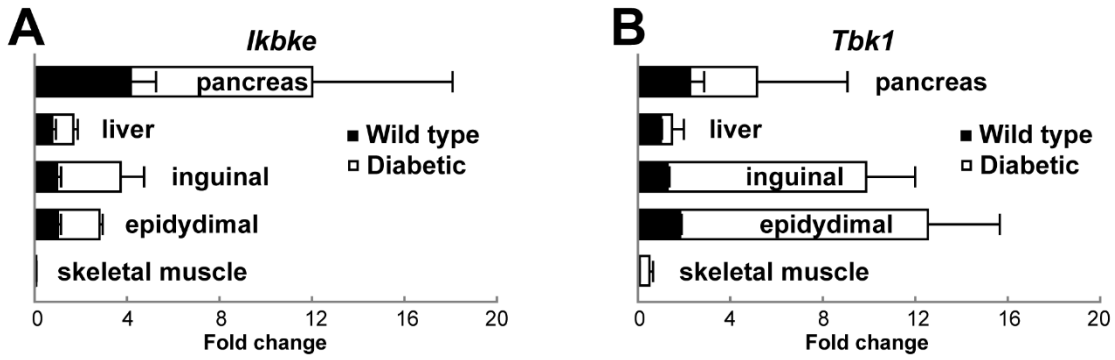

Figure 3.21 Prominent expression of TBK1/IKKε in murine pancreas and white adipose tissue.

(A-B) qRT-PCR results of *Ikbke* and *Tbk1* in wild-type or STZ-induced diabetic mice, comparing the fold changes of their expression in relevant tissues/organs. *Ikbke* and *Tbk1* show prominent basal and induced expression in the pancreas and white adipose tissue (WAT) upon STZ treatment. n=3 mice per group, triplicate.

PIAA administration caused a substantial reduction of non-fasting blood glucose levels after 4-5 days of intraperitoneal injection (Figure 3.25A). Significant improvement of glucose tolerance was observed compared with vehicle treatment (Figure 3.25B).

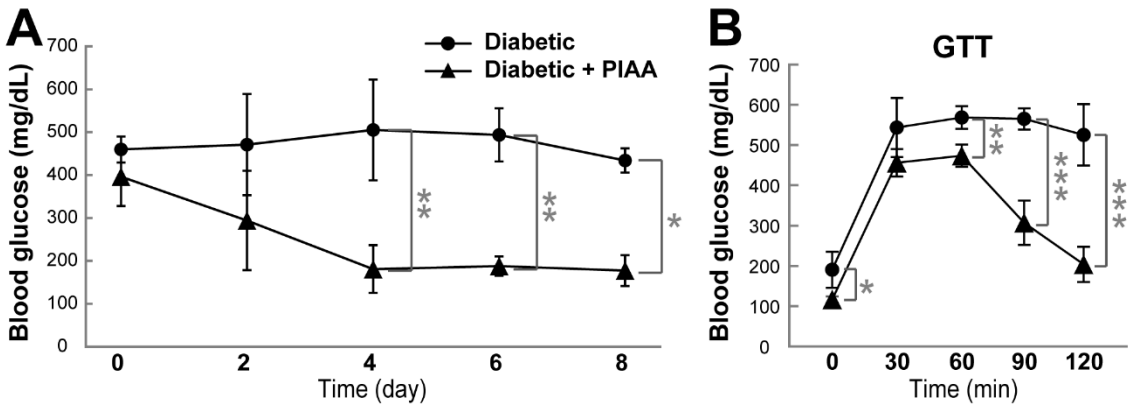

Figure 3.22 PIAA improves glucose control in the STZ-induced diabetes murine model.

(A-B) STZ-induced diabetic mice were treated with vehicle or PIAA for 8 days after disease induction (n=6 mice per group). (A) PIAA caused reduction of hyperglycemia (fed glucose measurement) relative to vehicle-treated animals. (B) PIAA-treated animals showed improved glucose tolerance. *, $P < 0.05$; **, $P < 0.01$; ***, $P < 0.001$.

Morphometric analysis of pancreas sections showed that the β-cells, not α-cells, in PIAA-treated mice were more likely to be $Ki67^{+}$, indicating that they were proliferating at a higher rate (Figure 3.26A-C). Moreover, β-cell area and insulin content were increased in PIAA-treated compared with vehicle-treated diabetic mice (Figure 3.26D-E). PIAA treatment also increased cAMP levels in the pancreas (Figure 3.26F). Taken together, these data suggest that inhibition of TBK1/IKKε leads to improvement of β-cell function and induction of β-cell replication across multiple species including primary human β-cells by stimulating a conserved mitotic pathway in β-cells, potentially the cAMP signaling.

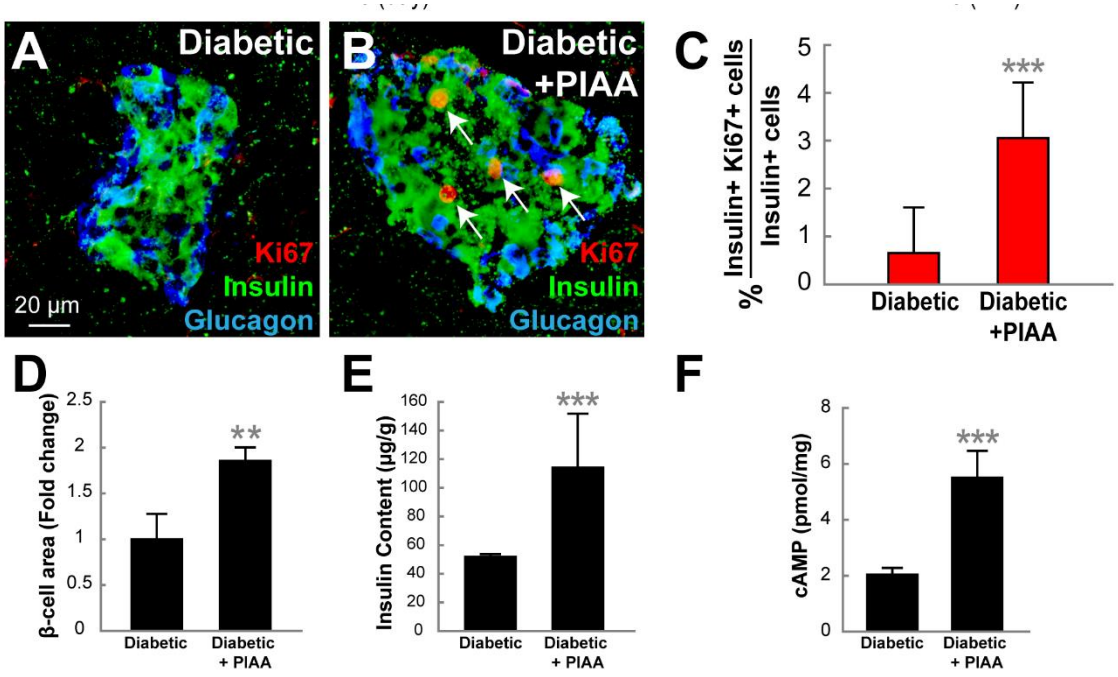

Figure 3.23 PIAA improves β-cell mass in the STZ-induced diabetes murine model.

(A-F) STZ-induced diabetic mice were treated with vehicle or PIAA for 8 days after disease induction (n=6 mice per group). Confocal images of diabetic pancreata treated with (A) vehicle and (B) PIAA, respectively, stained for Ki67 (red, white arrows), Insulin (green), and Glucagon (blue). (C) The percentage (mean±SD) of Ki67 and Insulin-double positive cells in diabetic islets increased with PIAA treatment (0.7±1.0% (vehicle) and 3.1±1.2% (PIAA)). Quantification (mean±SD) of (D) β-cell area (fold change, 1.0±0.3 (vehicle) and 1.9±0.1 (PIAA)), (E) insulin content (51.8±1.9 µg/g (vehicle) and 114.0±37.7 µg/g (PIAA)), and (F) cAMP levels (2.0±0.2 pmol/mg (vehicle) and 5.5±1.0 (PIAA)) in diabetic pancreata treated with vehicle or PIAA. *, $P < 0.05$; **, $P < 0.01$; ***, $P < 0.001$.

3.5 Conclusion

In the progenitors residing in the HPD system at later stages, Fhl1b regulates induction of pancreatic endocrine cells and regeneration of β-cells. Suppression of *fhl1b* increased *pdx1* and *neurod* expression in HPD progenitors, augmenting pancreatic endocrine cell formation and β-cell regeneration, whereas overexpression of *fhl1b* inhibited induction of pancreatic endocrine cells and β-cell regeneration.

We also identified TBK1/IKKε inhibitors as selective enhancers of β-cell proliferation in a transgenic zebrafish model of type I diabetes. We further demonstrated that inhibition of TBK1/IKKε promotes amplification of β-cells in mammalian systems including primary rat and human islets as well as STZ-induced diabetic mice. The proliferative effects of TBK1/IKKε inhibitors are likely to be mediated by the cAMP signaling via PDE3, indicating that TBK1/IKKε play a previously unappreciated role in modulating β-cell mass.

3.6 Discussion

Previous studies have suggested evident plasticity of cells in the HPD system, where differentiation into a specific lineage is suppressed by Fgf10 and Sox9b in zebrafish (Delous et al., 2012; Dong et al., 2007; Manfroid et al., 2012). Furthermore, expression analysis of Id2 has shown that Bmp signaling is blocked and/or excluded in the tissues, including those of the HPD system, that retain the potential to form pancreatic endocrine cells (Chung et al., 2010). Our data provide the intriguing evidence that Bmp2b signaling controls the induction of pancreatic endocrine cells from the HPD system by

inhibiting *pdx1* expression through its effector Fhl1b. The reciprocal expression pattern of *fhl1b* and *pdx1* further supports the suppressive effect of Fhl1b on *pdx1* expression. At 3 dpf, liver cells, which never express *pdx1* in lineage tracing analyses in mice (Fujitani et al., 2006; Gu et al., 2002) and in zebrafish (Chung et al., 2008), express high levels of *fhl1b*, while the HPD system expresses low levels of *fhl1b*. Consistently, the proximal intestine, which has been shown to have marked plasticity (Dong et al., 2007), expresses low levels of *fhl1b*. Most pancreatic cells do not express *fhl1b* except for a few cells in the principal islet. Intriguingly, these few pancreatic cells are located in the peripheral boundary of the principal islet, but are not overlapping with the core β-cells, which maintain a high-level of *pdx1* expression. Manipulating this antagonistic interplay may direct a common endodermal progenitor pool towards pancreatic endocrine, specifically β-cell, fate by modulating distinct levels of *pdx1* expression.

While the intrinsic transcriptional network that regulates β-cell development is well identified (Arda et al., 2013; Pan and Wright, 2011), the extrinsic signaling pathways that control β-cell regeneration remain largely elusive. Our studies for the first time suggest that Bmp signaling plays an essential role in the regeneration of β-cells, in part by modulating *pdx1* and *neurod* expression in the HPD system through its regulator Fhl1b. Although we are not able to exclude the possibility that newly generated β-cells came from α-cells (Thorel et al., 2010), our loss-of-function analyses of Fhl1b during normal development imply that increased formation of endocrine progenitors may lead to enhanced β-cell regeneration. In line with this hypothesis, in β-cell ablated *fhl1b* MO-injected larvae, multiple regenerating β-cells were found at the junction between the pancreas and the HPD system. In contrast, Adenosine signaling, one of the few signals

that has been shown to function during β-cell depletion in zebrafish (Andersson et al., 2012), plays a significant role in regulating β-cell mass during regeneration but not during normal conditions. Careful dissection of extrinsic signals and intrinsic factors acting on a specific aspect of β-cell regeneration will allow us to perform individual or combinatorial therapies to pinpoint the most valid regeneration strategy.

For the first time, we have pinpointed that inhibition of TBK1/IKKε promotes β-cell proliferation in multiple species including primary human islets. Of essential importance is that suppression of TBK1/IKKε with amlexanox and PIAA, which exhibited the highest potency among tested, can increase β-cell proliferation selectively without inducing a general increase in proliferation of other cell types/tissues and that a longer treatment with these small molecules did not lead to overproliferation of β-cells once normoglycemia was approached. Since oncogenicity can arise as a result of modulating mitogenic or regenerative pathways (Wang et al., 2015b), specific TBK1/IKKε inhibitors' selectivity to β-cells and ability to increase β-cell proliferation primarily during the most active period of β-cell regeneration present valid strategies for expanding β-cell mass. Furthermore, our results may support that Diarylamide WS6, which was previously suggested to target IKKε with increasing β-cell proliferation potency in primary human islet culture (Boerner et al., 2015; Shen et al., 2013), had modest effect on human β-cell proliferation (Wang et al., 2015a). Therefore, further design and validation of new molecular structures with potent TBK1- and/or IKKε-inhibition activities and minimal toxicity using the PIAA as a scaffold will allow us to identify legitimate strategies for developing human β-cell-specific proliferogens.

In progression of T1DM and T2DM, which is the most prevalent form of diabetes, decreasing β-cell mass is a common feature. T2DM patients with impaired fasting glucose show a relatively reduced β-cell mass regardless of obesity. This characteristic highlights a critical urgency to develop strategies to expand functionally relevant β-cell mass in diabetic therapy. TBK1/IKKε have shown to mainly act on IRFs, specifically IRF-3 and IRF-7, that are crucially involved in innate and adaptive immune responses and in pathogenesis of autoimmune diseases (Sharma et al., 2003). In the presence of IRF-induced type I interferon (IFN) (Honda et al., 2005; Sato et al., 2000), IKKε phosphorylates the Signal Transducer and Activator of Transcription 1 (STAT1) protein (Tenoever et al., 2007), which is critical to promote apoptosis upon viral infection. Accordingly, it is plausible to speculate that suppression of TBK1/IKKε can preserve residual β-cells in part by inhibiting STAT1-induced apoptosis. As our analyses suggest that repression of TBK1/IKKε increases the number of β-cells by stimulating cAMP, a careful dissection and elucidation of TBK1/IKKε-controlled signaling networks will shed light on modulating the immune response with concomitant increase in β-cell mass, opening up new avenues of immunotherapies for alleviating diabetes.

CONCLUSION AND DISCUSSION

The work in this thesis identified *fhl1b* as a novel target of Bmp2b signaling. By expression analysis, loss-of-function and gain-of-function studies, we showed that *fhl1b* promotes specification of liver and suppresses induction of pancreatic cells. Combined with single-cell lineage tracing experiments, we indicated that manipulation of *fhl1b* levels in the progenitors could lead to fate switch of endodermal progenitors.

Furthermore, Fhl1b also regulates the regeneration of β-cells by modulating *pdx1* and *neurod* expression in the HPD system. Loss-of-function and gain-of-function studies suggested *fhl1b* mainly regulates the neogenesis of β-cells from the progenitor cell population residing in the HPD system.

In addition to Bmp2b signaling pathway, we identified TBK1/IKKε inhibitors as enhancers of β-cell regeneration. These inhibitors promoted β-cell regeneration through enhancing β-cell-specific proliferation. Our results also suggested that this effect is achieved by up-regulating cAMP levels via suppressing activation of Pde3a in zebrafish. This effect is conserved in mammalian islets culture and STZ-induced diabetic mice.

These data firstly described the function of Fhl1b as a Bmp2b downstream target, regulating the fate decision of endodermal progenitor cells. It also supports the speculation that besides actively initiating the expression of hepatic lineage program, Bmp signaling may actively suppress the onset of pancreatic lineage gene expression. These data provide novel insights in β-cell regeneration as well. As previously expected, various sources can contribute to β-cell regeneration. Here we showed that two of them, the progenitors in the ductal system and the remaining endogenous β-cells, can be

regulated by signaling pathways. Depletion of *fhl1b* resulted in more progenitors converting to β-cells upon injury. This knowledge can also be applied to induce the directed differentiation of progenitor cells *in vitro*. The new connection between suppression of TBK1/IKKε pathway and β-cell proliferation during regeneration opened many possibilities for future treatment development.

It is important to further uncover how Bmp signaling pathway, especially through Fhl1b, regulates the fate decision process. A few studies linked the roles of Bmp signaling in fate decision with alterations of chromatin states and histone modifications. It's suggested that Bmp activates liver gene expression by recruiting factors to induce histone acetylation in the regulatory regions of liver genes. The pancreatic gene regulatory elements are poised by both active and suppressive histone marks. Loss of the suppressive marks led to pancreatic gene activation. These studies indicate that epigenetic modulation of lineage specification gene program is another layer of regulation in liver and pancreas fate decision. And Bmp is involved in this layer as well. Considering the characters of LIM-domain-only proteins, it is reasonable to speculate that Fhl1b may participate in epigenetic regulation of the histone marks via protein-protein interaction with some other histone modifying complexes. To answer this question, it would be very necessary and useful to identify proteins and factors binding with Fhl1b. Meanwhile, investigation of binding sites of Fhl1b in the genome could potentially tell the gene programs regulated by Fhl1b. By comparing the histone modification marks at those sites using control and altered-*fhl1b*-level samples, we can gain clues on how this regulation is achieved.

To exploit the potential of TBK1/IKKε inhibitors in future diabetes treatment, there are a few more questions need to be answered. First, a genetic validation is necessary to fully support the results from inhibitor treatment, and to provide confidence in exploring possible novel targets in this pathway. Nevertheless, the downstream network and effectors of TBK1/IKKε are not clear yet. Dissecting the regulatory pathways may help us to better understand the mechanism and specificity of this proliferative effect on β-cell regeneration. A few more screenings on inhibitors suppressing β-cell proliferation could provide information on possible downstream effectors. The discoveries of more downstream targets could also contribute to identifying new therapy strategies. The exploration of the immunosuppression side of TBK1/IKKε inhibitors will be an interesting mission and may lead to the development of multi-effect compounds.

REFERENCES

Aamodt, K.I., Aramandla, R., Brown, J., Fiaschi-Taesch, N., Wang, P., Stewart, A.F., Brissova, M., and Powers, A.C. (2016). Development of a reliable, automated screening system to identify small molecules and biologics that promote human beta cell regeneration. American journal of physiology. Endocrinology and metabolism, ajpendo 00515 02015.

Alexander, J., Stainier, D.Y., and Yelon, D. (1998). Screening mosaic F1 females for mutations affecting zebrafish heart induction and patterning. Developmental genetics *22*, 288-299.

Alonso, L.C., Yokoe, T., Zhang, P., Scott, D.K., Kim, S.K., O'Donnell, C.P., and Garcia-Ocana, A. (2007). Glucose infusion in mice: a new model to induce beta-cell replication. Diabetes *56*, 1792-1801.

Andersson, O., Adams, B.A., Yoo, D., Ellis, G.C., Gut, P., Anderson, R.M., German, M.S., and Stainier, D.Y. (2012). Adenosine signaling promotes regeneration of pancreatic beta cells in vivo. Cell metabolism *15*, 885-894.

Annes, J.P., Ryu, J.H., Lam, K., Carolan, P.J., Utz, K., Hollister-Lock, J., Arvanites, A.C., Rubin, L.L., Weir, G., and Melton, D.A. (2012). Adenosine kinase inhibition selectively promotes rodent and porcine islet beta-cell replication. Proc Natl Acad Sci U S A *109*, 3915-3920.

Arda, H.E., Benitez, C.M., and Kim, S.K. (2013). Gene regulatory networks governing pancreas development. Dev Cell *25*, 5-13.

Baeyens, L., Lemper, M., Leuckx, G., De Groef, S., Bonfanti, P., Stange, G., Shemer, R., Nord, C., Scheel, D.W., Pan, F.C., et al. (2014). Transient cytokine treatment induces acinar cell reprogramming and regenerates functional beta cell mass in diabetic mice. Nature biotechnology *32*, 76-83.

Bajoghli, B., Aghaallaei, N., Heimbucher, T., and Czerny, T. (2004). An artificial promoter construct for heat-inducible misexpression during fish embryogenesis. Dev Biol *271*, 416-430.

Biemar, F., Argenton, F., Schmidtke, R., Epperlein, S., Peers, B., and Driever, W. (2001). Pancreas development in zebrafish: early dispersed appearance of endocrine hormone expressing cells and their convergence to form the definitive islet. Dev Biol *230*, 189-203.

Boerner, B.P., George, N.M., Mir, S.U., and Sarvetnick, N.E. (2015). WS6 induces both alpha and beta cell proliferation without affecting differentiation or viability. Endocrine journal *62*, 379-386.

Bonner-Weir, S., Deery, D., Leahy, J.L., and Weir, G.C. (1989). Compensatory growth of pancreatic beta-cells in adult rats after short-term glucose infusion. Diabetes *38*, 49-53.

Brezar, V., Carel, J.C., Boitard, C., and Mallone, R. (2011). Beyond the hormone: insulin as an autoimmune target in type 1 diabetes. Endocrine reviews *32*, 623-669.

Byun, H.R., Choi, J.A., and Koh, J.Y. (2014). The role of metallothionein-3 in streptozotocin-induced beta-islet cell death and diabetes in mice. Metallomics : integrated biometal science *6*, 1748-1757.

Caillaud, A., Hovanessian, A.G., Levy, D.E., and Marie, I.J. (2005). Regulatory serine residues mediate phosphorylation-dependent and phosphorylation-independent activation of interferon regulatory factor 7. J Biol Chem *280*, 17671-17677.

Chang, D.F., Belaguli, N.S., Iyer, D., Roberts, W.B., Wu, S.P., Dong, X.R., Marx, J.G., Moore, M.S., Beckerle, M.C., Majesky, M.W., et al. (2003). Cysteine-rich LIM-only proteins CRP1 and CRP2 are potent smooth muscle differentiation cofactors. Dev Cell *4*, 107-118.

Chau, T.L., Gioia, R., Gatot, J.S., Patrascu, F., Carpentier, I., Chapelle, J.P., O'Neill, L., Beyaert, R., Piette, J., and Chariot, A. (2008). Are the IKKs and IKK-related kinases TBK1 and IKK-epsilon similarly activated? Trends in biochemical sciences *33*, 171-180.

Chocron, S., Verhoeven, M.C., Rentzsch, F., Hammerschmidt, M., and Bakkers, J. (2007). Zebrafish Bmp4 regulates left-right asymmetry at two distinct developmental time points. Dev Biol *305*, 577-588.

Chung, W.S., Andersson, O., Row, R., Kimelman, D., and Stainier, D.Y. (2010). Suppression of Alk8-mediated Bmp signaling cell-autonomously induces pancreatic beta-cells in zebrafish. Proc Natl Acad Sci U S A *107*, 1142-1147.

Chung, W.S., Shin, C.H., and Stainier, D.Y. (2008). Bmp2 signaling regulates the hepatic versus pancreatic fate decision. Dev Cell *15*, 738-748.

Chung, W.S., and Stainier, D.Y. (2008). Intra-endodermal interactions are required for pancreatic beta cell induction. Dev Cell *14*, 582-593.

Clement, J.F., Meloche, S., and Servant, M.J. (2008). The IKK-related kinases: from innate immunity to oncogenesis. Cell research *18*, 889-899.

Cogger, K., and Nostro, M.C. (2015). Recent advances in cell replacement therapies for the treatment of type 1 diabetes. Endocrinology *156*, 8-15.

Collombat, P., Mansouri, A., Hecksher-Sorensen, J., Serup, P., Krull, J., Gradwohl, G., and Gruss, P. (2003). Opposing actions of Arx and Pax4 in endocrine pancreas development. Genes Dev *17*, 2591-2603.

Conti, M., and Beavo, J. (2007). Biochemistry and physiology of cyclic nucleotide phosphodiesterases: essential components in cyclic nucleotide signaling. Annual review of biochemistry *76*, 481-511.

Curado, S., Anderson, R.M., Jungblut, B., Mumm, J., Schroeter, E., and Stainier, D.Y. (2007). Conditional targeted cell ablation in zebrafish: a new tool for regeneration studies. Developmental dynamics : an official publication of the American Association of Anatomists *236*, 1025-1035.

Delous, M., Yin, C., Shin, D., Ninov, N., Debrito Carten, J., Pan, L., Ma, T.P., Farber, S.A., Moens, C.B., and Stainier, D.Y. (2012). Sox9b is a key regulator of pancreaticobiliary ductal system development. PLoS Genet *8*, e1002754.

Delporte, F.M., Pasque, V., Devos, N., Manfroid, I., Voz, M.L., Motte, P., Biemar, F., Martial, J.A., and Peers, B. (2008). Expression of zebrafish pax6b in pancreas is regulated by two enhancers containing highly conserved cis-elements bound by PDX1, PBX and PREP factors. BMC developmental biology *8*, 53.

Dereeper, A., Guignon, V., Blanc, G., Audic, S., Buffet, S., Chevenet, F., Dufayard, J.F., Guindon, S., Lefort, V., Lescot, M., et al. (2008). Phylogeny.fr: robust phylogenetic analysis for the non-specialist. Nucleic Acids Res *36*, W465-469.

diIorio, P.J., Moss, J.B., Sbrogna, J.L., Karlstrom, R.O., and Moss, L.G. (2002). Sonic hedgehog is required early in pancreatic islet development. Dev Biol *244*, 75-84.

Donath, M.Y., and Shoelson, S.E. (2011). Type 2 diabetes as an inflammatory disease. Nature reviews. Immunology *11*, 98-107.

Dong, P.D., Munson, C.A., Norton, W., Crosnier, C., Pan, X., Gong, Z., Neumann, C.J., and Stainier, D.Y. (2007). Fgf10 regulates hepatopancreatic ductal system patterning and differentiation. Nat Genet *39*, 397-402.

Dooley, K., and Zon, L.I. (2000). Zebrafish: a model system for the study of human disease. Current opinion in genetics & development *10*, 252-256.

Dor, Y., Brown, J., Martinez, O.I., and Melton, D.A. (2004). Adult pancreatic beta-cells are formed by self-duplication rather than stem-cell differentiation. Nature *429*, 41-46.

El Ouaamari, A., Dirice, E., Gedeon, N., Hu, J., Zhou, J.Y., Shirakawa, J., Hou, L., Goodman, J., Karampelias, C., Qiang, G., et al. (2015). SerpinB1 Promotes Pancreatic beta Cell Proliferation. Cell metabolism.

El Ouaamari, A., Dirice, E., Gedeon, N., Hu, J., Zhou, J.Y., Shirakawa, J., Hou, L., Goodman, J., Karampelias, C., Qiang, G., et al. (2016). SerpinB1 Promotes Pancreatic beta Cell Proliferation. Cell metabolism *23*, 194-205.

Esser, N., Legrand-Poels, S., Piette, J., Scheen, A.J., and Paquot, N. (2014). Inflammation as a link between obesity, metabolic syndrome and type 2 diabetes. Diabetes research and clinical practice *105*, 141-150.

Farooq, M., Sulochana, K.N., Pan, X., To, J., Sheng, D., Gong, Z., and Ge, R. (2008). Histone deacetylase 3 (hdac3) is specifically required for liver development in zebrafish. Dev Biol *317*, 336-353.

Field, H.A., Dong, P.D., Beis, D., and Stainier, D.Y. (2003a). Formation of the digestive system in zebrafish. II. Pancreas morphogenesis. Dev Biol *261*, 197-208.

Field, H.A., Ober, E.A., Roeser, T., and Stainier, D.Y. (2003b). Formation of the digestive system in zebrafish. I. Liver morphogenesis. Dev Biol *253*, 279-290.

Fujitani, Y., Fujitani, S., Boyer, D.F., Gannon, M., Kawaguchi, Y., Ray, M., Shiota, M., Stein, R.W., Magnuson, M.A., and Wright, C.V. (2006). Targeted deletion of a cis-regulatory region reveals differential gene dosage requirements for Pdx1 in foregut organ differentiation and pancreas formation. Genes Dev *20*, 253-266.

Godinho, L., Mumm, J.S., Williams, P.R., Schroeter, E.H., Koerber, A., Park, S.W., Leach, S.D., and Wong, R.O. (2005). Targeting of amacrine cell neurites to appropriate synaptic laminae in the developing zebrafish retina. Development *132*, 5069-5079.

Gu, G., Dubauskaite, J., and Melton, D.A. (2002). Direct evidence for the pancreatic lineage: NGN3+ cells are islet progenitors and are distinct from duct progenitors. Development *129*, 2447-2457.

Guillemain, G., Filhoulaud, G., Da Silva-Xavier, G., Rutter, G.A., and Scharfmann, R. (2007). Glucose is necessary for embryonic pancreatic endocrine cell differentiation. J Biol Chem *282*, 15228-15237.

Hao, J., Ho, J.N., Lewis, J.A., Karim, K.A., Daniels, R.N., Gentry, P.R., Hopkins, C.R., Lindsley, C.W., and Hong, C.C. (2010). In vivo structure-activity relationship study of dorsomorphin analogues identifies selective VEGF and BMP inhibitors. ACS chemical biology *5*, 245-253.

Hesselson, D., Anderson, R.M., Beinat, M., and Stainier, D.Y. (2009). Distinct populations of quiescent and proliferative pancreatic beta-cells identified by HOTcre mediated labeling. Proc Natl Acad Sci U S A *106*, 14896-14901.

Ho, C.Y., Houart, C., Wilson, S.W., and Stainier, D.Y. (1999). A role for the extraembryonic yolk syncytial layer in patterning the zebrafish embryo suggested by properties of the hex gene. Current biology : CB *9*, 1131-1134.

Honda, K., Yanai, H., Negishi, H., Asagiri, M., Sato, M., Mizutani, T., Shimada, N., Ohba, Y., Takaoka, A., Yoshida, N., et al. (2005). IRF-7 is the master regulator of type-I interferon-dependent immune responses. Nature *434*, 772-777.

Hua, H., Zhang, Y.Q., Dabernat, S., Kritzik, M., Dietz, D., Sterling, L., and Sarvetnick, N. (2006). BMP4 regulates pancreatic progenitor cell expansion through Id2. J Biol Chem *281*, 13574-13580.

Huang, H., Vogel, S.S., Liu, N., Melton, D.A., and Lin, S. (2001). Analysis of pancreatic development in living transgenic zebrafish embryos. Molecular and cellular endocrinology *177*, 117-124.

Huang, M., Chang, A., Choi, M., Zhou, D., Anania, F.A., and Shin, C.H. (2014). Antagonistic interaction between Wnt and Notch activity modulates the regenerative capacity of a zebrafish fibrotic liver model. Hepatology *60*, 1753-1766.

Hutti, J.E., Porter, M.A., Cheely, A.W., Cantley, L.C., Wang, X., Kireev, D., Baldwin, A.S., and Janzen, W.P. (2012). Development of a high-throughput assay for identifying inhibitors of TBK1 and IKKepsilon. PLoS One *7*, e41494.

Hwang, W.Y., Fu, Y., Reyon, D., Maeder, M.L., Tsai, S.Q., Sander, J.D., Peterson, R.T., Yeh, J.R., and Joung, J.K. (2013). Efficient genome editing in zebrafish using a CRISPR-Cas system. Nature biotechnology *31*, 227-229.

Imai, Y., Dobrian, A.D., Morris, M.A., and Nadler, J.L. (2013). Islet inflammation: a unifying target for diabetes treatment? Trends in endocrinology and metabolism: TEM *24*, 351-360.

Inada, A., Hamamoto, Y., Tsuura, Y., Miyazaki, J., Toyokuni, S., Ihara, Y., Nagai, K., Yamada, Y., Bonner-Weir, S., and Seino, Y. (2004). Overexpression of inducible cyclic AMP early repressor inhibits transactivation of genes and cell proliferation in pancreatic beta cells. Mol Cell Biol *24*, 2831-2841.

Inoue, H., Ogawa, W., Ozaki, M., Haga, S., Matsumoto, M., Furukawa, K., Hashimoto, N., Kido, Y., Mori, T., Sakaue, H., et al. (2004). Role of STAT-3 in regulation of hepatic gluconeogenic genes and carbohydrate metabolism in vivo. Nature medicine *10*, 168-174.

Jao, L.E., Wente, S.R., and Chen, W. (2013). Efficient multiplex biallelic zebrafish genome editing using a CRISPR nuclease system. Proc Natl Acad Sci U S A *110*, 13904-13909.

Jinek, M., Chylinski, K., Fonfara, I., Hauer, M., Doudna, J.A., and Charpentier, E. (2012). A programmable dual-RNA-guided DNA endonuclease in adaptive bacterial immunity. Science *337*, 816-821.

Kadrmas, J.L., and Beckerle, M.C. (2004). The LIM domain: from the cytoskeleton to the nucleus. Nat Rev Mol Cell Biol *5*, 920-931.

Kawakami, K., Koga, A., Hori, H., and Shima, A. (1998). Excision of the tol2 transposable element of the medaka fish, Oryzias latipes, in zebrafish, Danio rerio. Gene *225*, 17-22.

Khaliq, M., Choi, T.Y., So, J., and Shin, D. (2015). Id2a is required for hepatic outgrowth during liver development in zebrafish. Mechanisms of development.

Kimmel, R.A., Onder, L., Wilfinger, A., Ellertsdottir, E., and Meyer, D. (2011). Requirement for Pdx1 in specification of latent endocrine progenitors in zebrafish. BMC biology *9*, 75.

Kinkel, M.D., Eames, S.C., Alonzo, M.R., and Prince, V.E. (2008). Cdx4 is required in the endoderm to localize the pancreas and limit beta-cell number. Development *135*, 919-929.

Korzh, V., Sleptsova, I., Liao, J., He, J., and Gong, Z. (1998). Expression of zebrafish bHLH genes ngn1 and nrd defines distinct stages of neural differentiation. Developmental dynamics : an official publication of the American Association of Anatomists *213*, 92-104.

Kroon, E., Martinson, L.A., Kadoya, K., Bang, A.G., Kelly, O.G., Eliazer, S., Young, H., Richardson, M., Smart, N.G., Cunningham, J., et al. (2008). Pancreatic endoderm derived from human embryonic stem cells generates glucose-responsive insulin-secreting cells in vivo. Nature biotechnology *26*, 443-452.

Lancman, J.J., Zvenigorodsky, N., Gates, K.P., Zhang, D., Solomon, K., Humphrey, R.K., Kuo, T., Setiawan, L., Verkade, H., Chi, Y.I., et al. (2013). Specification of hepatopancreas progenitors in zebrafish by hnf1ba and wnt2bb. Development *140*, 2669-2679.

Leung, L., Klopper, A.V., Grill, S.W., Harris, W.A., and Norden, C. (2011). Apical migration of nuclei during G2 is a prerequisite for all nuclear motion in zebrafish neuroepithelia. Development *138*, 5003-5013.

Ma, X., Helgason, E., Phung, Q.T., Quan, C.L., Iyer, R.S., Lee, M.W., Bowman, K.K., Starovasnik, M.A., and Dueber, E.C. (2012). Molecular basis of Tank-binding kinase 1 activation by transautophosphorylation. Proc Natl Acad Sci U S A *109*, 9378-9383.

Manfroid, I., Ghaye, A., Naye, F., Detry, N., Palm, S., Pan, L., Ma, T.P., Huang, W., Rovira, M., Martial, J.A., et al. (2012). Zebrafish sox9b is crucial for hepatopancreatic duct development and pancreatic endocrine cell regeneration. Dev Biol *366*, 268-278.

McLin, V.A., Rankin, S.A., and Zorn, A.M. (2007). Repression of Wnt/beta-catenin signaling in the anterior endoderm is essential for liver and pancreas development. Development *134*, 2207-2217.

Meier, J.J., Butler, A.E., Saisho, Y., Monchamp, T., Galasso, R., Bhushan, A., Rizza, R.A., and Butler, P.C. (2008). Beta-cell replication is the primary mechanism subserving the postnatal expansion of beta-cell mass in humans. Diabetes *57*, 1584-1594.

Michalopoulos, G.K. (2007). Liver regeneration. Journal of cellular physiology *213*, 286-300.

Miyazono, K., and Miyazawa, K. (2002). Id: a target of BMP signaling. Science's STKE : signal transduction knowledge environment *2002*, pe40.

Moss, J.B., Koustubhan, P., Greenman, M., Parsons, M.J., Walter, I., and Moss, L.G. (2009). Regeneration of the pancreas in adult zebrafish. Diabetes *58*, 1844-1851.

Mowers, J., Uhm, M., Reilly, S.M., Simon, J., Leto, D., Chiang, S.H., Chang, L., and Saltiel, A.R. (2013). Inflammation produces catecholamine resistance in obesity via activation of PDE3B by the protein kinases IKKepsilon and TBK1. eLife *2*, e01119.

Murtaugh, L.C., Stanger, B.Z., Kwan, K.M., and Melton, D.A. (2003). Notch signaling controls multiple steps of pancreatic differentiation. Proc Natl Acad Sci U S A *100*, 14920-14925.

Ninov, N., Borius, M., and Stainier, D.Y. (2012). Different levels of Notch signaling regulate quiescence, renewal and differentiation in pancreatic endocrine progenitors. Development *139*, 1557-1567.

Nostro, M.C., Sarangi, F., Ogawa, S., Holtzinger, A., Corneo, B., Li, X., Micallef, S.J., Park, I.H., Basford, C., Wheeler, M.B., et al. (2011). Stage-specific signaling through TGFbeta family members and WNT regulates patterning and pancreatic specification of human pluripotent stem cells. Development *138*, 861-871.

Ober, E.A., Verkade, H., Field, H.A., and Stainier, D.Y. (2006). Mesodermal Wnt2b signalling positively regulates liver specification. Nature *442*, 688-691.

Obholzer, N., Wolfson, S., Trapani, J.G., Mo, W., Nechiporuk, A., Busch-Nentwich, E., Seiler, C., Sidi, S., Sollner, C., Duncan, R.N., et al. (2008). Vesicular glutamate transporter 3 is required for synaptic transmission in zebrafish hair cells. The Journal of neuroscience : the official journal of the Society for Neuroscience *28*, 2110-2118.

Ostrom, M., Loffler, K.A., Edfalk, S., Selander, L., Dahl, U., Ricordi, C., Jeon, J., Correa-Medina, M., Diez, J., and Edlund, H. (2008). Retinoic acid promotes the generation of pancreatic endocrine progenitor cells and their further differentiation into beta-cells. PLoS One *3*, e2841.

Pagliuca, F.W., Millman, J.R., Gurtler, M., Segel, M., Van Dervort, A., Ryu, J.H., Peterson, Q.P., Greiner, D., and Melton, D.A. (2014). Generation of functional human pancreatic beta cells in vitro. Cell *159*, 428-439.

Pan, F.C., and Wright, C. (2011). Pancreas organogenesis: from bud to plexus to gland. Developmental dynamics : an official publication of the American Association of Anatomists *240*, 530-565.

Pisharath, H., Rhee, J.M., Swanson, M.A., Leach, S.D., and Parsons, M.J. (2007). Targeted ablation of beta cells in the embryonic zebrafish pancreas using E. coli nitroreductase. Mechanisms of development *124*, 218-229.

Porat, S., Weinberg-Corem, N., Tornovsky-Babaey, S., Schyr-Ben-Haroush, R., Hija, A., Stolovich-Rain, M., Dadon, D., Granot, Z., Ben-Hur, V., White, P., et al. (2011). Control of pancreatic beta cell regeneration by glucose metabolism. Cell metabolism *13*, 440-449.

Pozzilli, P., Maddaloni, E., and Buzzetti, R. (2015). Combination immunotherapies for type 1 diabetes mellitus. Nature reviews. Endocrinology *11*, 289-297.

Pyne, N.J., and Furman, B.L. (2003). Cyclic nucleotide phosphodiesterases in pancreatic islets. Diabetologia *46*, 1179-1189.

Reilly, S.M., Ahmadian, M., Zamarron, B.F., Chang, L., Uhm, M., Poirier, B., Peng, X., Krause, D.M., Korytnaya, E., Neidert, A., et al. (2015). A subcutaneous adipose tissue-liver signalling axis controls hepatic gluconeogenesis. Nature communications *6*, 6047.

Reilly, S.M., Chiang, S.H., Decker, S.J., Chang, L., Uhm, M., Larsen, M.J., Rubin, J.R., Mowers, J., White, N.M., Hochberg, I., et al. (2013). An inhibitor of the protein kinases TBK1 and IKK-varepsilon improves obesity-related metabolic dysfunctions in mice. Nature medicine *19*, 313-321.

Rennekamp, A.J., and Peterson, R.T. (2015). 15 years of zebrafish chemical screening. Current opinion in chemical biology *24*, 58-70.

Reyon, D., Tsai, S.Q., Khayter, C., Foden, J.A., Sander, J.D., and Joung, J.K. (2012). FLASH assembly of TALENs for high-throughput genome editing. Nature biotechnology *30*, 460-465.

Rezania, A., Bruin, J.E., Arora, P., Rubin, A., Batushansky, I., Asadi, A., O'Dwyer, S., Quiskamp, N., Mojibian, M., Albrecht, T., et al. (2014). Reversal of diabetes with insulin-producing cells derived in vitro from human pluripotent stem cells. Nature biotechnology *32*, 1121-1133.

Rezania, A., Bruin, J.E., Riedel, M.J., Mojibian, M., Asadi, A., Xu, J., Gauvin, R., Narayan, K., Karanu, F., O'Neil, J.J., et al. (2012). Maturation of human embryonic stem cell-derived pancreatic progenitors into functional islets capable of treating pre-existing diabetes in mice. Diabetes *61*, 2016-2029.

Robu, M.E., Larson, J.D., Nasevicius, A., Beiraghi, S., Brenner, C., Farber, S.A., and Ekker, S.C. (2007). p53 activation by knockdown technologies. PLoS Genet *3*, e78.

Rossi, J.M., Dunn, N.R., Hogan, B.L., and Zaret, K.S. (2001). Distinct mesodermal signals, including BMPs from the septum transversum mesenchyme, are required in combination for hepatogenesis from the endoderm. Genes Dev *15*, 1998-2009.

Russ, H.A., Parent, A.V., Ringler, J.J., Hennings, T.G., Nair, G.G., Shveygert, M., Guo, T., Puri, S., Haataja, L., Cirulli, V., et al. (2015). Controlled induction of human

pancreatic progenitors produces functional beta-like cells in vitro. EMBO J *34*, 1759-1772.

Sang, M., Ma, L., Sang, M., Zhou, X., Gao, W., and Geng, C. (2014). LIM-domain-only proteins: multifunctional nuclear transcription coregulators that interacts with diverse proteins. Molecular biology reports *41*, 1067-1073.

Sato, M., Suemori, H., Hata, N., Asagiri, M., Ogasawara, K., Nakao, K., Nakaya, T., Katsuki, M., Noguchi, S., Tanaka, N., et al. (2000). Distinct and essential roles of transcription factors IRF-3 and IRF-7 in response to viruses for IFN-alpha/beta gene induction. Immunity *13*, 539-548.

Schmittgen, T.D., and Livak, K.J. (2008). Analyzing real-time PCR data by the comparative C(T) method. Nature protocols *3*, 1101-1108.

Sharma, S., tenOever, B.R., Grandvaux, N., Zhou, G.P., Lin, R., and Hiscott, J. (2003). Triggering the interferon antiviral response through an IKK-related pathway. Science *300*, 1148-1151.

Shathasivam, T., Kislinger, T., and Gramolini, A.O. (2010). Genes, proteins and complexes: the multifaceted nature of FHL family proteins in diverse tissues. Journal of cellular and molecular medicine *14*, 2702-2720.

Shaw, J.E., Sicree, R.A., and Zimmet, P.Z. (2010). Global estimates of the prevalence of diabetes for 2010 and 2030. Diabetes research and clinical practice *87*, 4-14.

Shen, W., Taylor, B., Jin, Q., Nguyen-Tran, V., Meeusen, S., Zhang, Y.Q., Kamireddy, A., Swafford, A., Powers, A.F., Walker, J., et al. (2015). Inhibition of DYRK1A and GSK3B induces human beta-cell proliferation. Nature communications *6*, 8372.

Shen, W., Tremblay, M.S., Deshmukh, V.A., Wang, W., Filippi, C.M., Harb, G., Zhang, Y.Q., Kamireddy, A., Baaten, J.E., Jin, Q., et al. (2013). Small-molecule inducer of beta cell proliferation identified by high-throughput screening. Journal of the American Chemical Society *135*, 1669-1672.

Shih, H.P., Kopp, J.L., Sandhu, M., Dubois, C.L., Seymour, P.A., Grapin-Botton, A., and Sander, M. (2012). A Notch-dependent molecular circuitry initiates pancreatic endocrine and ductal cell differentiation. Development *139*, 2488-2499.

Shin, D., Lee, Y., Poss, K.D., and Stainier, D.Y. (2011). Restriction of hepatic competence by Fgf signaling. Development *138*, 1339-1348.

Shin, D., Shin, C.H., Tucker, J., Ober, E.A., Rentzsch, F., Poss, K.D., Hammerschmidt, M., Mullins, M.C., and Stainier, D.Y. (2007). Bmp and Fgf signaling are essential for liver specification in zebrafish. Development *134*, 2041-2050.

Sosa-Pineda, B., Wigle, J.T., and Oliver, G. (2000). Hepatocyte migration during liver development requires Prox1. Nat Genet *25*, 254-255.

Soyer, J., Flasse, L., Raffelsberger, W., Beucher, A., Orvain, C., Peers, B., Ravassard, P., Vermot, J., Voz, M.L., Mellitzer, G., et al. (2010). Rfx6 is an Ngn3-dependent winged helix transcription factor required for pancreatic islet cell development. Development *137*, 203-212.

Spagnoli, F.M., and Brivanlou, A.H. (2008). The Gata5 target, TGIF2, defines the pancreatic region by modulating BMP signals within the endoderm. Development *135*, 451-461.

Spence, J.R., Lange, A.W., Lin, S.C., Kaestner, K.H., Lowy, A.M., Kim, I., Whitsett, J.A., and Wells, J.M. (2009). Sox17 regulates organ lineage segregation of ventral foregut progenitor cells. Dev Cell *17*, 62-74.

Stafford, D., and Prince, V.E. (2002). Retinoic acid signaling is required for a critical early step in zebrafish pancreatic development. Current biology : CB *12*, 1215-1220.

Stanger, B.Z., and Hebrok, M. (2013). Control of cell identity in pancreas development and regeneration. Gastroenterology *144*, 1170-1179.

Tenoever, B.R., Ng, S.L., Chua, M.A., McWhirter, S.M., Garcia-Sastre, A., and Maniatis, T. (2007). Multiple functions of the IKK-related kinase IKKepsilon in interferon-mediated antiviral immunity. Science *315*, 1274-1278.

Thorel, F., Nepote, V., Avril, I., Kohno, K., Desgraz, R., Chera, S., and Herrera, P.L. (2010). Conversion of adult pancreatic alpha-cells to beta-cells after extreme beta-cell loss. Nature *464*, 1149-1154.

Untergasser, A., Cutcutache, I., Koressaar, T., Ye, J., Faircloth, B.C., Remm, M., and Rozen, S.G. (2012). Primer3--new capabilities and interfaces. Nucleic Acids Res *40*, e115.

Uribe, R.A., and Gross, J.M. (2010). Id2a influences neuron and glia formation in the zebrafish retina by modulating retinoblast cell cycle kinetics. Development *137*, 3763-3774.

Vetere, A., Choudhary, A., Burns, S.M., and Wagner, B.K. (2014). Targeting the pancreatic beta-cell to treat diabetes. Nature reviews. Drug discovery *13*, 278-289.

Walpita, D., Hasaka, T., Spoonamore, J., Vetere, A., Takane, K.K., Fomina-Yadlin, D., Fiaschi-Taesch, N., Shamji, A., Clemons, P.A., Stewart, A.F., et al. (2012). A human islet cell culture system for high-throughput screening. Journal of biomolecular screening *17*, 509-518.

Wandzioch, E., and Zaret, K.S. (2009). Dynamic signaling network for the specification of embryonic pancreas and liver progenitors. Science *324*, 1707-1710.

Wang, H., Maechler, P., Ritz-Laser, B., Hagenfeldt, K.A., Ishihara, H., Philippe, J., and Wollheim, C.B. (2001). Pdx1 level defines pancreatic gene expression pattern and cell lineage differentiation. J Biol Chem *276*, 25279-25286.

Wang, J., Kilic, G., Aydin, M., Burke, Z., Oliver, G., and Sosa-Pineda, B. (2005). Prox1 activity controls pancreas morphogenesis and participates in the production of "secondary transition" pancreatic endocrine cells. Dev Biol *286*, 182-194.

Wang, P., Alvarez-Perez, J.C., Felsenfeld, D.P., Liu, H., Sivendran, S., Bender, A., Kumar, A., Sanchez, R., Scott, D.K., Garcia-Ocana, A., et al. (2015a). A high-throughput chemical screen reveals that harmine-mediated inhibition of DYRK1A increases human pancreatic beta cell replication. Nature medicine *21*, 383-388.

Wang, P., Fiaschi-Taesch, N.M., Vasavada, R.C., Scott, D.K., Garcia-Ocana, A., and Stewart, A.F. (2015b). Diabetes mellitus--advances and challenges in human beta-cell proliferation. Nature reviews. Endocrinology *11*, 201-212.

Wang, W., Walker, J.R., Wang, X., Tremblay, M.S., Lee, J.W., Wu, X., and Schultz, P.G. (2009). Identification of small-molecule inducers of pancreatic beta-cell expansion. Proc Natl Acad Sci U S A *106*, 1427-1432.

Wang, Y.J., Park, J.T., Parsons, M.J., and Leach, S.D. (2015c). Fate mapping of ptf1a-expressing cells during pancreatic organogenesis and regeneration in zebrafish. Developmental dynamics : an official publication of the American Association of Anatomists *244*, 724-735.

Wells, J.M., and Melton, D.A. (2000). Early mouse endoderm is patterned by soluble factors from adjacent germ layers. Development *127*, 1563-1572.

Westerfield, M. (2000). The zebrafish book: A guide for the laboratory use of zebrafish (Danio rerio). (Eugene: Univ. of Oregon Press).

Xie, T., Chen, M., Zhang, Q.H., Ma, Z., and Weinstein, L.S. (2007). Beta cell-specific deficiency of the stimulatory G protein alpha-subunit Gsalpha leads to reduced beta cell mass and insulin-deficient diabetes. Proc Natl Acad Sci U S A *104*, 19601-19606.

Xu, C.R., Cole, P.A., Meyers, D.J., Kormish, J., Dent, S., and Zaret, K.S. (2011). Chromatin "prepattern" and histone modifiers in a fate choice for liver and pancreas. Science *332*, 963-966.

Xu, X., D'Hoker, J., Stange, G., Bonne, S., De Leu, N., Xiao, X., Van de Casteele, M., Mellitzer, G., Ling, Z., Pipeleers, D., et al. (2008). Beta cells can be generated from endogenous progenitors in injured adult mouse pancreas. Cell *132*, 197-207.

Ye, L., Robertson, M.A., Hesselson, D., Stainier, D.Y., and Anderson, R.M. (2015). Glucagon is essential for alpha cell transdifferentiation and beta cell neogenesis. Development *142*, 1407-1417.

Zaret, K.S. (2008). Genetic programming of liver and pancreas progenitors: lessons for stem-cell differentiation. Nature reviews. Genetics *9*, 329-340.

Zhang, D., Golubkov, V.S., Han, W., Correa, R.G., Zhou, Y., Lee, S., Strongin, A.Y., and Dong, P.D. (2014). Identification of Annexin A4 as a hepatopancreas factor involved in liver cell survival. Dev Biol *395*, 96-110.

Zhao, Z., Low, Y.S., Armstrong, N.A., Ryu, J.H., Sun, S.A., Arvanites, A.C., Hollister-Lock, J., Shah, N.H., Weir, G.C., and Annes, J.P. (2014). Repurposing cAMP-modulating medications to promote beta-cell replication. Molecular endocrinology *28*, 1682-1697.

Zhou, Q., Brown, J., Kanarek, A., Rajagopal, J., and Melton, D.A. (2008). In vivo reprogramming of adult pancreatic exocrine cells to beta-cells. Nature *455*, 627-632.

Ziv, O., Glaser, B., and Dor, Y. (2013). The plastic pancreas. Dev Cell *26*, 3-7.

Zmuda-Trzebiatowska, E., Oknianska, A., Manganiello, V., and Degerman, E. (2006). Role of PDE3B in insulin-induced glucose uptake, GLUT-4 translocation and lipogenesis in primary rat adipocytes. Cellular signalling *18*, 382-390.

Zorn, A.M., and Wells, J.M. (2009). Vertebrate endoderm development and organ formation. Annual review of cell and developmental biology *25*, 221-251.